Dipolar Bose-Einstein condensates in optical lattices

VON DER FAKULTÄT FÜR MATHEMATIK UND PHYSIK DER
GOTTFRIED WILHELM LEIBNIZ UNIVERSITÄT HANNOVER

ZUR ERLANGUNG DES GRADES
DOKTOR DER NATURWISSENSCHAFTEN
DR. RER. NAT

GENEHMIGTE DISSERTATION VON

M.SC. KAZIMIERZ ŁAKOMY

GEBOREN AM 11. APRIL 1984 IN WARSCHAU, POLEN

2013

Referent: Prof. Dr. Luis Santos
Koreferent: Prof. Dr. Manfred Lein
Tag der Promotion: 3. April 2013

to my mother

I do not know what I may appear to the world, but to myself
I seem to have been only like a boy playing on the sea-shore,
and diverting myself in now and then
finding a smoother pebble or a prettier shell than ordinary,
whilst the great ocean of truth lay all undiscovered before me.

SIR ISAAC NEWTON

Abstract

In this thesis we study theoretically a quantum degenerate ultracold dipolar gas of bosons. In particular, we focus on a dipolar Bose-Einstein condensate confined in an optical lattice and we demonstrate extensively how such arrangement can be employed to investigate on novel phenomena that arise as a consequence of both the long-range character and the anisotropy of the dipole-dipole interactions.

We examine a stack of quasi-one-dimensional traps and we show that the dipolar interactions support the formation of intersite soliton dimers and trimers, which constitute a paradigm of soliton molecules. We investigate in detail the stability of these two- and three-soliton bound states and we prove their existence in a regime where their molecular counterparts are precluded. Moreover, we find that in contrast to the dimers of polar molecules the soliton dimers exhibit a nontrivial behavior of the elementary excitations that stems from the competition between onsite and intersite dipole-dipole interactions. We demonstrate that the soliton molecules that we report are well feasible under realistic experimental conditions.

Furthermore, we show that the destabilization of a dipolar condensate confined in such a stack of nonoverlapping quasi-one-dimensional tubes induces an interesting dynamics characterized by the development of a correlated modulational instability in the disjoint sites. Careful analysis of this phenomenon reveals that for a sufficiently large dipole moment this correlated instability may be followed by the spontaneous self-assembly of stable soliton filaments (comprised of the soliton dimers) or a two-dimensional checkerboard soliton crystal (comprised of the soliton trimers), providing a route for the first realization of self-sustained two-dimensional arrangements of matter-wave solitons. Our numerical simulations show that these self-assembled structures may be observed within current experimental feasibilities.

In addition, we explore consequences of a parametric modulation of the dipolar interactions in a quasi-one-dimensional dipolar condensate in the stack. Showing that the emerging Faraday patterns differ significantly with respect to the two-dimensional case, we demonstrate the nontrivial role of the confinement dimensionality in dipolar gases. Moreover, considering two sites in the stack, we present nonlocal effects that originate in the dipolar coupling between the patterns in the nonoverlapping tubes. Namely, we show that, for a critical driving frequency, the unfolding of the excitations spectrum into symmetric and antisymmetric modes gives rise to a transition between correlated and anticorrelated Faraday patterns in the two condensates. Furthermore, we find that for the critical driving the emergent pattern differs from one realization to another, resulting from a spontaneous symmetry-breaking mechanism.

Finally, we focus on a two-dimensional geometry and we show that the density dependence of the excitations spectrum in a trapped dipolar condensate gives rise to an effective potential that traps elementary excitations in the region of highest density of the condensate, leading to a roton confinement. Moreover, we demonstrate that in a pancake dipolar condensate the roton confinement is of a fundamental relevance for the dynamics of the roton instability. In particular, we find that a roton-unstable condensate develops a density pattern that is localized in the trap center. We show that this atypical modulational instability leads to local collapses, followed by an elaborate atoms loss dynamics, which differs radically from both the usual global collapse in a nonpolar gas and the d-wave collapse in a dipolar gas. Inducing such roton instability dynamically and next arresting the collapse we illustrate the formation of a robust and long-living confined gas of rotons. Other consequences of the roton confinement are also discussed, including the local susceptibility of the condensate against density perturbation, which we exemplify with a vortex lattice.

Keywords: Bose-Einstein condensate, dipole-dipole interactions, optical lattice

Zusammenfassung

In der vorliegen den Arbeit wird die Theorie quantenmechanisch entarteter ultrakalter dipolarer bosonischer Gase untersucht. Von besonderem Interesse ist ein Bose-Einstein Kondensat, welches in einem optischen Gitter eingeschlossen ist. Es wird gezeigt, wie solch ein System dazu genutzt werden kann, um neuartige Phänomene zu studieren, welche sowohl auf dem langreichweitigen Charakter der Dipol-Dipol-Wechselwirkung basieren, als auch deren anisotrope Natur miteinbeziehen.

Erforscht werden Systeme aus Blöcken quasi-eindimensionaler Fallen, um zu zeigen, dass dipolare Wechselwirkungen die Bildung von ”inter-site“ Soliton-Dimeren und -Trimeren fördern, was als ein Beispiel für die Bildung von Solitonenmolekülen dient. Im Detail wird die Stabilität der genannten Zwei- und Drei-Solitonen-Bindungszustände untersucht und gezeigt, dass diese in einem Bereich tatsächlich existieren, wo die Bildung der den solitonischen Bindungszuständen entsprechenden Moleküle unterdrückt wird. Des Weiteren ergibt sich, dass, anders als im Fall von Dimeren von polaren Molekülen, die Solitondimere eine nichttriviale Art elementarer Anregungen aufweisen, welche ihren Ursprung im Zusammenspiel von ”on-site“ und ”inter-site“ Dipol-Dipol Wechselwirkungen haben. Dabei wird auch auf die experimentelle Realisierbarkeit der oben erwähnten solitonischen Moleküle eingegangen.

Darüber hinaus wird aufgezeigt, dass eine Destabilisierung des dipolaren Kondensates, welches in solchen Blöcken von nicht-überlappenden, quasi-eindimensionalen Röhren gefangen ist, interessante dynamische Effekte hervorruft, welche durch korrelierte modulierte Instabilitäten zwischen disjunkten ”sites“ charakterisiert werden. Eine detaillierte Analyse besagter Phänomene lässt darauf schließen, dass für ausreichend große Dipolmomente die korrelierten Instabilitäten abgelöst werden durch spontan geordnete stabile Soliton-Filamente (bestehend aus Solitonendimeren), oder durch zweidimensionale schachbrettartige Solitonenkristalle (bestehend aus Solitontrimeren), was wiederum einen Weg zur Realisierung selbsterhaltender, zweidimen-

sionaler Anordnungen von Materiewellen-Solitonen aufzeigt. Numerische Simulationen geben einen Hinweis darauf, dass auch diese sich selbst organisierenden Strukturen in bestehenden Experimenten beobachtet werden können.

Zusätzlich werden die Auswirkungen einer parametrischen Modulation der dipolaren Wechselwirkung in einem quasi eindimensionalen dipolaren Kondensat in der oben eingeführten Blockanordnung studiert. Dabei wird gezeigt, dass die auftretenden Faraday-Muster sich signifikant von denen im zweidimensionalen Fall unterscheiden. Daraus lässt sich eine nicht triviale Rolle der Einschluss-Geometrie im Fall von dipolaren Gasen schlussfolgern. Ferner, im Fall von zwei ”sites“ im Fallenblock, werden nichtlokale Effekte vorgestellt, welche ihren Ursprung in der dipolaren Kopplung zwischen den ausgebildeten Mustern in den nicht-überlappenden Fallenröhren haben. Konkret wird gezeigt, dass für kritische Modulationsfrequenzen die Aufspaltung des Anregungsspektrums in symmetrische und antisymmetrische Moden einen Übergang zwischen korrelierten und unkorrelierten Faraday Mustern in den zwei Kondensaten ermöglicht. In diesem Rahmen variieren die auftretenden Muster im Bereich der kritischen Modulation je nach Ausführung, was ein Resultat spontaner Symmetriebrechung ist.

Zum Schluss wird die zweidimensionale Geometrie genauer betrachtet und gezeigt, dass die Dichteabhängigkeit des Anregungsspektrums in einem eingeschlossenen dipolaren Kondensat ein effektives Potential hervorruft, welches elementare Anregungen in Regionen hoher Dichte im Kondensat einschliest, was in einem Roton-Confinement resultiert. Darüber hinaus ist das Roton-Confinement in oblaten dipolaren Kondensaten von fundamentaler Bedeutung für die Dynamik der Rotoninstabilität. Im Detail wird gezeigt, dass eine Roton-Instabilität ein Dichtemuster ausbildet, welches im Fallenzentrum konzentriert ist. Es wird nachgewiesen, dass diese untypische Modulationsinstabilität zu einem lokalen Kollaps führt, gefolgt von einem plötzlichen Stoppen des Atomverluste. Dies unterscheidet sich grundlegend sowohl von einem globalen Kollaps in einem un-polaren Gas, als auch vom d-Wellen Kollaps in einem dipolaren Gas. Es wird gezeigt, dass das dynamische Erzeugen einer solchen Roton-Instabilität, gefolgt von einer Unterdeckung des Kollapses, zu der Ausbildung eines stabilen und langlebigen eingeschlossenen Gases aus Rotonen führt. Auch weitere Konsequenzen des Roton-Confinement werden diskutiert und untersucht, wie zum Beispiel die lokale Suszeptibilität des Kondensats gegenüber Dichtefluktuationen, welche an einem Vortexgitter veranschaulicht werden können.

Schlagworte: Bose-Einstein Kondensat, Dipol-Wechselwirkung, optisches Gitter

Contents

I Introduction and Overview **1**

II Bose-Einstein condensation **3**
- II.A Cooling and trapping of neutral atoms 4
  - II.A.1 Cooling 4
  - II.A.2 Atomic traps 6
  - II.A.3 Optical lattices 7
- II.B An ideal Bose gas 9
- II.C A weakly interacting Bose gas 12
  - II.C.1 Elastic scattering 12
  - II.C.2 Mean-field description 13
  - II.C.3 Gross-Pitaevskii equation 14
  - II.C.4 Thomas-Fermi limit 15
  - II.C.5 Stability of the condensate 16
  - II.C.6 Quasi-low-dimensional Gross-Pitaevskii equation 18
  - II.C.7 Solitons 19
  - II.C.8 Elementary excitations 22

III Dipolar Bose-Einstein condensates **27**
- III.A Dipole-dipole interaction in a polar gas 28
- III.B Geometrical stabilization 32
- III.C Collapse dynamics 34
- III.D Excitations 36
- III.E Roton-Maxon spectrum 38
- III.F Dipolar solitons 42

IV Soliton molecules in dipolar BECs **45**
- IV.A Introduction 46
- IV.B Model 47
- IV.C Dipolar soliton in a single quasi-1D trap 48

IV.D Soliton dimers 49
IV.E Soliton trimers 54
IV.F Summary 58

V Spontaneous self-assemblies of solitons in dipolar BECs 59
V.A Introduction 60
V.B Model 61
V.C Linear regime: Bogoliubov modes 62
V.D Filamentation 64
V.E Checkerboard soliton crystal 68
V.F Summary 71

VI Faraday patterns in coupled quasi-1D dipolar BECs 73
VI.A Introduction 74
VI.B Model 75
VI.C Faraday Patterns in a single quasi-1D dipolar BEC 77
VI.D Faraday Patterns in two quasi-1D dipolar BECs 80
VI.E Summary 85

VII Roton confinement in trapped dipolar BECs 87
VII.A Introduction 88
VII.B Analytical model 89
VII.C Local modulational instability and collapse 91
VII.D Confined roton gas 94
VII.E Spatially dependent susceptibility 95
VII.F Summary 96

VIII Conclusions and Outlook 97

A Dimensionally reduced GPE 101

B Analytical expressions for the energy functional 105

C Bogoliubov-de Gennes equations 109

D Derivation of the Mathieu equations 113

Bibliography 117

Curriculum Vitae 145

Publications 147

Acknowledgements 149

I

Introduction and Overview

The impact of ultracold atomic quantum gases on present-day physics is linked to the extraordinary degree of control that such systems offer to investigate the fundamental behavior of quantum matter under various conditions. This controllability extends also to the interatomic interactions that acutely influence intrinsic properties of a gas. Until recently, only short-range isotropic interactions had been investigated. Lately, however, theoretical and experimental developments in ultracold gases have attracted a major focus of the community on the frontier of long-range interactions, and soon new discipline of polar gases emerged. Within this vast field the research has been pursued in three branches: heteronuclear molecules, Rydberg gases and highly magnetic atoms. In this thesis we focus on the last case, and specifically on a quantum degenerate dipolar gas of bosons, which recently has been realized in several experiments.

Remarkably, the long-range dipole-dipole interactions result in an inherently nonlocal nature of dipolar gases, particularly striking in a deep optical lattice. For a nondipolar system, atoms trapped in different sites of a deep lattice do not interact with each other. Hence, for a vanishing intersite hopping, different lattice sites may be considered as mutually independent, uncorrelated experiments. In contrast, even in the absence of hopping, the dipole-dipole interactions couple the disjoint sites and play a decisive role in the collective excitations spectrum, dynamics, and stability properties of the condensate, as we will learn throughout.

Dipolar effects are also particularly relevant to what concerns the nonlinear properties of dipolar Bose-Einstein condensates, the leitmotif of this thesis. Crucially, whereas a nondipolar BEC presents a local Kerr-like type of nonlinearity, the nonlinearity in a dipolar BEC exhibits a nonlocal character. This, in turn, fundamentally modifies the physics of dipolar solitons and density patterns, and becomes especially striking in a quasi-one-dimensional condensate where, contrary to higher dimensions, an instability is not followed with a collapse.

The long-range character and anisotropy of the interactions in a dipolar condensate give rise to yet another phenomenon, which links this system directly to superfluid helium. Namely, the elementary excitations spectrum in a dipolar gas is distinguished by the presence of the celebrated roton minimum at intermediate momenta, a phenomenon absent in nonpolar gases. As we will see, the occurrence of the roton has fundamental consequences for the stability of a condensate, and for the understanding of its collapse dynamics.

In the following chapter we present the fundamental ideas in the physics of ultracold degenerate Bose gases, for the cases of an ideal gas and a gas with short-range, and isotropic interactions. In chapter III we introduce the concept of a Bose-Einstein condensate with long-range and anisotropic dipole-dipole interactions and we discuss the central novel phenomena that occur in such systems. In chapter IV we discuss the physics of a dipolar condensate in deep optical lattice that results effectively in a stack of disjoint quasi-one-dimensional condensates and we show that the interplay between the onsite and intersite dipolar interactions gives rise to soliton bound states. In chapter V a destabilization of such stack is investigated and it is demonstrated that the dipole-dipole interactions between the nonoverlapping condensates results in a correlated modulational instability that evolves spontaneously into soliton filaments or a soliton crystal, depending on the sign of interactions. In chapter VI we study Faraday patterns formation in the stack and we find, for the case of two sites, that the dipolar intersite interactions render the patterns in the two condensates correlated or anticorrelated, depending on the frequency with which the strength of the interactions is modulated. Finally, in chapter VII we present the results of our study on the roton confinement in a trapped dipolar Bose-Einstein condensate and we discuss its far-reaching consequences. We conclude in chapter VIII, providing an outlook for the further research on the discussed subjects.

⁂

II

Bose-Einstein condensation

Since the first theoretical works of Satyendra Nath Bose and Albert Einstein [1, 2], the Bose-Einstein condensation remained merely an obscure idea for seventy years, with the major experimental obstacle laying in ultracold temperatures required to observe the condensate. Finally, this long quest reached its goal in the year 1995, when the first BEC was observed in dilute alkali gases (rubidium, lithium and sodium) in JILA, Rice University and MIT [3–5]. For this achievement Eric A. Cornell, Carl E. Wieman and Wolfgang Ketterle were jointly awarded the Nobel prize in physics in 2001. In this chapter we discuss briefly the fundamental concepts behind the ultracold Bose gases. Comprehensive coverage of this vast discipline, along with recent developments, can be found in a number of reviews and monographs that ensued from the wide interest in this field [6–11].

II.A

Cooling and trapping of neutral atoms

The genuine idea of cooling and trapping of neutral atoms is based on their interactions with light. It was essentially the progress on novel experimental techniques in these two fields in the second half of the 20th century that paved the way to the observation of ultracold degenerate quantum gases. The success in the development of methods to cool and trap atoms with laser light was awarded with the Nobel prize in physics in 1997 for Steven Chu, Claude Cohen-Tannoudji and William D. Phillips.

II.A.1 Cooling

The simplest form of cooling is Doppler cooling [12, 13], which can be understood considering a semi-classical picture of interactions of a two-level atom with the electric field of a laser. For sufficiently small intensity of the field, the force $\mathbf{F}$ acting on the atom reads in general $\mathbf{F} = \mathbf{F}_\mathrm{D} + \mathbf{F}_\mathrm{R}$, where $\mathbf{F}_\mathrm{D}$ is the dipole force proportional to the gradient of the light intensity, and $\mathbf{F}_\mathrm{R}$ is the radiation pressure force [14]. A two-level atom, with the transition frequency ω_0, moving at velocity $\mathbf{v}$ in a monochromatic light field $\mathbf{E}(\mathbf{r},t) = \hat{\varepsilon}\mathscr{E}\cos(\omega t - \mathbf{kr})$, experiences the Doppler effect and hence the frequency detuning $\delta = \omega - \omega_0$ is modified, according to $\delta_d = \delta - \omega_d$, with $\omega_d = \mathbf{kv}$ as the Doppler frequency shift. In consequence, while the dipole force vanishes, the radiation pressure force reads [15]

$$\mathrm{F}_\mathrm{R}(v) = \mathrm{F}_\mathrm{R}(v=0) - \eta v, \tag{II.1}$$

where the coefficient

$$\eta = -\hbar k^2 \Gamma \left[\frac{\delta \Omega^2/2}{\left(\delta^2 + \Gamma^2/4 + \Omega^2/2\right)^2} \right] \tag{II.2}$$

depends on the detuning, spontaneous emission rate Γ and Rabi frequency Ω. Clearly, for $\delta < 0$ (red-detuned light) η becomes positive and the second term in Eq. II.2 plays the role of a friction force that slows the atoms down. In other words, since photons in the field propagating towards the atom are now closer to the resonance $\omega_0 = \omega$, the atom will absorb them more likely than the ones from the field propagating in the same direction and therefore will decelerate. Cooling of a gas can therefore be readily achieved by combing two counterpropagating red-detuned laser beams that will turn the gas into so-called optical molasses. Nonetheless, the possibilities of the Doppler cooling are limited by the randomness of spontaneous emission and randomness of light absorption processes [15]. In consequence, the precise analysis of these effects finds the so-called Doppler limit T_Doppler, that is that the minimum temperature achievable with the Doppler cooling technique, $k_B T_\mathrm{Doppler} \approx \hbar\Gamma/2$, obtained for the detuning $\delta = -\Gamma/2$. For typical alkali atoms the Doppler limit is of the order of $100-200\,\mu$K and it was long believed to be the fundamental limit of laser cooling.

However, the experimental results [16] found temperatures of the molasses well below the Doppler limit and soon the theoretical explanation followed [17] proposing the idea of Sisyphus cooling. The key feature of this model that distinguish it from the earlier picture is the inclusion of both the multiplicity of sublevels that make up the atomic state and spatially dependent optical potential, which can be produced, e.g., with two counterpropagating lasers with orthogonal or oppositely circulating polarizations (polarization gradient). For atoms moving in a light field that varies in space, optical pumping acts to adjust populations of some of the Zeeman sublevels of the ground state hyperfine levels to the changing conditions of the light field. The central parameter that governs the populations is the light shift ΔE_g, i.e., the shift of the energies of the ground magnetic substates induced by the atom-light interaction [18],

$$\Delta E_g = \frac{2\hbar\delta\Omega^2}{\Gamma^2 + 4\delta^2}\mathscr{C}_{ge}^2, \tag{II.3}$$

with $\mathscr{C}_{ge}$ as the Clebsch-Gordan coefficient that describes the coupling between the atom and the light field. Crucially, this parameter not only depends on the magnetic quantum numbers but also on the polarization of the field. Thus, for a field with nonzero polarization gradient, while traveling through the wavelength of the field atoms are continuously pumped into most negatively shifted state, readjusting their population completely from one Zeeman sublevel to another, and back again. Under appropriate conditions, the atom preferentially jumps from one ground state to another when it is near the maxima of the initial optical potential (most positively shifted state) and hence the minima of the final one (most negatively shifted state). As a result, the atom moves mostly uphill the potential and transfers its kinetic energy to the potential energy that is subsequently radiated away due to the spontaneous emission [15]. Therefore, the atom seems always to be climbing potential hills and loosing energy in the process, which eventually can lead to temperatures orders of magnitude smaller than the Doppler cooling. Here again, the minimum attainable temperatures are however fundamentally limited by the randomness of the recoil process. Indeed, more detailed calculations show that the bottleneck of the Sisyphus cooling is few recoil temperatures $T_{\mathrm{rec}} = \hbar^2k^2/2mk_B$ [18]. For typical alkali atoms this translates into $1-50\,\mu$K.

Interestingly, even this limitation has been yet finally overcome with the ideas of employing states insensitive to the light field, so called dark states [19, 20]. In the context of optical cooling, a particularly gripping class of these superposition states are those whose excitable component vanishes exactly when their de Broglie wave is characterized by a particular momentum. Such velocity selective population trapping (VSCPT) allows arbitrarily narrow momentum distributions and has been demonstrated to yield temperatures orders of magnitude smaller than the recoil limit [21]. A detailed theory of VSCPT can be found in Ref. [22]. Another technique that proved itself successful in subrecoil cooling is referred to as Raman cooling [23]. In Ref. [24] this method was used for cesium atoms and temperature below 3 nK was reached, i.e., less than 1/70 of the single photon recoil temperature.

Yet, the laser cooling methods by itself do not suffice to reach the regime of Bose-Einstein condensation. The difficulty stems from the fact that the quantum degeneracy limit calls not only for ultra-low temperatures but also for sufficiently high densities of the atomic sample (see Sec. II.B) that have not been achieved with laser cooling, mostly due to absorption of light, radiation trapping and excited state collisions [25]. Crucially for the long sought goal of attaining the condensate, all these problems have been surmounted with evaporative cooling. First proposed and experimentally applied for atomic hydrogen [26, 27], the method was finally extended to alkali atoms [28–30]. Evaporative cooling is based on the idea of energetic (hot) particles from the Maxwell-Boltzmann distribution tail escaping a confined sample carrying energy larger than the average thermal energy, followed by a rethermalization of the remaining gas through elastic collisions. The process results in cooling. Due to the lower temperature, the cooling rate decreases, unless evaporation is forced by modifying the system, e.g. with the radio frequency knife [31, 32], in such a way that less energetic particles can still escape. A canonical example of evaporative cooling is that of a cooling of a cup of coffee. In this case, the liquid is converted to a gaseous state as the hottest molecules evaporate escaping the cup and leaving the remaining molecules in the liquid cooler. Furthermore, such cooling requires the evaporation of only a small fraction of the coffee to cool it by a considerable amount. Thus, even though the method results in the removal of some particles, those that remain have much lower average energy and, occupying a smaller volume, increase the density. Comprehensive reviews on evaporative cooling can be found in Refs. [25, 33].

II.A.2 Atomic traps

The two main groups of atomic traps are dissipative traps and conservative traps. The traps from the former group provide a trapping mechanism both in position space and in velocity space (cooling). The ones that belong to the latter group confine atoms in a restricted volume in space with no influence on their velocity distribution (no cooling).

The basic example of a dissipative trap is the magneto-optical trap (MOT), usually the step number one in an experimental sequence towards BEC. The MOT consists of two counterpropagating laser beams with opposite circular polarizations and a static magnetic field directed along the lasers axis, with magnitude proportional to the distance from the trap center $z = 0$ and reversing its sign in that point [34, 35]. Such field may be created by a pair of anti-Helmholtz coils [15]. Through combination of arguments related to both the molasses technique and the radiative selection rules we find that the laser detuning acquires now a spatially dependent character due to the Zeeman effect, which shifts the atomic transitions in and out of the resonance with the laser field. In result, the total radiation pressure force $\mathbf{F}_\mathrm{R}$ can be written as [18]

$$\mathrm{F}_\mathrm{R} = -\beta v - m\omega^2_\mathrm{trap} z, \tag{II.4}$$

which is not only a cooling force but also a restoring force that brings the atoms towards the center of the trap.

The actual condensation and the target measurements on the BEC typically take place in a conservative trap, such as a magnetic trap or a dipole trap, where the precooled atoms are loaded from the MOT and cooled further evaporatively. The design of various quasistatic magnetic traps is principally based on the fact that a neutral atom with a permanent magnetic moment $\boldsymbol{\mu}$ can be confined in a minimum of an inhomogeneous field $\mathbf{B}$ by a force $\mathbf{F} = \nabla(\boldsymbol{\mu} \cdot \mathbf{B})$, provided that the atomic state was prepared in the so-called weak-field seeking state [15]. The general features of most common magnetic traps' configurations, i.e. quadrupole traps, spherical hexapole traps and Ioffe-Pritchard traps are discussed in Ref. [36].

In the case of a dipole trap, the oscillating electric field of a laser induces an oscillating atomic electric dipole moment that interacts with the field. If the laser intensity $I(\mathbf{r})$ is spatially inhomogeneous, the coupling and the corresponding ac-Stark shifts of atomic energy levels vary in space, producing a potential $U(\mathbf{r}) \propto I(\mathbf{r})/\delta$ [14] that gives rise to the dipole force $\mathbf{F}_\mathrm{D} = -\nabla U(\mathbf{r})$ (see Fig. II.1.a). Clearly, for a red-detuned light ($\delta < 0$), the sign of the interactions is such that $U(\mathbf{r})$ is attractive and the atoms are being pulled into a region with maximum laser intensity (strong-field seekers). For a blue-detuned light ($\delta > 0$) the potential $U(\mathbf{r})$ is repulsive and the dipole force pushes the atoms out to a region with minimum laser intensity (weak-field seekers). The atoms can be thus trapped in minima or maxima of the laser field, depending on the frequency of the lasers. An all-optical formation of the condensate was initially facing some major obstacles [37] and turned successful [38] only some time after the Boulder, MIT and Rice groups employed magnetic traps in the first observation of the BEC [3–5]. An extensive review on optical dipole traps can be found in Ref. [37].

II.A.3 Optical lattices

A periodic lattice potential with tightly confining potential wells can be created by realizing a dipole trap with superimposed counter propagating laser beams. These beams interfere and the interference pattern results in a periodic potential landscape, which, depending on the lasers arrangement acquire one-, two- or three-dimensional character (see Fig. II.1). In the center of the trap, for distances much smaller than the beam waist, the trapping potential $V(\mathbf{r})$ in three-dimensions can be approximated as the sum of a homogeneous periodic lattice potential

$$V_p(\mathbf{r}) = V_p\left(\sin^2(kx) + V_y \sin^2(ky) + V_z \sin^2(kz)\right), \tag{II.5}$$

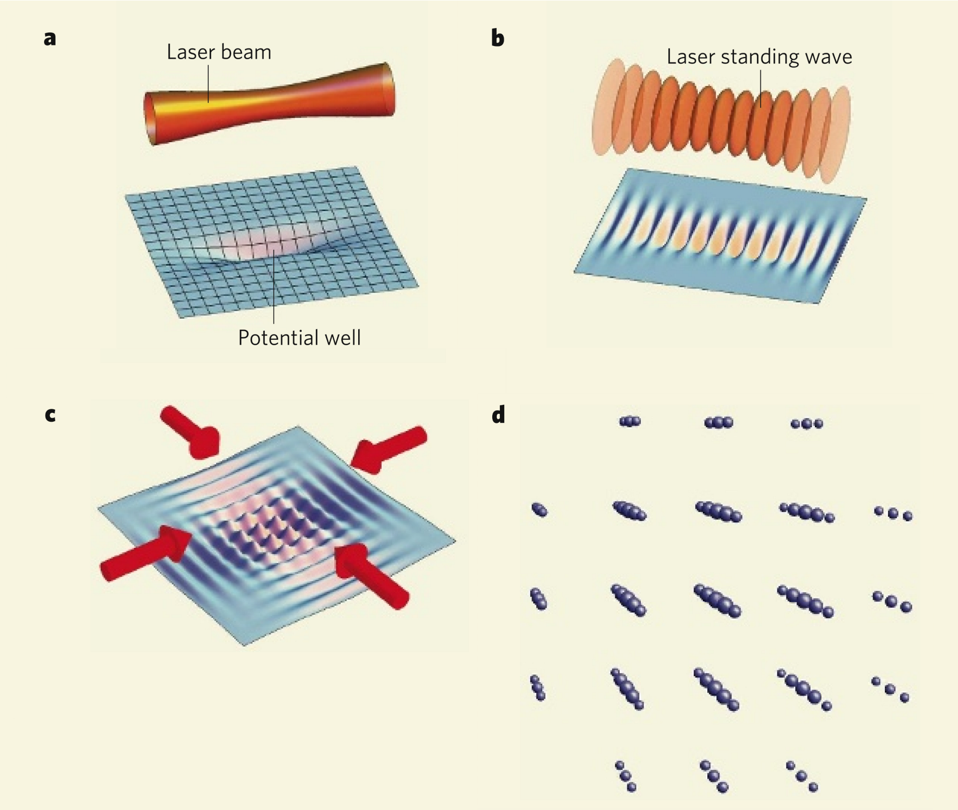

Figure II.1: (a) Laser light potential proportional to the gradient of the laser's intensity. The repulsive or attractive character of the potential depends on the sign of the laser's detuning from the atomic transition frequency. The simplest imaginable trap of this type consists of a single, strongly focused Gaussian laser beam [18]. (b) Two counterpropagating laser beams form a standing wave through interference and hence, effectively, an array of 2D disk-like trapping potentials. Ultracold atoms can be trapped in the potential minima (or maxima) that occur every half of the wavelength, separated from the neighboring minima by potential walls. This is the basis of a one-dimensional optical lattice. (c) Adding an additional pair of lasers we obtain a two-dimensional optical lattice that gives rise to an array of tightly confining 1D potential tubes. (d) A three-dimensional lattice can be created by combining three standing waves. Reprinted from Nature **453**, 736 (2008).

and an additional external harmonic confinement due to the Gaussian laser beam profiles [39]. In an experiment a supplementary confinement can be accomplished with a magnetic trapping potential. For deep optical lattice potentials, the confinement on a single lattice site is approximately harmonic. Atoms are then tightly confined at a single lattice site, with trapping frequencies ω_l of up to 100 kHz. The energy $\hbar\omega_p = 2E_r\left(V_p/E_R\right)^{1/2}$ of local oscillations in the well is of the order of several recoil energies $E_r = \hbar^2k^2/2m$, which is a natural measure of energy scales in optical lattice potentials [8].

Optical lattices are often referred to as artificial crystals of light and indeed the ultracold atoms in lattice sites play the part of electrons in a solid. However, real solid materials are incredibly complex, mostly due to the inevitable effects of vibrations of the crystal lattice and defects, which render both theoretical and experimental studies particularly troublesome. The optical lattices offer a way out becoming quantum simulators [40, 41] that realize simplified models of condensed-matter physics, with all relevant parameters such as the lattice potential depth, lattice geometry and interaction strength between particles being easily tunable over a wide range [42]. Utilizing this controllability, ultracold gases paved way to answers for fundamental questions in physics regarding, e.g., quantum magnetism, strongly correlated systems, effects of dimensionality or quantum information processing. Thorough reviews on optical lattices are presented in Refs. [8, 42–44].

II.B

An ideal Bose gas

The thermodynamics of an ideal Bose gas has been widely studied and the results are summarized in a number of works [45–48]. It is most commonly the grand canonical ensemble, with temperature T and chemical potential μ as the control parameters, that is employed to describe the phenomenon of condensation. In this ensemble, in which external conditions determine only the average total number of particles $\langle N\rangle$, the average occupation number of the i-th energy level reads

$$\langle n_i\rangle = \frac{1}{e^{(E_i-\mu)/k_BT}-1}. \tag{II.6}$$

Naturally, Eq. (II.6) is consistent only if the chemical potential is smaller than the energy of the ground state of the gas, $\mu < E_0$. However, crucially, when $\mu \to E_0$ the occupation number of the ground state $\langle n_0\rangle$ becomes macroscopic. This phenomenon, which occurs at a finite temperature, is the trademark of the Bose-Einstein condensation [1, 2].

Employing Eq. (II.6) and assuming that k_BT is much larger than the average energy difference between the energy levels of the single particle Hamiltonian, the average total number of particles in an ideal Bose gas can be approximated by the integral

$$\langle N\rangle = \int_0^\infty \frac{g(E)E}{e^{(E-\mu)/k_BT}-1}, \tag{II.7}$$

where $g(E)$ is the energy density of states that essentially contains the entire information about the system and hence determines its behavior. In the case of a uniform Bose gas in a box potential of the volume V in d dimensions, which in case of one- and two-dimensional systems can be well implemented in experiments employing atom chips techniques [49], we find that $g(E) \propto E^{d/2-1}$. In particular, when $d = 3$, we can evaluate the integral Eq. (II.7) to obtain

$$\lambda^3 \frac{\langle n_0\rangle}{V} = \lambda^3 \frac{\langle N\rangle}{V} - \mathrm{Li}_{3/2}(z) \tag{II.8}$$

where $\lambda = (2\pi\hbar^2/mk_BT)^{1/2}$ is the thermal wavelength, with m is the mass of an atom, $\mathrm{Li}_s(x)$ is the the polylogarithm function and $z = e^{\mu/k_BT}$, which in case of Bosons obeys the condition $0 \le z \le 1$, is the fugacity of the gas. Eq. (II.8) implies that when the temperature and the density of particles, $n = \langle N\rangle/V$, are such that $\lambda^3 n > \mathrm{Li}_{3/2}(z)$, a finite fraction of the particles occupies the ground state of the system and the Bose-Einstein condensation occurs. Evaluating the polylogarithm function we find that this condition reads explicitly $\lambda^3 n = \rho \gtrsim 2.6$, where ρ is commonly referred to as the phase space density. Even more physically insightful is the observation that Eq. (II.8) means also that the phase transitions begins when the average distance between the atoms becomes comparable to their de Broglie wavelength, i.e., $n^{-1/3} \lesssim \lambda$ (*quantum regime*). In typical experiments with quantum gases the temperature is ranging from 100 nK to 1 μK, and the density is in the range from $10^{12}\mathrm{cm}^{-3}$ to $10^{15}\mathrm{cm}^{-3}$.

Interestingly, the occurrence of the condensation depends crucially on the dimensionality of the system and properties of the trapping potential. In particular, in a 1D box potential $g(E) \propto E^{-1/2}$ and in a 2D box the $g(E)$ is independent of the energy E. In consequence, analyzing Eq. (II.7), we come to the conclusion that in these two cases the chemical potential increases monotonically with decreasing temperature and remains negative at any $T \neq 0$, which indicates that the population of the groundstate is microscopic. One thus can say that there is no BEC in a finite temperature ideal uniform 1D and 2D, respectively, Bose gas.

For harmonically trapped bosons, for which $g(E) \propto E^{d-1}$, the situation dramatically changes [50]. In a 3D harmonic trap, such as in the 3D box potential, the atoms again condense. Strikingly, in contrast with the result for a 2D box potential, in a 2D harmonic trap a macroscopic occupation of the ground state of the system occurs for a finite critical temperature T_c and one can speak of an ordinary BEC transition [51]. The 1D harmonic case

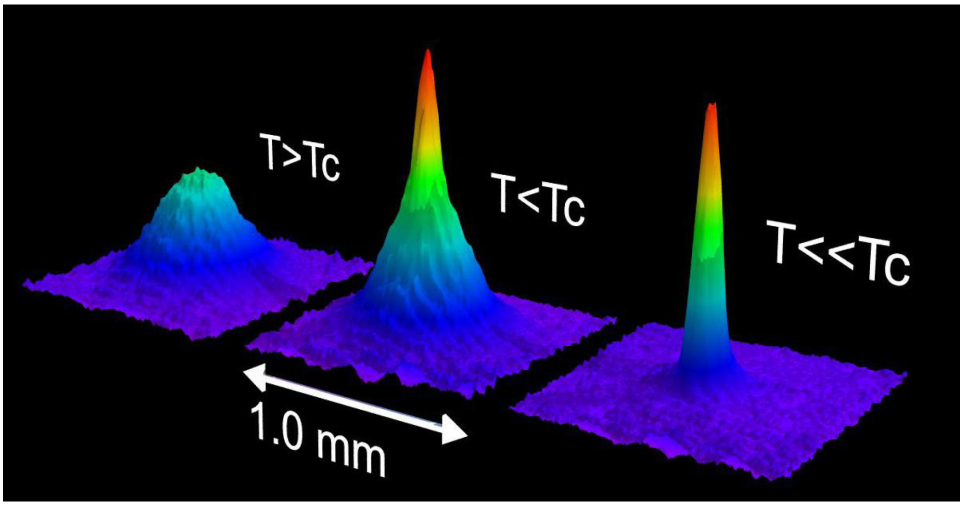

Figure II.2: Observation of Bose-Einstein condensation by absorption imaging of an expanding Bose gas in the position space. Here the snapshot of the cloud was taken after 6 ms of the time of flight. The Bose-Einstein condensate is characterized by its slow expansion. Left picture: an expanding cloud cooled to temperature just above the transition point, $T > T_c$. Middle picture: just after the condensate appeared, $T = T_c$. Right picture: after further evaporative cooling has left an almost pure condensate, $T \ll T_c$. The total number of atoms at the phase transition is about 7×10^5, the temperature at the transition point is 2 μK. Reprinted from the W. Ketterle's Nobel lecture, Rev. Mod. Phys. **74**, 1131 (2002).

is particularly interesting because the standard result is that BEC is not possible, based on the use of the continuous spectrum. However, when the discrete structure of the lowest energy levels is properly taken into account, one finds that for a finite size 1D Bose gas in a harmonic potential that for below certain finite temperature the population of the ground state rapidly grows with decreasing T and becomes macroscopic [52].

The discussion of an ideal Bose gas is mostly academic and the fundamental question concerns the influence of interparticle interactions on the presence and character of BEC. These questions, particularly relevant in physics of low-dimensional gases, have been widely addressed both theoretically and experimentally in number of works [53–62]. In the next section we present basic concepts of the well established theory.

II.C

A weakly interacting Bose gas

II.C.1 Elastic scattering

Let us first consider a general problem of two atoms interacting via potential $V(\mathbf{r}_1 - \mathbf{r}_2)$. In the center of mass reference frame the motion of atoms is described by the Hamiltonian

$$\mathscr{H} = \frac{\mathbf{p}^2}{2m_r} + V(\mathbf{r}), \tag{II.9}$$

with $m_r = m/2$ the reduced mass. In a sufficiently dilute gas the mean interatomic distance is much larger than the radius of interatomic interactions r_0, i.e., $n^{-1/3} \ll r_0$ (*dilute regime*), which means that the wave functions of particles at the mean interparticle separation are not influenced by the interactions between them. Employing this assumption, equivalent to $V(r > r_0) = 0$, and solving the Schrödinger equation with the Hamiltonian (II.9), we find the corresponding asymptotic ($\mathbf{r} \to \infty$) form of the wave function

$$\psi(\mathbf{r}) = e^{\imath \mathbf{r}\mathbf{k}} + f_{\mathbf{k}}(\mathbf{n}) \frac{e^{\imath k r}}{r}, \tag{II.10}$$

where $\mathbf{n}$ is the direction of the scattering and f is called the scattering amplitude, whose form can be found in standard textbooks [63]. Note, that provided the condition $n r_0^3 \ll 1$ is satisfied, the shape of the potential at short distances, i.e., $V(r \simeq 0)$, is irrelevant and the asymptotic form of the wave function in Eq. (II.10) is sufficient to characterize the atomic interactions, which will be sensitive solely to $f_{\mathbf{k}}(\mathbf{n})$. If the de Broglie wavelength greatly exceeds r_0, i.e., $\lambda \gg r_0$, which yields $k r_0 \ll 1$ (*ultracold regime*), further simplifications of Eq. (II.10) can be made and in turn we find that

$$f_{k\to 0}(\mathbf{n}) = -\frac{m}{4\pi\hbar^2} \int d^3\mathbf{r}\, V(\mathbf{r}) \psi(\mathbf{r}) = -a_{sc}, \tag{II.11}$$

where a_{sc} is called the scattering length. Eq. (II.11) means that the scattered wave function is spherically symmetric, even if $V(\mathbf{r})$ itself is not, and that the entire scattering process is characterized merely by a single atomic parameter a_{sc} [64]. This type of scattering, commonly called the s-wave scattering, occurs only when the momentum of the relative motion of atoms is equal $l = 0$. For nonzero values of the angular momentum, the centrifugal barrier inhibits collisions in the ultracold regime.

The most straightforward model of the potential $V(\mathbf{r})$ working accordingly with the assumptions above is the zero-range potential

$$V(\mathbf{r} - \mathbf{r}') = g\delta(\mathbf{r} - \mathbf{r}'), \tag{II.12}$$

which, together with Eq. (II.11) and the Born approximation [65], yields the celebrated formula

$$g = \frac{4\pi\hbar^2 a_{sc}}{m}. \tag{II.13}$$

Interestingly, the scattering length of atoms, and hence properties of BEC, can be controllably manipulated through magnetic or optical Feshbach resonances [66–70] that are strong variations of the scattering length, induced by an external field, which occur when a molecular state (closed channel) has nearly zero energy and couples resonantly to the free states (open channel) of the colliding atoms. The magnetic field governs the closed-open channels coupling strength [71], shifting the energies of two free atoms relative to the molecular state, and thereby controls the interatomic interaction strength. In particular, a magnetically tuned Feshbach resonance can be described with the expression for the s-wave scattering as a function of the magnetic field B

$$a_{sc}(B) = a_{bg}\left(1 - \frac{\Delta}{B - B_0}\right). \tag{II.14}$$

Here, a_{bg} is the so-called background scattering length, summarizing the effect of the direct scattering processes in the open channel, B_0 denotes the resonance position, where the scattering length diverges ($a_{sc} \to \pm\infty$), and the parameter Δ is the resonance width [70]. Eq. (II.14) demonstrates clearly vast capabilities of the Feshbach resonances that allow not only to control the strength of interactions but also, by changing the sign of a_{sc}, to change entirely their character. This versatility has been utilized in various experiments, including formation of matter-wave bright solitons [72, 73], controlled collapse of the condensate [74], BEC-BCS crossover [75] and formation of ultracold molecules [76, 77].

II.C.2 Mean-field description

The many-body Hamiltonian of N bosons interacting through a two-body interatomic potential $V(\mathbf{r}-\mathbf{r}')$ takes the standard form

$$\begin{aligned}\mathscr{H} = &\int d^3\mathbf{r}\,\hat{\Psi}^\dagger(\mathbf{r})\left[-\frac{\hbar^2\nabla^2}{2m} + U(\mathbf{r})\right]\hat{\Psi}(\mathbf{r}) \\ &+ \frac{1}{2}\int d^3\mathbf{r}d^3\mathbf{r}'\,\hat{\Psi}^\dagger(\mathbf{r})\hat{\Psi}^\dagger(\mathbf{r}')V(\mathbf{r}-\mathbf{r}')\hat{\Psi}(\mathbf{r})\hat{\Psi}(\mathbf{r}'),\end{aligned} \tag{II.15}$$

with $U(\mathbf{r})$ as an external potential and $\hat{\Psi}^\dagger(\mathbf{r})$, and $\hat{\Psi}(\mathbf{r})$ denoting the bosonic creation and annihilation field operators, respectively, acting at the position $\mathbf{r}$. While the characteristics of the system can be calculated starting directly from the Hamiltonian (II.15), employing, e.g., Monte Carlo methods, the full many-body Schrödinger problem may become particularly impractical numerically, especially for large N values. Mean-field methods are commonly developed to overcome this problem and to provide a clear physical insight into a considered system. The experiments with the ultracold bosons have proved these theoretical mean-field models particularly effective [6].

The cornerstone of the mean-field theory for bosons was laid by N. N. Bogolyubov in his work on superfluidity [78]. The key point consists in separating out the condensate contribution to the bosonic field operator. In general, in a given basis of single-particle wave functions $\varphi_\nu(\mathbf{r})$, the field operator can be expressed as $\hat{\Psi}(\mathbf{r}) = \sum \varphi_\nu(\mathbf{r})\hat{a}_\nu$, where $\hat{a}_\nu$ are the corresponding annihilation operators acting in the Fock space and obeying the standard commutation relations, and n_ν is the eigenvalue of the operator $\hat{n}_\nu = \hat{a}^\dagger_\nu \hat{a}_\nu$. The Bose-Einstein condensation occurs when the number of atoms n_0 of a particular single-particle state becomes macroscopic and the ratio n_0/N remains finite in the thermodynamic limit $N \to \infty$. In this limit the states with n_0 and $n_0 \pm 1 \simeq n_0$ particles correspond to the same physical configuration and, in consequence, the operators $\hat{a}_0$ and $\hat{a}^\dagger_0$ can be treated like complex numbers $\hat{a}_0 = \hat{a}^\dagger_0 = \sqrt{n_0}$. Hence, we can decompose the field operator into

$$\hat{\Psi}(\mathbf{r}) = \Psi(\mathbf{r}) + \hat{\Psi}'(\mathbf{r}) \tag{II.16}$$

where $\Psi(\mathbf{r})$ is a complex valued classical field (*condensate wave function*) defined as the expectation value of the field operator, i.e., $\Psi(\mathbf{r}) = \langle \hat{\Psi}(\mathbf{r}) \rangle$, which fixes the BEC density through $n_0(\mathbf{r}) = |\Psi(\mathbf{r})|^2$. The operator $\hat{\Psi}'(\mathbf{r})$ represents the noncondensed fraction of atoms that in the ultracold regime remains small and can be treated perturbatively.

II.C.3 Gross-Pitaevskii equation

The time evolution of the field operator $\hat{\Psi}(\mathbf{r})$ is described by the Heisenberg equation of motion $\imath\hbar\partial_t \hat{\Psi}(\mathbf{r},t) = [\hat{\Psi}(\mathbf{r},t), \mathcal{H}]$. At zero temperature all N particles are in the condensate [79] and we can restrict the perturbative treatment of Eq. (II.16) to its zero order, plainly replacing the field operator in the Heisenberg equation with the classical field $\Psi(\mathbf{r})$. Employing Eq. (II.12) for the interatomic potential we arrive at the Gross-Pitaevskii equation [80, 81], often referred to as nonlinear Schrödinger equation, describing the dynamics of the condensate wave function

$$\imath\hbar\partial_t \Psi(\mathbf{r},t) = \left(-\frac{\hbar^2 \nabla^2}{2m} + U(\mathbf{r}) + g|\Psi(\mathbf{r},t)|^2 \right) \Psi(\mathbf{r},t). \tag{II.17}$$

Clearly, the validity of the Gross-Pitaevskii equation (GPE) relies on the assumptions that the number of atoms is macroscopic, i.e., that the gas is in the quantum regime, and that the average interatomic distance is much larger than the interatomic interactions range, i.e., that the gas is in the dilute regime. Recalling that, within the hitherto considerations, the effective length scale of the interactions is set by a_{sc}, the latter condition can be written as $na_{sc}^3 \ll 1$, with n as the average density of the gas. Note, however, that a small value of the parameter na_{sc}^3 does not imply necessarily small effects of interactions and that also a dilute gas can exhibit an important nonideal behavior. The reason for that stems from the fact that in order to estimate the significance of interactions one should rather compare the interactions energy with the kinetic energy of the atoms in the trap $U(\mathbf{r})$. This, in turn, yields Na_{sc}/l_{ho}, with l_{ho} the harmonic oscillator length, as the pertinent parameter [6]. Accordingly, one can find that at the same time $na_{sc}^3 \ll 1$ and $Na_{sc}/l_{ho} \gg 1$, and hence the interactions in a dilute gas can be indeed relevant.

The ground state of the condensate can be simply calculated assuming the Hartree-Fock ansatz for the condensate wave function, $\Psi(\mathbf{r}) = \sqrt{N}\prod \phi_0(\mathbf{r}_i)$, with $\phi_0(\mathbf{r}_i)$ as a normalized to unity single-particle wave function, to be determined. With this ansatz and Hamiltonian (II.15) the energy of the system, i.e., $\langle \Psi(\mathbf{r})|\mathscr{H}|\Psi(\mathbf{r})\rangle$, takes the form

$$E\left[\phi_0,\phi_0^*\right] = N\int d^3\mathbf{r}\left(\frac{\hbar^2}{2m}|\nabla\phi_0(\mathbf{r})|^2 + U(\mathbf{r})|\phi_0(\mathbf{r})|^2 + \frac{g}{2}N|\phi_0(\mathbf{r})|^4\right). \tag{II.18}$$

Introducing a Lagrange multiplier μ that governs the normalization of the $\phi_0(\mathbf{r})$ function, we minimize a new functional

$$X\left[\phi_0,\phi_0^*\right] = E\left[\phi_0,\phi_0^*\right] - \mu N\int d^3\mathbf{r}\,|\phi_0(\mathbf{r})|^2, \tag{II.19}$$

and we arrive at the time independent GPE

$$\mu\phi_0(\mathbf{r}) = \left(-\frac{\hbar^2\nabla^2}{2m} + U(\mathbf{r}) + gN|\phi_0(\mathbf{r})|^2\right)\phi_0(\mathbf{r}). \tag{II.20}$$

Furthermore, we calculate the chemical potential of the gas, by definition, differentiating Eq. (II.18) with respect to the number of particles, i.e., $\partial E/\partial N$. Successively, multiplying Eq. (II.20) with $\phi_0^*(\mathbf{r})$ and integrating with respect to $\mathbf{r}$, we find that $\mu = \partial E/\partial N$, and hence its interpretation. Note, that in the particular case of a homogeneous gas in a box with volume V, $\mu = gN/V = gn$. With all these considerations it is clear now that a stationary solution of Eq. (II.17) in general takes the form

$$\Psi(\mathbf{r},t) = \phi_0(\mathbf{r})e^{-\imath\mu t/\hbar}. \tag{II.21}$$

II.C.4 Thomas-Fermi limit

At this point it is worth to consider solutions of the Gross-Pitaevskii equation in the afore mentioned limit $Na_{sc}/l_{ho} \gg 1$, which is particularly interesting since the condition behind it is well satisfied by most of the current experiments. This so-called Thomas-Fermi (TF) regime assumes that the interactions energy of the condensate in a trap greatly exceeds its kinetic energy or, in other words, that the size of the condensate wave function is much larger than the harmonic oscillator length, i.e., $R \gg \sqrt{\hbar/m\omega}$, with R the radius of the condensate. In consequence, this means that one can neglect the quantum kinetic energy term (*quantum pressure*) in Eq. (II.20) and the solution of the GPE takes form of the inverted potential

$$\phi_0(\mathbf{r}) = \sqrt{\frac{\mu}{Ng}\left(1 - \frac{r^2}{R_{TF}^2}\right)}\theta(R_{TF} - r), \tag{II.22}$$

with the Thomas-Fermi radius $R_{TF} = \sqrt{2\mu/m\omega^2}$ and $\theta(r)$ the Heaviside function. In particular, normalizing Eq. (II.22) we find that due to the spatial inhomogeneity, $\mu \sim N^{2/5}$ as opposed to $\mu \sim N$ for the homogeneous case. Moreover, we note that the balance between the quantum pressure and the interactions energy of the condensate fixes a typical length scale, called the healing length ξ. This is the minimum distance over which the condensate wave function can heal or, in other words, adapt to boundary conditions, and it is set by equating the quantum pressure $\sim \hbar^2/m\xi^2$ and the interactions energy $\sim ng$, $\xi = \hbar/\sqrt{mgn}$. Note that under normal BEC conditions ($na_{sc}^3 \ll 1$) ξ is large compared to a_{sc} but generally small with respect to typical trap sizes l_{ho}. This quantity is particularly relevant for solitons physics (see Sec. II.C.7) and for superfluid effects, such as, e.g., properties of vortices [10, 11].

II.C.5 Stability of the condensate

Another physically insightful class of solutions of the GPE is a Gaussian function, which becomes the exact solution in the limit of vanishing interactions. Assuming a spherical trap and employing the variational ansatz

$$\phi_0(r) = \left(\frac{1}{\pi^{1/2}\sigma}\right)^{3/2} e^{-r^2/2\sigma^2}, \tag{II.23}$$

into Eq. (II.18) we arrive at the

$$\frac{E(\sigma)}{N\hbar\omega_{ho}} = \frac{3}{4}\left(\frac{1}{\sigma^2} + \sigma^2\right) + \frac{\chi}{2\sigma^3}, \tag{II.24}$$

with $\chi = \sqrt{2/\pi}(Na_{sc}/l_{ho})$. In Eq. (II.24) the first term corresponds to the kinetic energy, the second one to the potential energy of the trap and the last one to the energy of interactions, which is proportional to the density $\sim N/\sigma^3$. Finding the ground state solution amounts to solving $dE/d\sigma = 0$, which yields $\sigma^5 - \sigma - \chi = 0$.

In case of a positive scattering length, for $\chi \ll 1$ we find the solution of the noninteracting gas, i.e., $\sigma = 1$, and for $\chi \gg 1$ we obtain $\sigma \approx \chi^{1/5} \sim N^{1/5}$, which means that the more atoms are in the trap the less localized is the condensate

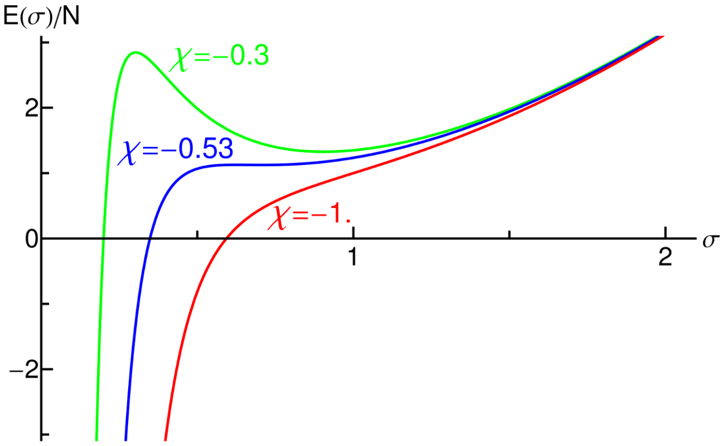

Figure II.3: Energy per particle (II.24), in units of $\hbar\omega_{ho}$, for atoms in a spherical trap interacting with attractive forces, as a function of the width of the Gaussian wave function (II.23). The curves are plotted for three different values of $\chi \sim Na_{sc}/l_{ho}$: $\chi = -0.3$, with a local minimum in the energy functional, $\chi = \chi_c = -0.53$, with a saddle point, and $\chi = -1$, where it is only a collapsed state $\sigma = 0$ that minimizes the energy.

wave function (II.23), i.e., the atoms repel each other. In this limit the kinetic energy scales like $\sim 1/N^{2/5}$, the trap potential energy $\sim N^{2/5}$ and similarly the interactions energy $\sim N^{2/5}$. This means that the kinetic energy is negligible and the ground state configuration is attained through equilibration between the atomic interactions energy and the trap potential. Hence, the condensate is always stable.

For $a_{sc} < 0$, the interactions energy becomes negative and the global minimum $E(\sigma) = -\infty$ exists for all χ values at $\sigma = 0$, i.e., in a state where the BEC cloud collapses to a point [74, 82–86]. However, if $|\chi|$ is smaller than a certain critical value $|\chi_c|$, the negative interactions energy are compensated by the trap potential energy, resulting in a local minimum in the energy functional (see Fig. II.3), which supports a (meta)stable configuration. Calculating $d^2E/d\sigma^2 = 0$ we find that $\chi_c = -0.53$, which refers to the critical number of particles in the condensate $N_c = -0.671 l_{ho}/a_{sc}$. More precise numerical simulations of the GPE show that $N_c = -0.575 l_{ho}/a_{sc}$, which is consistent with recent experimental measurements [87, 88].

In the above discussed studies the critical number of particles N_c has been found to depend very weakly on the trap aspect ratio [89]. In a dipolar BEC the anisotropy of the dipole-dipole interactions thoroughly modifies the situation, with stability properties strongly dependent on the geometry of the condensate. We will learn the details of this effect in section III.B, which remains inherently linked with chapter VII.

II.C.6 Quasi-low-dimensional Gross-Pitaevskii equation

With the discussion presented in Sec. II.B and Sec. II.C.3, it is worth to consider the description a quasi-low-dimensional condensate. Such systems have been studied theoretically [53, 54, 57, 59, 90–93] and realized experimentally in one and two dimensions, in magnetic traps [55, 56, 94], optical lattices [60, 61] and atom chips [49, 95, 96].

In a three-dimensional BEC the radial extension of the cloud $R_\perp$ and its axial length R_z are determined by the interactions and (greatly) exceed the healing length ξ, hence fulfilling the relation $R_\perp, R_z \gg \xi$. The progress in the trapping techniques allows however to tightly confine the motion of the trapped atoms in one (two) direction and create quasi-two-dimensional (quasi-one-dimensional) gas, in which the particles undergo only zero point oscillations in the frozen direction. The effective dynamics of such gas can be obtained by averaging the three-dimensional interactions over the radial (axial) density profile.

For a quasi-two-dimensional (*pancake*) condensate $R_z \ll \xi \ll R_\perp$, which is equivalent to $\hbar\omega_z \gg ng \gg \hbar\omega_\perp$, so that the interactions energy is smaller than the energy difference between ground and first excited state of the harmonic oscillator in the axial direction. Hence, we can assume the ground state of a harmonic oscillator for the axial part of the wave function and factorize $\Psi(\mathbf{r},t)$ in Eq. (II.17) into

$$\Psi(\mathbf{r},t) = \Psi(x,y,t)\Psi_{ho}(z) = \Psi(x,y,t)\pi^{-1/4} l_z^{-1/2} e^{-z^2/2l_z^2}, \tag{II.25}$$

where $l_z = \sqrt{\hbar/m\omega_z}$ is the axial harmonic oscillator length. Employing this factorization and integrating Eq. (II.17) wit respect to z, we arrive at the two-dimensional Gross-Pitaevskii equation

$$\imath\hbar\partial_t\Psi(x,y,t) = \left(-\frac{\hbar^2}{2m}\left(\partial_x^2 + \partial_y^2\right) + U(x,y) + g_{2\mathrm{D}}|\Psi(x,y,t)|^2\right)\Psi(x,y,t), \tag{II.26}$$

with the effective coupling parameter $g_{2\mathrm{D}} = g/\sqrt{2\pi}l_z$.

For a quasi-one-dimensional (*cigar*) condensate $R_\perp \ll \xi \ll R_z$, which is equivalent to $\hbar\omega_\perp \gg ng \gg \hbar\omega_z$, so that the interactions energy is smaller than the energy difference between ground and first excited state of the harmonic oscillator in the radial direction. Similarly to the previous case we can then assume the ground state of the harmonic oscillator for the radial part of the wave function and factorize as follows

$$\Psi(\mathbf{r},t) = \Psi(z,t)\Psi_{ho}(x,y) = \Psi_z(z,t)\pi^{-1/2} l_\perp^{-1} e^{-(x^2+y^2)/2l_\perp^2}, \tag{II.27}$$

where $l_\perp$ is the radial harmonic oscillator length. Inserting this ansatz into Eq. (II.17) and integrating the x, y dependence we obtain the effective one-dimensional Gross-Pitaevskii equation

$$\imath\hbar\partial_t\Psi(z,t) = \left(-\frac{\hbar^2}{2m}\partial_z^2 + U(z) + g_{1\mathrm{D}}|\Psi(z,t)|^2\right)\Psi(z,t), \tag{II.28}$$

with $g_{1\mathrm{D}} = g/2\pi l_\perp^2$.

We comment on the dimensional reduction of the GPE describing a dipolar gas in section III.A.

In Sec. II.C.5 we considered stability properties of a three-dimensional gas. Following the same procedures, together with the results of this section, we can now examine the stability of a condensate with a negative scattering length in lower dimensions. For a pancake condensate the energy functional reads

$$\frac{E(\sigma_\perp)}{N\hbar\omega_\perp} = \frac{1}{2}\left(\frac{1}{\sigma_\perp^2} + \sigma_\perp^2\right) - \frac{1}{\sigma_\perp^2}\left(\frac{N|a_{sc}|}{l_\perp}\right). \tag{II.29}$$

Clearly, for $N|a_{sc}|/l_\perp < 1/2$, i.e., when the kinetic energy dominates over the interactions energy, a global minimum $\sigma_\perp \neq 0$ exists. Otherwise, the condensate collapses to a point. Interestingly, in a cigar-shaped condensate a finite global minimum always exists, independently of the number of particles, and the $\sim 1/\sigma_z$ scaling of the interactions energy

$$\frac{E(\sigma_z)}{N\hbar\omega_z} = \frac{1}{4}\left(\frac{1}{\sigma_z^2} + \sigma_z^2\right) - \frac{1}{\sigma_z}\left(\sqrt{2\pi}\frac{N|a_{sc}|}{l_z}\right), \tag{II.30}$$

renders the condensate always stable against a collapse.

II.C.7 Solitons

In the quasi-two-dimensional case, see Eq. (II.29), it is the presence of the trapping potential that sustains the local minimum, and switching off the trap will cause the free expansion or the collapse of the gas, depending on the value of $N|a_{sc}|/l_\perp$. Crucially, in a quasi-one-dimensional condensate, see Eq. (II.30), the minimum exists even in the absence of the trap. Such localized states with the quantum pressure (dispersion of the wave packet) being balanced by the nonlinearity are called solitons (solitary waves). These wave packets maintain their shape while they travel at constant speed and can interact with each other, and emerge from the collision unchanged, except for a phase shift [97]. Several exactly integrable nonlinear equations, admitting an infinite number of conservation laws and exact solutions, emerge as universal models of solitons. These include Kortweg-de Vries equation, nonlinear Schrödinger equation, sine-Gordon equation and others [98]. Today, experimental and theoretical studies of solitons remain an active field in several branches of science, including applied mathematics, astrophysics, chemistry and molecular biology [99]. In physics a large part of work on solitons is concentrated in the fields of nonlinear optics (light waves) and BECs (matter waves).

Optical solitons [100] may be naturally subdivided into three broad categories- temporal, spatial, and spatiotemporal (light bullets). They may exist in the form of one-dimensional or multidimensional objects [101]. One-dimensional temporal solitons in optical fibers with a cubic (Kerr) nonlinearity were predicted [102] and observed experimentally [103], while stable self-trapping of light in the spatial domain was first observed in planar waveguides [104]. Spatial two-dimensional solitary waves were first studied and observed in photorefractive crystals [105, 106] and in optical media with quadratic nonlinearity [107], where spatiotemporal self-trapping of light in two-dimensional quasi-soliton objects was also observed [108]. Stable fully three-dimensional optical solitons were predicted [109, 110] and only recently observed in a discrete setting of waveguide arrays [111].

In ultracold gases the long sought solitons [90, 112–124] were first observed experimentally for condensates with repulsive interactions (*dark solitons*) in three dimensions [125] and in a quasi-one-dimensional BEC [126]. These solitons are characterized by a notch in the BEC density profile with a phase step across the soliton center. Solitons in condensates with attractive interactions (*bright solitons*), with a peak in the BEC density profile, were created shortly after in a quasi-one-dimensional gas [72, 73]. Also, a mechanism based on temporal and spatial variation of the scattering length has been proposed to stabilize bright solitons in higher dimensions [127–129]. More recently, spontaneous formation of *gray solitons* in quasi-one-dimensional condensates was predicted as a result of the Kibble-Zurek mechanism [130, 131] and rapid evaporative cooling [132].

Dark solitons

In three-dimensional geometry dark solitons ($a_{sc} > 0$) are inherently unstable against the decay into vortex rings (snake instability), both in self-defocusing media (optical dark solitons) [133, 134] and in Bose-Einstein condensates (matter wave dark solitons) [135]. In order to suppress the decay the system has to be effectively one-dimensional (cigar condensate). Then the one-dimensional Gross-Pitaevskii equation, without the trapping potential, admits the nontrivial analytical solution [136]

$$\Psi(z,t) = \sqrt{n_0}\left[\imath\frac{v}{c} + \sqrt{1-\frac{v^2}{c^2}}\tanh\left(\frac{z-vt}{\xi}\sqrt{1-\frac{v^2}{c^2}}\right)\right], \tag{II.31}$$

where n_0 is the BEC density far away from the density notch, $\mu = n_0 g_{\text{1D}}$ is the chemical potential, $c = \sqrt{n_0 g_{\text{1D}}/m}$ is the sound velocity, and $\xi = \hbar/\sqrt{m\mu}$ is the healing length. Solution (II.31) describes a density distribution $n(z - vt)$ that has a minimum in the center of the soliton corresponding to $n(0) = n_0 v^2/c^2$. For a soliton at rest this value is equal to zero and hence the name black soliton. For a soliton propagating with velocity $0 < v < c$ the density in the center is finite and thus such solitons are called gray. When $v \to c$, the soliton disappears, as its width becomes infinitely large. The phase of the wave function ϕ, defined through $\Psi(z,t) = \sqrt{n(z,t)}\exp(\imath\varphi(z,t))$, changes along the soliton according to the formula

$$\Delta\varphi = \varphi(\infty,t) - \varphi(-\infty,t) = 2\arctan\left(\frac{v}{\sqrt{c^2 - v^2}}\right) - \pi, \tag{II.32}$$

hence the probability current flows in the direction opposite to the propagation of the soliton, i.e., the atoms seep through the density notch [48]. For a black soliton the phase change is given by $\Delta\varphi = \pi$ and it was this finite phase difference that gave rise to the idea of creating a dark soliton in an experiment with phase imprinting technique [125, 126]. It is finally worth noticing that the velocity of the soliton increases when its energy decreases. This implies that dissipative effects will result in an acceleration of the soliton until it will eventually disappear [10].

Bright solitons

As already noted, in a condensate with a (constant) negative scattering length, i.e., with attractive interactions, the bright solitons can exist only if the system is effectively one-dimensional. Then, the analytical solution of the one-dimensional GPE, without the trapping potential, reads [112, 137]

$$\Psi(z,t) = \frac{l_\perp}{\lambda\sqrt{2|a_{sc}|}}\operatorname{sech}\left(\frac{z - vt}{\lambda}\right)\exp\left[\imath\frac{mv}{\hbar}z - \frac{\imath}{\hbar}\left(\frac{mv^2}{2} - \frac{\hbar^2\lambda^2}{2m}\right)t\right], \tag{II.33}$$

where the soliton width $\lambda = l_\perp^2/a_{sc}N$ and v is the soliton velocity. Notably, κ is inversely proportional to N and thus, even though the tight radial confinement stabilizes the condensate, for a large number of atoms the width of the soliton will tend to zero, rendering the soliton prone to the collapse to a point.

Yet another intriguing type of stationary solutions of the nonlinear Schrödinger equation are bright multisoliton states (*soliton train*) [112, 124]. Interestingly, such soliton trains have been observed in experiments of Strecker *et al.* [73] (see Fig. II.4), and it has been found that, despite the attractive inter-atomic interactions, the solitons in the train repel each other with a force that depends on their separation. It was proposed that, similarly to the mechanisms in optical fibers [138, 139], the trains originate in the modulational instability of the condensate that is seeded by quantum mechanical phase fluctuations, and that the source of the repulsive force is a phase difference of π between two neighboring solitons [140, 141]. Recently, however, it has been suggested that quantum fluctuations cause the fragmentation of a soliton train [142, 143] and may already be more important in experiments than previously thought. The dipolar counterpart of soliton trains will be of

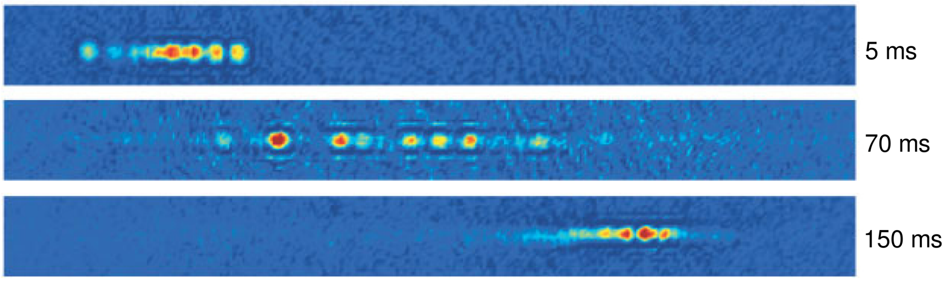

Figure II.4: Oscillations of a soliton train in a harmonic potential, observed in the experiment of Strecker *et al.* [73]. The three images show a soliton train near the two turning points and near the centre of oscillation. Noninteracting solitons, simultaneously released from different points in a harmonic potential, would be expected to pass through one another. However, the figures show that the spacing between solitons is compressed at the turning points, and spread out at the centre of the oscillation. This is evidence of a short-range repulsive force between the solitons. Reprinted from Nature **417**, 150 (2002).

the major focus in chapter V.

Currently available experimental methods [144] together with various theoretically sophisticated schemes [145–147] make bright solitons especially interesting branch of research in the field of nonlinear matter-wave optics [148–150], and in particular in the context of atom lasers [151–158] and interferometry [159–162]. Furthermore, quantum effects in bright solitons have been studied in the context of mesoscopic quantum superposition states (Schrödinger cats) [163, 164] and entanglement [165–167].

In section III.F we will inquire into the field of solitons in dipolar gases with long-range and anisotropic interactions. We will learn there how these features alter the soliton physics and introduce new effects absent for the case that we have discussed in this section.

II.C.8 Elementary excitations

The matter-wave solitons can be viewed as macroscopic nonlinear excitations of a condensate. In this section we will consider small amplitude excitations (*elementary excitations*), where the changes in space and time of the condensate wave function with respect to the stationary configuration are small. In other words, where only a small fraction of particles is excited out of the condensate. In many cases these solutions provide a deep insight into the collective behavior of an interacting Bose gas [10, 11, 168–170].

Employing the idea of the mean-field description presented in Sec. II.C.2, we now want to investigate phenomena arising in a Bose gas due to the presence of the quantum (noncondensed) correction $\hat{\Psi}'(\mathbf{r})$ in the field operator decomposition $\hat{\Psi}(\mathbf{r}) = \Psi(\mathbf{r}) + \hat{\Psi}'(\mathbf{r})$. To this end, we consider the grand canonical Hamiltonian $\mathscr{K} = \mathscr{H} - \mu\hat{N}$, where $\mathscr{H}$ is the many-body Hamiltonian defined in Eq. II.15, and $\hat{N} = \int d^3\mathbf{r}\,\hat{\Psi}^\dagger(\mathbf{r})\hat{\Psi}(\mathbf{r})$ is the particle number operator. Substituting the field-operator $\hat{\Psi}(\mathbf{r})$ into the Hamiltonian $\mathscr{K}$ we find that the terms which are linear in $\hat{\Psi}'(\mathbf{r})$ and $\hat{\Psi}'^\dagger(\mathbf{r})$ vanish due to the stationary Gross-Pitaevskii equation (II.20), and thus, following the fundamental mean-field restriction $N - N_0 \ll N_0$, and hence omitting cubic and fourth-order terms in $\hat{\Psi}'(\mathbf{r})$ and $\hat{\Psi}'^\dagger(\mathbf{r})$, we arrive at $\mathscr{K} = h_0 + \mathscr{H}_B$, where h_0 is the c-number part and the Bogoliubov Hamiltonian $\mathscr{H}_B$ reads

$$\begin{aligned}\mathscr{H}_B = &\int d^3\mathbf{r}\,\hat{\Psi}'^\dagger(\mathbf{r})\left[-\frac{\hbar^2\nabla^2}{2m} + U(\mathbf{r}) + 2g\,|\Psi(\mathbf{r})|^2 - \mu\right]\hat{\Psi}'(\mathbf{r})\\ &+\frac{g}{2}\int d^3\mathbf{r}\left(\Psi^2(\mathbf{r})\hat{\Psi}'^\dagger(\mathbf{r})\hat{\Psi}'^\dagger(\mathbf{r}) + \Psi^{*2}(\mathbf{r})\hat{\Psi}'(\mathbf{r})\hat{\Psi}'(\mathbf{r})\right).\end{aligned} \tag{II.34}$$

Substituting Hamiltonian $\mathscr{H}_B$ into the Heisenberg equation of motion for the noncondensed field $\hat{\Psi}'(\mathbf{r})$, $\imath\hbar\partial_t\hat{\Psi}'(\mathbf{r},t) = [\hat{\Psi}'(\mathbf{r},t), \mathscr{K}]$, we find

$$\imath\hbar\partial_t\hat{\Phi}(\mathbf{r}) = \left(-\frac{\hbar^2\nabla^2}{2m} + U(\mathbf{r}) + 2g\,|\Psi(\mathbf{r})|^2 - \mu\right)\hat{\Phi}(\mathbf{r}) + g\Psi^2(\mathbf{r})\hat{\Phi}^\dagger(\mathbf{r}), \tag{II.35}$$

where we have introduced $\hat{\Phi}(\mathbf{r}) = \hat{\Psi}'(\mathbf{r})e^{-\imath\mu t/\hbar}$. We now employ the generalized Bogoliubov transformation [171] to write $\hat{\Phi}(\mathbf{r})$ as

$$\hat{\Phi}(\mathbf{r}) = \sum_\nu u_\nu(\mathbf{r})\hat{b}_\nu e^{-\imath\epsilon_\nu t/\hbar} - v_\nu^*(\mathbf{r})\hat{b}_\nu^\dagger e^{\imath\epsilon_\nu t/\hbar}, \tag{II.36}$$

where index ν labels quantum states of elementary excitations, $\hat{b}_\nu$ and $\hat{b}_\nu^\dagger$ are the annihilation and creation operators of the elementary excitations (*quasiparticles*), respectively, ϵ_ν are their energies, and u_ν (*particles*) and v_ν (*holes*) are their eigenfunctions. Furthermore, the operators $\hat{b}_\nu$ and $\hat{b}_\nu^\dagger$ obey the canonical commutation relations, $[\hat{b}_\nu, \hat{b}_\mu^\dagger] = \delta_{\nu,\mu}$ and $[\hat{b}_\nu, \hat{b}_\mu] = [\hat{b}_\nu^\dagger, \hat{b}_\mu^\dagger] = 0$. Calculating the commutators of $\hat{b}_\nu$ and $\hat{b}_\nu^\dagger$ with both sides of Eq. (II.35) we arrive [172] at the set of coupled equations

$$\left\{\begin{aligned} \epsilon_\nu u_\nu(\mathbf{r}) &= \left(-\frac{\hbar^2\nabla^2}{2m} + U(\mathbf{r}) + 2g\,|\Psi(\mathbf{r})|^2 - \mu\right)u_\nu(\mathbf{r}) - g\Psi^2(\mathbf{r})v_\nu(\mathbf{r}), && \text{(II.37)}\\ -\epsilon_\nu v_\nu(\mathbf{r}) &= \left(-\frac{\hbar^2\nabla^2}{2m} + U(\mathbf{r}) + 2g\,|\Psi(\mathbf{r})|^2 - \mu\right)v_\nu(\mathbf{r}) - g\Psi^{*2}(\mathbf{r})u_\nu(\mathbf{r}), && \text{(II.38)}\end{aligned}\right.$$

that reduce the bilinear Bogoliubov Hamiltonian $\mathscr{H}_B$ to the diagonal form

$$\mathscr{H}_B = \sum_\nu \epsilon_\nu \hat{b}_\nu^\dagger \hat{b}_\nu. \tag{II.39}$$

Eqs. (II.37) and (II.38) are typically called Bogoliubov-de Gennes (BdG) equations [78, 173].

Further progress depends on the properties of the normal modes $u_\nu(\mathbf{r})$ and $v_\nu(\mathbf{r})$. In particular, we can derive the orthogonality conditions [171]

$$\left(\epsilon_\nu - \epsilon_\mu^*\right) \int d^3\mathbf{r} \left[u_\nu(\mathbf{r}) u_\mu^*(\mathbf{r}) - v_\nu(\mathbf{r}) v_\mu^*(\mathbf{r})\right] = 0. \tag{II.40}$$

If the system has a complex eigenvalue, the assumed ground state $\Psi(\mathbf{r})$ is not stable and the system exhibits a dynamical instability, with the zero norm of the corresponding elementary excitation. For real energies ϵ_ν, the amplitudes are normalized so that they satisfy the conditions

$$\int d^3\mathbf{r} \left[u_\nu(\mathbf{r}) u_\mu^*(\mathbf{r}) - v_\nu(\mathbf{r}) v_\mu^*(\mathbf{r})\right] = \delta_{\nu,\mu} \tag{II.41}$$

and, if $\epsilon_\nu + \epsilon_\mu \neq 0$, the orthogonality condition reads

$$\int d^3\mathbf{r} \left[u_\nu(\mathbf{r}) v_\mu(\mathbf{r}) - u_\nu(\mathbf{r}) v_\mu(\mathbf{r})\right] = 0. \tag{II.42}$$

Moreover, it can be seen from the Bogoliubov-de Gennes equations allow a simple symmetry operation [171, 174]. Namely, if (u_ν, v_ν) is a solution with eigenvalue ϵ_ν and positive normalization, i.e., $\int d^3r\, |u_\nu(\mathbf{r})| - |v_\nu(\mathbf{r})| = 1$, then there is always another solution (v_ν^*, u_ν^*) with eigenvalue $-\epsilon_\nu$ and negative normalization, $\int d^3r\, |u_\nu(\mathbf{r})| - |v_\nu(\mathbf{r})| = -1$. For uniform condensates with plane wave solutions, the positive normalization always leads to positive eigenvalues. However, nonuniform condensates such as one with a vortex or a dark soliton can have physical states with positive normalization and negative eigenvalues [175]. If a positive norm solution has a negative eigenvalue, the system exhibits Landau instability because it can lower the energy by exciting quasiparticles with negative eigenvalues [11].

Typically, the BdG equations (II.37)-(II.38) call for numerical methods in order to obtain solutions for the eigenfrequencies and the normal modes of the system. However, an insightful analytical solution is provided by the collective oscillations around the ground state of a uniform gas. In this case the excitations eigenfunctions are simply the plane waves $u_\nu(\mathbf{r}) = u_\mathbf{k} e^{\imath \mathbf{k}\mathbf{r}}/\sqrt{V}$ and $v_\nu(\mathbf{r}) = v_\mathbf{k} e^{\imath \mathbf{k}\mathbf{r}}/\sqrt{V}$, with V the volume of the system, whereas the ground state $\Psi(\mathbf{r})$ can be chosen to be real, $\Psi(\mathbf{r}) = \sqrt{n}$, and $\mu = gn$. In turn, the BdG equations yield the famous Bogoliubov spectrum of the elementary excitations in a homogeneous Bose gas

$$\epsilon_k = \sqrt{E_k^2 + 2ngE_k}, \tag{II.43}$$

with the kinetic energy $E_k = \hbar^2 k^2/2m$. The spectrum (II.43) is plotted in Fig. II.5. For small momenta, $k \ll \xi^{-1}$, which correspond to energies $\epsilon_k \ll \mu$, the excitations acquire collective phonon character and the dispersion rela-

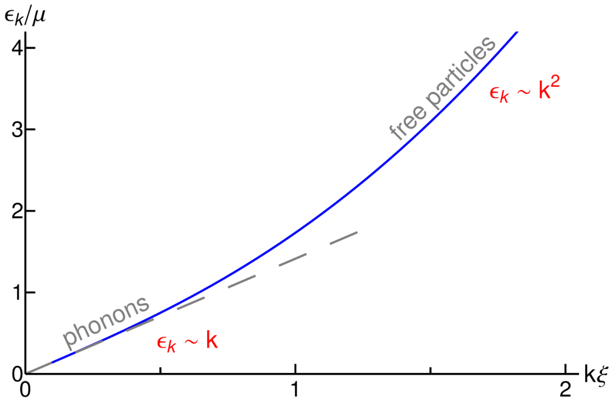

Figure II.5: Elementary excitations spectrum (II.43) for a uniform degenerate Bose gas with contact interactions, in units of the chemical potential $\mu = ng$, as a function of the momentum k, in units of the healing length $\xi = \hbar/\sqrt{2m\mu}$. For momenta smaller than the length scale set by the healing length, i.e., $k\xi \ll 1$, the excitations acquire collective phonon-like form $\epsilon_k \sim k$ (straight dashed line). When the excitation energy exceeds significantly the interactions per particle, i.e., $\epsilon_k \gg \mu$, the excitations behave like free particles $\epsilon_k \sim k^2$. Compare with the roton-maxon spectrum in a dipolar condensate, e.g., in Fig. III.7.

tion can be written as $\epsilon_k = c_s \hbar k$, where $c_s = \sqrt{ng/m}$ is the sound velocity. Interestingly, the Bogoliubov phonon quasiparticles have been observed experimentally [176, 177]. For $k \gg \xi^{-1}$, i.e., $\epsilon_k \gg \mu$, the excitations loose the collective character and behave like free particles, since their energy greatly exceeds the interactions per particle ng. In this case, Eq. (II.43) reduces to $\epsilon_k = \hbar^2 k^2/2m + ng$, with the ng term indicating interactions between high-energy particles and the condensate [172].

In section II.C.5 we saw that a three-dimensional uniform Bose gas with attractive interactions is unstable against a collapse to a point. The attractive interactions, $g < 0$, mean in terms of the elementary excitations (II.43) that the speed of sound c_s becomes imaginary and so do the energies of the phonon excitations. It is then clear from the Bogoliubov transformation (II.36) that the amplitudes of the phonon eigenfunctions, and hence the condensate wave function, will grow exponentially. This phenomenon, which is an example of dynamical instability, is called phonon instability.

In section III.E we will learn how the elementary excitations spectrum changes in the presence of dipole-dipole interactions and how these modifications give rise to a wealth of new physical phenomena, which we will be exploring throughout this thesis.

◆

III

Dipolar Bose-Einstein condensates

In chapter II we have seen how essential are the interparticle interactions for the properties of an ultracold gas. In particular, we concentrated hitherto on the short-range (contact) interactions. In the remainder of this thesis we will address novel physical phenomena arising in an ultracold gas due to the presence of long-range interactions. In general, the broad class of systems typified by such interactions, the so-called polar gases, consists of polar molecules [178–190], Rydberg gases [191–200] and dipolar gases of atoms with large magnetic moment. In this thesis we will inquire into the last branch, and specifically into dipolar Bose-Einstein condensates.

While the long-range interactions had been known for some time in other systems, e.g., in classical ferrofluids [201, 202] and liquid crystals [203], it was the theoretical proposal of K. Góral, K. Rzążewski and T. Pfau [204] together with experimental progress on trapping atoms with higher magnetic moments [205, 206] that boosted the interest in the field of ultracold atomic gases with dominant dipole-dipole interactions. Several seminal theoretical works had been published [207–211], regarding the mean-field description, possible ground state solutions, elementary excitations and stability properties of a dipolar condensate, until finally the experimental milestone has been set by the condensation of chromium atoms (^{52}Cr, dipole moment μ of 6 times the Bohr magneton μ_B) in T. Pfau's group [212]. Soon, another experiments followed, demonstrating directly the anisotropic and long-range character of dipolar interactions through studies of expansion [213, 214], stability properties [215] and unprecedented d-wave collapse dynamics [216] in a chromium BEC.

Yet, the interest in the field has been still increasing on both experimental and theoretical side. The major contributions on the former one are the very recently successfully condensed gases of dysprosium (^{164}Dy, $\mu = 10\mu_B$) in B. Lev's group [217] (followed with the first realization of quantum degenerate dipolar Fermi gas of ^{161}Dy [218]) and erbium (^{168}Er, $\mu = 7\mu_B$) in the group of F. Ferlaino [219]. The experimental group of B. Laburthe-Tolra has lent a number of influential results [220–224]. On the theory side various proposals have appeared for dipolar condensates, regarding, among others, phenomena in rotating traps [225–227], dipolar effects in spinor condensates [228–235] and in superfluidity [236, 237], dipole induced modifications of the Bogolibov modes [238–241] and ground state structures [242–246], manifestation of the dipolar interactions in the condensate stabilization and collapse [247–251], collective intersite physics in deep optical lattices [252–254], dipolar originating pattern formation [255–257], and atom optics, with particular emphasis on dipolar solitons [258–261]. Some of the these predictions have been investigated jointly with experimentalists who directly confirmed them. A broader summary of hitherto studied subjects in the field of degenerate dipolar Bose gases, together with further references and comprehensive coverage of equally interesting and extensive domain of ultracold dipolar Fermi gases, can be found in Refs. [262–264].

We continue this chapter presenting the basic physical principles of dipolar Bose-Einstein condensates.

III.A

Dipole-dipole interaction in a polar gas

In general, two dipoles with the same dipole moment (electric d or magnetic μ) oriented along $\hat{\mathbf{r}}_1$ and $\hat{\mathbf{r}}_2$, respectively, and joined by vector $\mathbf{r}$, interact via

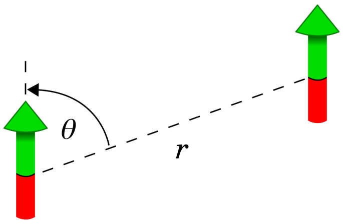

Figure III.1: Two dipoles polarized by an external field interacting through the dipolar potential (III.2). Clearly, for $\theta = 0$ the two particles attract each other, while for $\theta = \pi/2$ they repel (see text).

the dipole-dipole potential

$$V_d(\mathbf{r}) = g_d \frac{\hat{\mathbf{r}}_1\hat{\mathbf{r}}_2 - 3(\hat{\mathbf{r}}_1\hat{\mathbf{r}})(\hat{\mathbf{r}}_2\hat{\mathbf{r}})}{r^3}, \tag{III.1}$$

with $g_d = d^2/4\pi\varepsilon_0$ for electric dipoles (ε_0 is the vacuum permittivity), or $g_d = \mu_0\mu^2/4\pi$ for magnetic dipoles (μ_0 is the vacuum permeability). We note that for the theory of electromagnetism to be consistent an additional term $\propto\ \delta(\mathbf{r})$ appears on the left hand side of Eq. (III.1), which can be easily understood thinking in terms of the Laplace equation [265]. In the context of ultracold gases, exclusion of the delta term from the dipole-dipole potential (III.1) obviously does not affect the inherently long-range character of the dipolar physics. It can, however, bear upon short range phenomena, such as the dipole-dependent scattering length [247, 266], and thus should be on the whole included in the pseudopotential describing particles interacting via the dipolar forces [207, 208, 267]. We omit this term in Eq. (III.1) for the clarity.

If the dipoles are subjected to an external field that orients them along a particular direction, the dipole-dipole potential simplifies to

$$V_d(\mathbf{r}) = g_d \frac{1 - 3\cos^2\theta}{r^3}, \tag{III.2}$$

where θ is the angle between the direction of the dipole moments and the vector joining two particles (see Fig. III.1). Obviously, as it has been mentioned already, expression (III.2) is long-ranged (for more detailed discussion see Ref. [268]). Moreover, the presence of angle θ renders the potential anisotropic. Naturally, when dipoles are in the head-to-tail configuration ($\theta = 0$) they attract each other, for the so-called magic angle θ_m, such that $\cos\theta_m = 1/\sqrt{3}$, the interaction vanishes, and in the side-by-side configuration ($\theta = \pi/2$) the dipoles repel each other. Heteronuclear polar molecules can have permanent dipole moment along the internuclear axis with strength ranging between one tenth and ten Debye (1D = 1/2.54 au), for atomic species the dipole moment ranges between one and ten Bohr magneton ($1\mu_B = 1/274$ au). Similarly to the scattering length a_{sc} for the contact coupling strength g, Eq. (II.13), we can now introduce the characteristic length scale for the dipolar interactions $a_d = mg_d/\hbar^2$. And so, for alkali rubidium $a_d^{Rb} = 0.1\,\mathrm{nm}$, for chromium $a_d^{Cr} = 2.4\,\mathrm{nm}$, for erbium $a_d^{Er} = 10.6\,\mathrm{nm}$, and for dysprosium $a_d^{Dy} = 21.0\,\mathrm{nm}$. For most polar molecules a_d reaches up to 3500 nm [263, 264]. Obviously, the larger the ratio a_d/a_{sc} the more pronounced are the dipolar effects in a system.

We have seen in section II.C.1 that the short-range interactions can be modified by means of the Feshbach resonances. Interestingly, it is also possible to manipulate the dipolar interactions (DDI). Namely, in the case of polar molecules it is possible to tailor the strength and the shape of the interaction potentials by means of, e.g., an additional microwave field [269, 270]. Dipolar atomic gases offer the possibility of engineering the strength and the sign of DDI as well [271]. In this case, the idea is based on combination of static magnetic field along the z-axis, $\mathbf{B}_z$, and a field in the perpendicular xy-plane, $\mathbf{B}_{xy}(t)$, that rotates with frequency Ω, (see Fig. III.2), such that $\mathbf{B}_z = B\cos\varphi\hat{\mathbf{z}}$, $\mathbf{B}_{xy}(t) = B\sin\varphi\big(\cos(\Omega t)\hat{\mathbf{x}} + \sin(\Omega t)\hat{\mathbf{y}}\big)$, and the total field $\mathbf{B}(t) = \mathbf{B}_z + \mathbf{B}_{xy}(t)$. In turn, over the period $T = 2\pi/\Omega$ the particles feel the time averaged potential

$$\langle V_d(\mathbf{r})\rangle_T = \frac{3\cos^2\varphi - 1}{2} V_d(\mathbf{r}), \tag{III.3}$$

with $V_d(\mathbf{r})$ as the original dipole-dipole introduced in Eq. (III.2). Clearly, the φ-dependent term in Eq. (III.3) can be changed continuously from 1 to $-1/2$. Hence, a variation of φ allows manipulation of the DDI, including the reversal of the sign of the potential or even its complete cancellation for $\varphi = \theta_m$. An analogous technique can be applied also to the electric dipole moments [264]. We will see in chapters IV and V how the tunability of the dipolar interactions

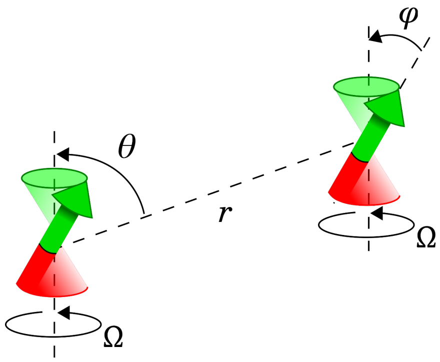

Figure III.2: Tuning of the dipolar interactions by means of a transverse magnetic field rotating with frequency Ω. The time-averaged dipole-dipole potential acquires the form of Eq. (III.3), allowing not only to tune the strength of the interaction but even to reverse its sign, depending on the value of the parameter φ.

gives rise to some unprecedented phenomena.

In the remainder of the thesis we will frequently use the Fourier representation $\hat{V}_d(\mathbf{k})$ of the dipole-dipole potential (III.2) for its analytical and numerical convenience. Derivation of $\hat{V}_d(\mathbf{k})$ is based on the expansion of a plane wave in the basis of spherical harmonics and is rather straightforward. The final result reads [204]

$$\hat{V}_d(\mathbf{k}) = \frac{4\pi}{3} g_d \left(3\cos^2\theta_k - 1\right), \tag{III.4}$$

with θ_k as the angle between the wave vector $\mathbf{k}$ and the direction of a dipole moment.

As we have discussed in section II.C.2, the mean-field description of a purely contact interacting Bose-Einstein condensate has been proven both theoretically and experimentally to work exceptionally well [6, 10]. The inclusion of the dipolar interactions in this formalism is attributed to pioneering works by You and Yi [207, 208] who constructed a pseudo-potential for a general case of anisotropic potentials. This result yields directly the nonlocal version of the Gross-Pitaevskii equation (II.17),

$$\begin{aligned} \imath\hbar\partial_t\Psi(\mathbf{r},t) = \Bigg[& -\frac{\hbar^2\nabla^2}{2m} + U(\mathbf{r}) + g|\Psi(\mathbf{r},t)|^2 \\ & + \int d^3\mathbf{r}' \, |\Psi(\mathbf{r}',t)|^2 V_d(\mathbf{r}-\mathbf{r}') \Bigg] \Psi(\mathbf{r},t), \end{aligned} \tag{III.5}$$

which describes a dipolar Bose-Einstein condensate and becomes now an involved integrodifferential equation. The validity of Eq. (III.5) has been additionally evaluated with many-body diffusion Monte-Carlo studies [247, 266, 272] and the results verified the applicability of the nonlocal GPE, provided that the gas is dilute, $na_{sc}^3 \ll 1$. In Eq. (III.5) we have ignored the contact part of the dipole-dipole pseudo-potential that contributes to the regularization of the short-range coupling parameter g. This is, however, legitimate as the main contribution to the mean-field dipolar interactions integral in Eq. (III.5) comes from large interparticle distances of the order of a spatial size of the condensate [262].

Dimensional reduction of the nonlocal Gross-Pitaevskii equation (III.5) is in general more elaborate than the same procedure in the nondipolar case discussed in section II.C.6, with details of calculations relying strongly on particular geometry that is considered. For the details of the nonlocal GPE describing a quasi-one-dimensional dipolar gas, which we will be employing in chapters IV, V and VI, reader is referred to appendix A.

III.B

Geometrical stabilization

In section II.C.5 we have found that the instability of a condensate with attractive contact interactions, i.e., $a_{sc} < 0$, can be suppressed in a trap, provided that the atoms number N is sufficiently small, $N < N_c = -0.575 l_{ho}/a_{sc}$. The stability of dipolar condensates in a trapping potential has been widely investigated. In particular, for studies of the critical number of atoms and the critical trap aspect ratio in a BEC with the interparticle interactions dominated by the dipole-dipole forces ($a_{sc} = 0$) the reader is referred to Refs. [209, 239, 242] and the review [262]. Here, we would like to focus on the influence of the trapping geometry on the BEC stability properties when both contact and dipolar interactions are present. In particular, the above recalled critical number of particles N_c for a condensate with solely contact interactions has been found to depend very weakly on the trap aspect ratio [89]. The anisotropy of the DDI renders the situation radically different for a dipolar BEC.

This can be intuitively understood considering a cylindrically symmetric trap with the symmetry axis z coinciding with the orientation of the dipoles. The axial and radial frequencies are denoted as ω_z and ω_ρ, respectively. It is then automatically clear that for a prolate trap (aspect ratio $\lambda = \omega_z/\omega_\rho < 1$), the DDI is essentially attractive and in such a trap a dipolar BEC will become unstable unless a large repulsive contact interactions will suppress the collapse. Then again, for an oblate trap ($\lambda > 1$), the DDI is essentially

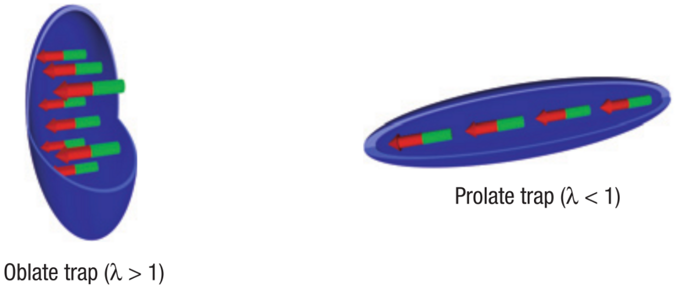

Figure III.3: Intuitive picture of the trap geometry dependence of the stability of a trapped dipolar BEC. For large trap aspect ratios λ (pancake-shape) the dipolar interactions are predominantly repulsive, stabilizing the condensate against a collapse. For small values of λ the dipole-dipole interactions are essentially attractive, rendering the BEC more prone to the collapse. Reprinted from Nat. Phys. **4**, 218 (2008)

repulsive and unless the contact interactions are strongly attractive, the BEC will remain stable. One can therefore expect that for a given trap aspect ratio λ, there exists a critical value of scattering length, below which the condensate becomes unstable.

These considerations can be expressed quantitatively employing the Gaussian ansatz (for details see Ref. [273] and references therein),

$$\Psi(\rho,z)=\sqrt{\frac{N}{\pi^{3/2}\sigma_\rho^2\sigma_z l_{ho}^3}}\exp\left[-\frac{1}{2l_{ho}^2}\left(\frac{\rho^2}{\sigma_\rho^2}+\frac{z^2}{\sigma_z^2}\right)\right], \tag{III.6}$$

with the harmonic oscillator length $l_{ho}=\sqrt{\hbar/m\bar{\omega}}$ and the average trap frequency $\bar{\omega}=(\omega_\rho^2\omega_z)^{1/3}$. Inserting Eq. (III.6) into the energy functional corresponding to the nonlocal GPE (III.5), one arrives at the expression for the

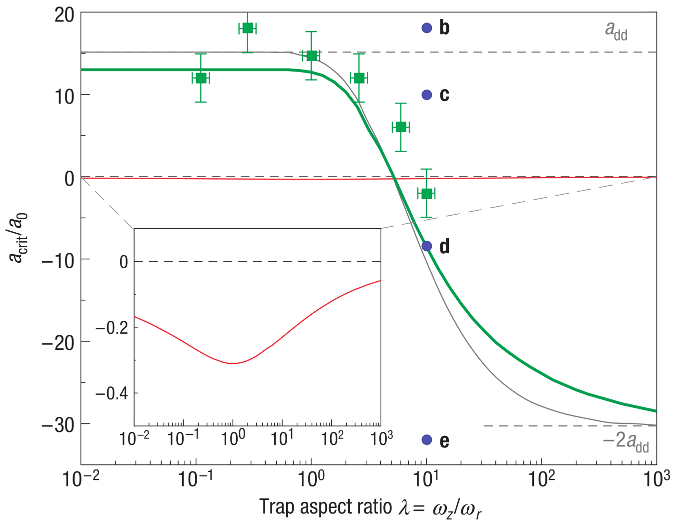

Figure III.4: Stability diagram of a dipolar BEC in the a_{sc}-λ plane. The figure shows experimental (green squares) and theoretical (green line) values of the critical scattering length $a_{\rm crit}$ as a function of the trap aspect ratio. The red curve (magnified in the inset) marks the stability threshold for a BEC with pure contact interactions using the same parameters. The asymptotic stability boundary ($Na_d/l_{ho}\gg 1$) is plotted in grey. For sufficiently large scattering lengths, (b), a global minimum of the energy $E(\sigma_\rho,\sigma_z)$ exists and the BEC is always stable. In the intermediate range, (c), for nonzero σ_ρ only a local minimum occurs and a (meta)stable state is supported against the collapse. For a critical value $a_{\rm crit}$, (d), the minimum disappears and the BEC becomes unstable. For certain value of the scattering length, (e), the condensate is always unstable as the dipolar interactions cannot suppress the collapse even for a large value of the trap aspect ratio λ. Reprinted from Nat. Phys. **4**, 218 (2008)

condensate energy $E(\sigma_\rho,\sigma_z)$, which depends on the widths of the condensate [215]. Then, to determine the scattering length stability threshold a_{crit}, one needs to minimize $E(\sigma_\rho,\sigma_z)$ with respect to σ_ρ and σ_z, keeping the parameters N, λ and $\bar{\omega}$ fixed (we will use an analogous method in chapter IV, see also appendix B). The theoretical and experimental results are summarized in Fig. III.4 showing the stability diagram. For sufficiently large scattering lengths, $a_{sc} \gg a_d$, Ref. [215] finds that $E(\sigma_\rho,\sigma_z)$ supports a global minimum for finite σ_ρ and σ_z independently of λ, and thus the BEC is stable. Going below $a_{sc} \sim a_d$, the absolute ground state is a collapsed infinitely thin cigar-shaped BEC ($\sigma_\rho \to 0$) and possible existence of a further local minimum (corresponding to a metastable state; compare with Fig. II.3) is determined by the trap aspect ratio. In particular, for a purely dipolar gas the criterion $\lambda > \lambda_c \approx 5.2$ for the stability has been found. Finally, below $a_{sc} \sim -6a_d$ (this corresponds to $a_{sc} \sim -2a_d$ in the notation of Ref. [215]), the local minimum vanishes for any λ and the condensate is always unstable.

We note at this point that the shape of a BEC cloud together with stability properties can be found analytically in the Thomas-Fermi limit that is reached when the kinetic energy is small in comparison to both the potential energy due to the trap and the interaction energy between atoms, and the term with derivatives in Eq. (III.5) can be neglected (see Sec. II.C.4). Then, surprisingly, it has been found that the ground state solution of a dipolar BEC in the cylindrically symmetric case has exactly the same form of an inverted parabola as in the case of pure contact-interactions, i.e., $n(\mathbf{r}) = n_0\left(1-\rho^2/\sigma_\rho^2 - z^2/\sigma_z^2\right)$, with the only difference in the explicit form of the radii [274, 275].

III.C

Collapse dynamics

In Sec. II.C.5 we have stated that an unstable nondipolar condensate collapses to a point. In reality, the dynamics of a collapsing BEC is far more complex, including the implosion of the cloud followed by inelastic losses and the explosion of the remnant condensate together with energetic jets [74, 82–86]. In the context of our developments that will be presented in chapter VII, it is instructive to analyze the so-called d-wave collapse of a dipolar condensate, which was reported in Ref. [216].

The experimental sequence was as follows. First, for a given number of particles and trap aspect ratio, and an external magnetic field B oriented along z direction, a stable chromium BEC was created with the scattering length larger than the critical scattering length, a_{crit}, that we commented on in the previous section. Next, with the Feshbach resonance technique, the scattering length was ramped down rapidly below the a_{crit}. After the ramp the cloud evolved for an adjustable time t_{hold} and then the trap was switched off. Subsequently, after the time of flight, the condensate was imaged by absorption of a resonant laser beam propagating along x direction. The results are presented in Fig. III.5.

Initially, due to the ramp into the regime of strong attractive contact interactions, the density of atoms in the center of the trap grows significantly. However, a strong rise of density in the collapsing condensate enhances intrinsic inelastic processes, with the most crucial recombination through the 3-body interatomic collisions. This process occurs at interparticle distances of the order of the characteristic radius of interaction between atoms and has a local character [82], which allows the description $\dot{n}(\mathbf{r},t) = -L_3 n^3(\mathbf{r},t)$, where L_3 is the recombination rate constant. It is important that the recombination simply leads to the loss of atoms (we stress that the recombination in the course of the collapse does not burn the condensate completely, i.e., the number of atoms in a BEC always remains finite) and does not break the coherence between the particles remaining in the condensate. Hence, the three-body recombination can be explicitly included in the nonlocal GPE, which now will read

$$\begin{aligned} \imath\hbar\partial_t\Psi(\mathbf{r},t) = \Bigg[& -\frac{\hbar^2\nabla^2}{2m} + U(\mathbf{r}) + g|\Psi(\mathbf{r},t)|^2 \\ & + \int d^3\mathbf{r}'\,|\Psi(\mathbf{r}',t)|^2 V_d(\mathbf{r}-\mathbf{r}') - \frac{\imath\hbar L_3}{2}|\Psi(\mathbf{r},t)|^4\Bigg]\Psi(\mathbf{r},t). \end{aligned} \tag{III.7}$$

Kagan *et al.* show in Ref. [82] that the accumulation of particles in the center is however limited and that the compression (implosion) of the condensate reaches a maximum and turns into expansion (explosion) when the density of the collapsing condensate becomes so high that the recombination losses dominate over attractive interparticle interaction. This argumentation has been confirmed with the experimental results in the case of purely contact interacting gas [74], and is also applicable in the case of a dipolar gas. In the former case the explosion is isotropic [86] which is intuitive, given the s-wave character of the contact interactions. Strikingly, Lahaye *et al.* found experimentally in Ref. [216] that for a dipolar condensate the explosion recovers the d-wave symmetry (cloverleaf pattern) of the dipolar potential $V_d(\mathbf{r}) \sim Y_2^0(\theta,\phi)/r^3$, with $Y_2^0(\theta,\phi)$ as the spherical harmonic function. In Fig. III.5, the collapse occurs mainly in the $x-y$ plane due to the anisotropy of the DDI (in the absence of the inelastic losses the condensate would indeed become an infinitely thin cigar-shaped cloud along z direction), and therefore the BEC explodes essentially radially, producing the anisotropic shape of the cloud.

We stress that the physical origin of this collapse is the phonon instability, related with small momenta, analogous to the one discussed in Sec. II.C.8 for nondipolar gases, and should not be mistaken with other possible collapse

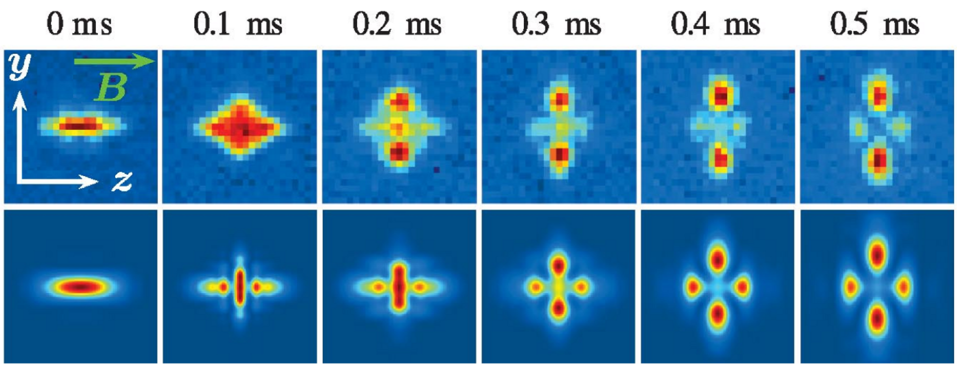

Figure III.5: Collapse dynamics of a dipolar condensate. The figure shows series of absorption images of the condensate for different values of t_{hold} (upper row) and the results of numerical simulations of the Eq. (III.7), with $L_3 = 2 \times 10^{-40} m^6/s$. Clearly, the d-wave angular symmetry of the dipolar interactions is recovered. Compare with the Fig. VII.3a and Fig. VII.3b. Reprinted from Phys. Rev. Lett. **101**, 080401 (2008)

mechanisms (see Sec. III.D). In particular, in chapter VII we will investigate the dynamics following the roton instability, related with dispersion minimum occurring at intermediate momenta (see Sec. III.E), and we will discuss what new physical consequences it bears.

We also note, that contrary to the three-dimensional case discussed in this section, in a two-dimensional geometry the phonon instability does not necessarily lead to a collapse of a dipolar condensate [248]. Furthermore, recently, stability properties have been examined and a novel type of deconfinement-induced collapse has been reported for an array of dipolar condensates formed by a one-dimensional optical lattice [250, 251].

III.D

Excitations

We have claimed in the previous section that the origin of the d-wave collapse of a dipolar gas is the phonon instability, which, as we have seen in Sec. II.C.8, occurs when the Bogoliubov excitations have imaginary frequencies at low momenta. Following the essential ideas of the stability analysis for a nondipolar gas, we now employ the Bogoliubov ansatz (II.36) for the wave function of a dipolar condensate,

$$\Psi(\mathbf{r},t) = \Psi(\mathbf{r}) + u(\mathbf{r})e^{-\imath\omega t} + v^*(\mathbf{r})e^{\imath\omega t} \qquad \text{(III.8)}$$

and linearizing the time dependent nonlocal Gross-Pitaevskii equation (III.5) around the stationary solution $\Psi(\mathbf{r})$, we arrive at corresponding Bogoliubov-de Gennes equations,

$$\begin{cases} u(\mathbf{r})\hbar\omega = \left[-\dfrac{\hbar^2\nabla^2}{2m} - \mu + U(\mathbf{r}) + 2\displaystyle\int d^3\mathbf{r}'\,V(\mathbf{r}-\mathbf{r}')\left|\Psi(\mathbf{r}')\right|^2\right]u(\mathbf{r}) \\ \qquad + \displaystyle\int d^3\mathbf{r}'\,V(\mathbf{r}-\mathbf{r}')\left|\Psi(\mathbf{r}')\right|^2 v(\mathbf{r}), & \text{(III.9)} \\ -v(\mathbf{r})\hbar\omega = \left[-\dfrac{\hbar^2\nabla^2}{2m} - \mu + U(\mathbf{r}) + 2\displaystyle\int d^3\mathbf{r}'\,V(\mathbf{r}-\mathbf{r}')\left|\Psi(\mathbf{r}')\right|^2\right]v(\mathbf{r}) \\ \qquad + \displaystyle\int d^3\mathbf{r}'\,V(\mathbf{r}-\mathbf{r}')\left|\Psi(\mathbf{r}')\right|^2 u(\mathbf{r}), & \text{(III.10)} \end{cases}$$

where we have combined the contact potential (II.12) together with the dipole-dipole potential (III.2) into $V(\mathbf{r}) = g\delta(\mathbf{r}) + V_d(\mathbf{r})$, for the sake of simplicity. It is easy to see that for a homogeneous dipolar BEC (compare with Eq. (II.43) for a nondipolar condensate) the solution of Eqs. (III.9)-(III.10) for the excitations spectrum reads

$$\begin{aligned} \epsilon_k &= \sqrt{E_k^2 + 2n\left(g + \hat{V}_d(\mathbf{k})\right)E_k} && \text{(III.11)} \\ &= \frac{\hbar k}{2m}\sqrt{\hbar^2k^2 + 4mng\left[1 + \varepsilon_{dd}\left(3\cos^2\theta_k - 1\right)\right]}, && \text{(III.12)} \end{aligned}$$

where $\varepsilon_{dd} = 4\pi g_d/3g = a_d/3a_{sc}$ measures the strength of the dipole-dipole interactions relative to the short-range interactions. It is then clear from Eq. (III.12) that a dipolar uniform condensate is unstable against phonon instability if $\varepsilon_{dd} > 1$, with the most unstable direction of the wavevector $\theta_k = \pi/2$. This is a direct consequence of the partially attractive nature of the DDI.

In general, due to the nonlocal character of the dipole-dipole interaction, the Bogoliubov-de Gennes equations (III.9)-(III.10) belong to the class of integrodifferential equations and are analytically, and numerically challenging. For a three-dimensional harmonic trap with cylindrical symmetry the solutions of the BdG equations were computed by Ronen *et al.* in Ref. [238]. Furthermore, for several low energy excitations modes it is possible to obtain analytic results by means of approximate methods such as Thomas-Fermi approximation [211, 274] or time-dependent Gaussian variational ansatz [207, 208, 210]

$$\Psi(x,y,z,t) = A(t)\prod_{\eta=x,y,z} e^{-\eta^2/2w_\eta^2(t) - \imath\eta^2\beta_\eta(t)}, \qquad \text{(III.13)}$$

with time-dependent variational Gaussian widths w_η and phases β_η, and normalization coefficient $A(t)$. Inserting Eq. (III.13) into the corresponding Lagrangian and applying the standard Euler-Lagrange procedure one can find the effective equations of motion for the variational parameters w_η and β_η. Most interestingly, Góral and Santos found in Ref. [210] that contrary

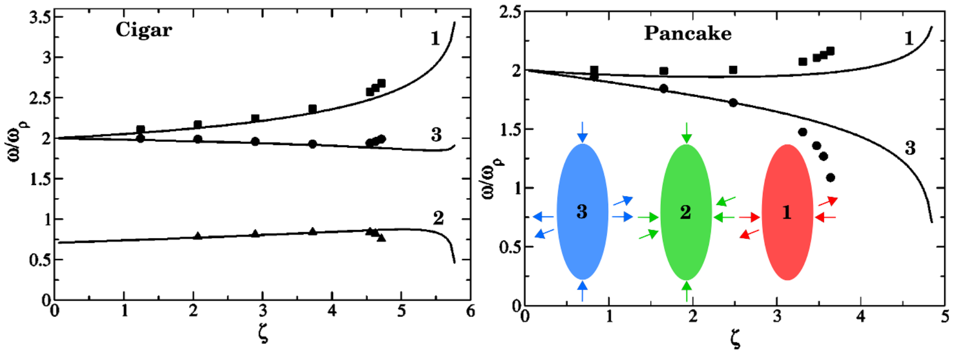

Figure III.6: Excitations frequencies of the oscillations modes in units of the radial frequency ω_ρ as a function of the dipolar parameter $\zeta \sim g_d$. In case of the cigar geometry (right panel) the lowest lying excited mode is the monopole breathing mode (2), which goes down, vanishing for a critical value of ζ_c at which the system becomes unstable. For pancake geometry, it is the quadrupole mode (3) which becomes the lowest one. The solid lines correspond to the variational results, based on the Eq. (III.13). The points (squares, circles, triangles) represent the data obtained through direct numerical simulation of the nonlocal GPE (III.5). The inset shows the graphical representation of the oscillations modes of a dipolar BEC. Reprinted from Phys. Rev. A **66**, 023613 (2002).

to the case of contact interactions the properties of the most unstable mode crucially depend on the geometry (trap aspect ratio). Namely, while for a purely contact interacting BEC it is always the monopole breathing mode (mode 2 in Fig. III.6) that becomes most unstable, for a dipolar BEC it is either the quadrupole mode (mode 3 in Fig. III.6) for $\lambda > 1$, or the monopole mode for $\lambda < 1$. These results are summarized in Fig. III.6.

III.E

Roton-Maxon spectrum

Since the appearance of the pioneering papers by Landau on the theory of superfluidity [276–278], the notion of the roton minimum in the collective modes dispersion of a system has played a pivotal role in explanation of the behavior of the superfluid phase of ^{4}He below the critical temperature $T_c = 2.17\,\mathrm{K}$. Crucially, the striking nonviscous flow and the frictionless motion of an impurity in the liquid break down above a critical flow velocity $v_{\max}$ [279]. In the Landau's theory, it is postulated that in order to explain this breakdown, the ϵ_k dispersion of the collective excitations must be non-monotonic, starting acoustically (phonon) $\epsilon_k = \hbar k c_s$, reaching a maximum (*maxon*), which is then followed by a minimum (*roton minimum*) around

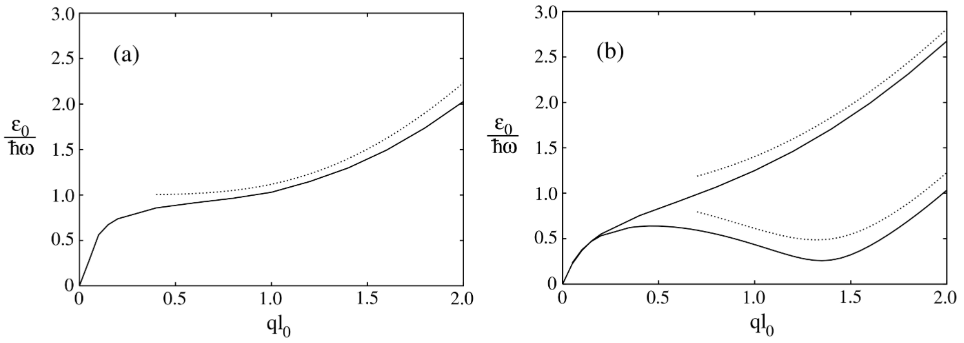

Figure III.7: Roton-Maxon excitations spectrum of a dipolar condensate. Dispersion law ϵ_q is calculated for (a) $\beta = 0.5$ and $\mu/\hbar\omega = 343$, and (b) $\beta = 0.53$ and $\mu/\hbar\omega = 46$ (upper curve), and $\beta = 0.47$ and $\mu/\hbar\omega = 54$ (lower curve). The solid lines depict the numerically solved BdG equations (III.9)-(III.10), the dotted lines show the results of Eq. (III.15). Reprinted from Phys. Rev. Lett. **90**, 250403 (2003).

$k = k_{\rm min}$, such that the line $\epsilon_k = \hbar k v_{\rm max}$ becomes tangent to the dispersion curve in the neighborhood of the minimum. Landau's original suggestion was that the development of the roton minimum had to be sought in the existence of a rotation-like collective excitation (vortical motion) of the fluid, hence the term by which the phenomenon has become to be known [280]. A milestone in understanding the phenomenon was set by Feynman and Cohen [281–283] who identified the relation between the static structure factor $S(\mathbf{k})$, which is related with the Fourier transform of the pair correlation function [284], and the collective modes dispersion,

$$\epsilon_k = E_k/S(\mathbf{k}), \tag{III.14}$$

supporting the argument that the physical origin of the roton appearance in the spectrum are the strong correlations prevailing in the system [280, 285]. In the subsequent years a series of experiments based on neutron scattering [286–289] followed the theoretical considerations and the existence of the roton at $k_{\rm min} = 1.93\,\text{Å}^{-1}$ has been confirmed. Furthermore, a number of phenomena arising in helium due to the presence of the deep roton minimum, such as density oscillations close to a defect or novel properties of vortices, have been predicted [290–294].

Crucially, Santos *et al.* showed in his seminal work [211] that a dipolar Bose-Einstein condensate can also exhibit the roton-maxon character of the excitations spectrum (see Fig. III.7). In particular, in Ref. [211] the authors consider an infinite pancake trap with dipoles perpendicular to the plane of the trap. In this configuration the collective modes dispersion allows a transparent physical interpretation. For in-plane momenta $\mathbf{q}$ much smaller than the inverse size L of the condensate in the confined direction, the excitations have two-dimensional character. Hence, since the dipoles are in the side-by-side configuration, particles effectively repel each other and the in-plane excitations are phonons. For $qL \gg 1$, the excitations acquire three-dimensional character and the interparticle repulsion is reduced. This decreases the excitations energy under an increase of q. The energy reaches a minimum and then starts to grow as the excitations continuously enter the free particle regime.

These considerations can be expressed quantitatively solving numerically the underlying Bogoliubov-de Gennes equations (III.9)-(III.10) (solid lines in Fig. III.7). For $qL \ll 1$, analytic results for the dispersion law ϵ_q can be found in the Thomas-Fermi limit [295], with the lowest excitations branch representing phonons propagating in the plane of the pancake. Interestingly, for the most involved three-dimensional regime, i.e., $qL \gg 1$, Santos *et al.* [211] have obtained an insightful analytical result,

$$\epsilon_q^2 = E_q^2 + \frac{(2\beta - 1)(5 + 2\beta)}{3(1 + \beta)(2 + \beta)} E_q \mu + \hbar^2 \omega^2, \tag{III.15}$$

with $E_q = \hbar^2 q^2/2m$, $\mu > 0$ as the chemical potential, ω as the axial trapping frequency, and $\beta = 3g/8\pi g_d$. From Eq. (III.15) (dotted lines in Fig. III.7) two possible types of behavior of the spectrum follow. For $\beta > 1/2$ the excitations energy monotonously increases with q and the condensate is stable for any momentum q and any density n. If $\beta < 1/2$, the dispersion law ϵ_q is characterized by the presence of a minimum. Since in the limit $qL \gg 1$ the energy ϵ_q is a growing function of q, the existence of this minimum indicates that the spectrum ϵ_q as a whole acquires the roton-maxon character. Crucially, with increasing density (chemical potential) of the BEC also the depth of the roton minimum increases until finally it reaches $\epsilon_q = 0$ at, approximately, $q = \sqrt{2}/l_z$. This is the onset of the roton instability. Any further increase of n (μ) renders ϵ_q imaginary and the condensate becomes dynamically unstable against a collapse with regard to these intermediate momentum excitations.

The complexity of the excitations spectrum in a dipolar condensate, and the existence of the roton minimum in particular, gives rise to a wealth of new physical phenomena, unprecedented in a nondipolar BEC. In particular, in the numerical study of the collective modes of a dipolar BEC in a three dimensional harmonic trap with cylindrical symmetry [238–240] two possible types of solution for a stable condensate have been found: a pancake (normal) shaped condensate with the maximum condensate density in the center of the trap, and a biconcave (blood cell) shaped condensate (Dutta and Meystre predicted structured ground states also in anisotropic traps [242]). In the former case, the mode with the frequency that goes to zero when approaching the instability (compare with Sec. III.D) has zero projection of the angular momentum on the z-axis, $m = 0$. This *radial roton* and its behavior are qualitatively similar to the roton mode in the infinite pancake that we analyzed above, in particular, collapsing due to density modulations in the radial direction. In contrast, for the biconcave condensate, the lowest excitation mode near the instability has nonzero projection of the angular momentum on the z-axis, $m \neq 0$. This is a kind of an *angular roton* in the trap. The appearance of the angular roton when the ground state has the biconcave shape may be understood in the light of the fact that the maximum density of such condensate lies along a ring. Hence, the instability may be considered a density distortion along this ring and indeed it has been found that a dipolar BEC may become unstable against the density modulations in the angular coordinate, followed with the characteristic angular collapse [249], which spontaneously breaks the cylindrical symmetry (compare with Fig. VII.3a). In chapter VII we will see how the confinement of the roton excitations in the center of a condensate cloud gives rise to yet different, unconventional collapse dynamics that originates in the roton instability.

The onset of the roton in a quasi-one-dimensional geometry was studied in Refs. [296, 297].

Touching zero energy at a finite wave vector is suggestive of a possible phase transition to a supersolid, i.e., a self-assembled density modulation [298, 299]. However, in Ref. [300] it has been found numerically that the putative supersolid states of a dipolar BEC are unstable.

Furthermore, the observation of dipolar effects in atom interferometry experiments [252] stimulated investigations on the collective excitations spectrum in a dipolar condensate in a one-dimensional optical lattice. For nondipolar systems, gases trapped in different sites of a deep lattice do not interact with each other. Hence, for a zero intersite hopping, different sites may be considered as independent, uncorrelated experiments. Remarkably, even in the absence of hopping, the long-range character of the dipolar interactions plays a key role for the occurring phenomena. In particular, dipolar BECs in nonoverlapping lattice sites share common excitations modes. This collective character enhances roton-like features in the excitation spectrum [253] and modifies the BEC stability, as recently demonstrated experimentally [250]. Similar intersite effects in a multilayer of dipolar BECs were examined also in the context of the phonon instability [254]. The idea of collective character of the excitations that are shared by all sites in the lattice will be the primal scope of our studies in chapter V. See also appendix C.

Finally, recently, the effects originating in anisotropy of the Bogoliubov spectrum with respect to the direction of the wave vector have received much attention, in particular in what regards anisotropic superfluidity [237] (see Ref. [236] as well), which has been also examined experimentally and the anisotropy of the speed of sound has been observed [224] (see also Ref. [221]). Moreover anisotropic coherence properties [301] and anisotropic density instability [302] have been investigated in the context of tilting the dipoles polarization angle (see also Ref. [303]).

III.F

Dipolar solitons

Dipolar effects are particularly relevant to what concerns the nonlinear properties of dipolar Bose-Einstein condensates (BECs). Crucially, whereas nondipolar BECs present a local Kerr-like type of nonlinearity (see Sec. II.C.7), the nonlinearity in dipolar BECs exhibits a nonlocal character, similar to that in plasmas [304], with the nonlocal response induced by heating and ionization, nematic liquid crystals [305, 306], where the nonlocality stems from long-range molecular interactions, and in photorefractive media [105, 106].

In particular, we have seen in section II.C.7 that the local nonlinearity in a nondipolar condensate gives rise to the stable bright soliton solutions but only in a one-dimensional geometry. Interestingly, however, it has been observed experimentally that in the systems mentioned above, the nonlocal nonlinearity stabilizes solitons also in two dimensions [307–310]. Strikingly, in Refs. [258, 259] two-dimensional bright solitons (isotropic and anisotropic) have been also predicted for a dipolar BEC.

The necessary conditions for the existence of the isotropic two-dimensional bright soliton in a pancake dipolar BEC can be understood utilizing the Gaussian ansatz (III.6) that we have employed in Sec.III.B when considering the stability of a dipolar condensate,

$$\Psi(\rho,z)=\sqrt{\frac{N}{\pi^{3/2}L_\rho^2 L_z l_z^3}}\exp\left[-\frac{1}{2l_z^2}\left(\frac{x^2+y^2}{L_\rho^2}+\frac{z^2}{L_z^2}\right)\right], \tag{III.16}$$

where $l_z = \sqrt{\hbar/m\omega_z}$ is the axial harmonic oscillator length and L_ρ, and L_z are the variational parameters, related to the widths in the xy-plane (pancake plane) and in the confined z-direction, which coincides with the direction of an external magnetic field, respectively. Inserting this ansatz into the corresponding energy functional Pedri and Santos [258] derive the energy of the system and they find that it admits a minimum, for a finite L_ρ and L_z, only if the dipole-dipole coupling strength g_d is negative or, equivalently, $a_d < 0$. This condition can be achieved utilizing the technique of tuning of the DDI that we discussed in section III.A. For $Na_{sc}/l_z \gg 1$, the explicit condition for the existence of the two-dimensional isotropic dipolar soliton reads $|g_d/g| > 3/8\pi$ or, equivalently, $|a_d/a_{sc}| > 1/2$, which has been additionally verified with direct numerical simulations of the nonlocal GPE (III.5).

Furthermore, employing the time-dependent Gaussian variational ansatz, such as the one in Eq. (III.13), the authors of Ref. [258] examined stability properties of the two-dimensional isotropic dipolar soliton (see Fig. III.8) and they found that for any value of $\beta = g_d/g$ it is the breathing mode which is the lowest-lying mode (compare with Sec. III.D). For sufficiently small values of $|\beta|$, the frequency of the breathing mode tends to zero, and eventually

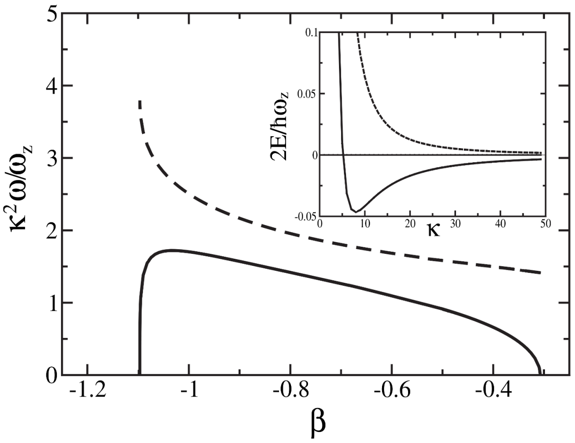

Figure III.8: Energy of elementary excitation modes of a two-dimensional isotropic dipolar soliton. The solid line corresponds to the breathing mode while the dashed line depicts the result for the quadrupole modes (see Fig. III.6) for $g = 10\hbar\omega_z l_z^3$, with $\kappa = L_\rho/L_z$ (see Eq. (III.16)). Clearly, for small values of $|\beta|$, the dipolar interactions do not suffice to stabilize a soliton and the breathing mode touches zero while the condensate wave packet expands. In contrast, when $|\beta|$ becomes large, the three-dimensional character of the dipole-dipole interactions becomes decisive and the attractive part of the DDI renders the soliton eventually unstable against the collapse. Hence, the dipole-dipole interactions support the stable soliton solutions only in a certain range of the strength of the dipolar coupling. Inset: Energy of the system E for $g = 500\hbar\omega_z l_z^3$ and $\beta = -0.1$ (instability against expansion, dashed line), and $\beta = -0.2$ (stable soliton, solid line). Reprinted from Phys. Rev. Lett. **95**, 200404 (2005).

the systems becomes unstable against expansion. This corresponds to the disappearance of the minimum in the energy of the system in the inset of the Fig. III.8. In this regime, the two-dimensional picture provides a good description of the physics of the problem. For sufficiently large values of $|\beta|$, the three-dimensional character of the system becomes decisive, rendering the soliton unstable against collapse. This is reflected in the decrease of the frequency of the breathing mode. In chapter IV we will present an analogous stability analysis of soliton molecules, i.e., compounds that consist of several dipolar solitons.

Finally, Pedri and Santos [258] performed numerical analysis of a scattering process of two dipolar solitons and they observed that, in contrast to collisions of nondipolar solitons in one dimension, the scattering was inelastic. In particular, the dipolar solitons may transfer their center-of-mass kinetic energy into internal vibrational modes. This process, in turn, may result in soliton fusion into a single localized oscillating structure or even in destruction of the solitons. Similar analysis of scattering properties of dipolar solitons in a double-well potential with no hopping was performed in Ref. [260] and interesting intersite effects have been observed. In particular, a new scattering scenario has been found, in which inelastic spiraling occurs, scattering resonances have been discussed and the molecular-like interlayer potential has been investigated. In chapters IV and V we will see how a proper engineering of such intersite interactions between disjoint one-dimensional dipolar BECs can pave the way towards involved soliton structures.

Following the same formalism as the one employed by Pedri and Santos [258], Tikhonenkov *et al.* [259] considered a pancake dipolar BEC with dipoles polarized perpendicularly to the confinement direction and they found the necessary conditions for the existence of the bright anisotropic dipolar solitons. In particular, they concluded that in such arrangement no sign reversal of the DDI is required in order to observe the solitons. In addition, as for the case of the isotropic solitons, the anisotropic solitons in a three-dimensional geometry have been proven unstable against collapse.

We note that recently a scheme for the creation of stable three-dimensional bright solitons in a Rydberg-dressed Bose-Einstein condensate has been proposed [311]. For a general discussion of collapse arrest and soliton stabilization in nonlocal nonlinear media the reader is referred to Ref. [312].

As we discussed in section II.C.7, nondipolar dark solitons in a three-dimensional geometry are inherently unstable against the snake instability. Interestingly, the presence of dipole-dipole interactions may stabilize a three-dimensional dark soliton, provided that the condensate is loaded into a sufficiently deep two-dimensional optical lattice. This effect was studied in Ref. [261].

❧

IV

Soliton molecules in dipolar BECs

Dipolar interactions support the formation of intersite soliton molecules in a stack of quasi-one-dimensional traps. In this chapter we show that the stability and properties of individual solitons and soliton molecules in such a geometry crucially depend on the interplay between contact and dipolar interactions. In particular, two different quasi-one-dimensional soliton regimes are possible: a one-dimensional soliton characterized by purely repulsive dipole-dipole interactions and a three-dimensional soliton for which a sufficiently large dipole moment renders the dipole-dipole interactions attractive. Furthermore, we find that in contrast to the dimers of polar molecules the soliton dimers exhibit a nontrivial behavior of the elementary excitations that stems from the competition between onsite and intersite interactions. Finally, we prove the existence of soliton trimers in a regime where molecular trimers do not occur. We demonstrate that the soliton molecules that we report are well feasible under realistic experimental conditions.

IV.A

Introduction

As we have broadly discussed in Sec. III.F, dipole-dipole interactions are particularly relevant to what concerns the nonlinearity in dipolar Bose-Einstein condensates. Namely, as opposed to nonpolar gases, the nonlinearity in dipolar BECs exhibits a nonlocal character, which becomes clear from the nonlocal Gross-Pitaevskii equation (III.5). This feature results in a range of novel physical phenomena, being especially striking in the physics of dipolar solitons.

We have also learned in sections III.C, III.E and III.F that the nonlocal character of the DDI plays a substantial role in the physics of dipolar gases in optical lattices, even in the absence of the intersite hopping. Namely, the long-range dipole-dipole interactions couple the disjoint sites and thus fundamentally modify the excitations spectrum and the stability properties of a dipolar BEC. Furthermore, as we will see in chapter V, the intersite dipolar interactions between nonoverlapping condensates may also lead to a correlated modulational instability. Interestingly, the intersite dipole-dipole coupling is also of the prime importance in the field of polar molecules, leading to a variety of unprecedented few-body bound states such as intersite dimers [313, 314], trimers [315, 316] and filaments [317, 318].

In this chapter we analyze in detail the physics of dipolar bright solitons in a stack of quasi-1D condensates, created by means of an optical lattice. We focus on the stability and properties of soliton dimers and trimers, which constitute the building blocks of the soliton filaments and crystals, respectively, created during the above-mentioned correlated modulational instability. These two- and three-soliton bound states are an paradigms of the so-called soliton molecules. Recently, an optical equivalent of such objects has been realized experimentally in optical fibers [319, 320] and a variety of theoretical proposals to create atomic soliton molecules have been presented [321–323]. Soliton dimers share some properties with molecular dimers. However, as we discuss in detail below, intrasoliton interactions (of course absent in the case of individual polar molecules) are decisive for their stability and elementary excitations. Moreover, whereas molecular trimers may be found (in the absence of any additional lattice [316]) only for a rather narrow window of the dipole moment orientations [315], soliton trimers may exist for the orientations for which trimers of individual polar molecules are precluded.

The chapter is structured as follows. Sec. IV.B introduces the general formalism. In Sec. IV.C we compute the universal stability diagram for a single dipolar soliton in a quasi-1D trap and we show that such geometry supports two stable soliton regimes differing substantially in the character of the dipolar interactions. Section IV.D is devoted to the study of properties of the soliton dimers. We discuss the intersoliton binding potential and the nontrivial dependence of the dimer elementary excitations on the dipolar coupling. In Sec. IV.E we analyze the trimer case, showing that soliton trimers may be found in a regime where molecular trimers would be unstable.

IV.B

Model

In the following of this chapter we consider a dipolar BEC loaded in a stack of M parallel quasi-1D traps (tubes), formed by a 2D optical lattice with sites located at $y_j = j\Delta$ (Fig. IV.1). The intertube potential barrier is considered sufficiently large to suppress any hopping. In each tube we assume a strong harmonic confinement of frequency $\omega_\perp$ in the xy plane and no confinement along the z direction. The atoms possess a magnetic dipole moment μ (the results are equally valid for electric dipoles, such as polar molecules) oriented along the y axis, in the side-by-side configuration, by a sufficiently large external field. Introducing a wavefunction $\Psi_j(\mathbf{r})$ that describes an atomic cloud in a site j holding N atoms, the system of nonlocal coupled Gross-Pitaevskii equations reads

$$\begin{aligned}\imath\hbar\partial_t\Psi_j(\mathbf{r}) = \Bigg[& -\frac{\hbar^2}{2m}\nabla^2 + U_j(\mathbf{r}) + gN\left|\Psi_j(\mathbf{r})\right|^2 \\ & + \sum_{m=0}^{M-1}\int d\mathbf{r}' V_d\left(\mathbf{r}-\mathbf{r}'\right)\left|\Psi_m\left(\mathbf{r}'\right)\right|^2\Bigg]\Psi_j(\mathbf{r},t). \qquad \text{(IV.1)}\end{aligned}$$

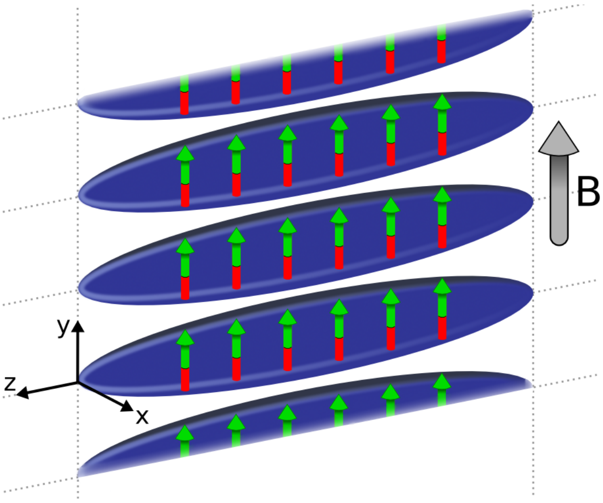

Figure IV.1: Scheme of a stack of quasi-1D tubes of dipolar Bose-Einstein condensates.

Here, $U_j(\mathbf{r}) = \frac{1}{2}m\omega_\perp^2[x^2 + (y - y_j)^2]$ and $V_d(\mathbf{r} - \mathbf{r}') = g_d N(1 - 3\cos^2\theta)/|\mathbf{r} - \mathbf{r}'|^3$ is the dipole-dipole potential where $g_d = \mu_0\mu^2/4\pi$ with μ_0 being the vacuum permeability and θ the angle between the vectors joining two interacting particles and the direction of the dipole moment. The short-range interactions are characterized by $g = 4\pi a_{sc}\hbar^2/m$ with a_{sc} being the s-wave scattering length. In this chapter we consider only attractive short-range interactions ($a_{sc} < 0$).

IV.C

Dipolar soliton in a single quasi-1D trap

We discuss first the conditions of existence of a stable bright soliton in a single quasi-1D trap ($M = 1$). To this end we assume a 3D anisotropic Gaussian ansatz

$$\Psi_0(\mathbf{r}) = \frac{1}{\pi^{3/4}(l_x l_y l_z)^{1/2}} \exp\left(-\frac{x^2}{2l_x^2} - \frac{y^2}{2l_y^2} - \frac{z^2}{2l_z^2}\right), \tag{IV.2}$$

where l_x, l_y, and l_z are the variational widths along x, y and z directions, respectively. Employing this ansatz into Eq. (IV.1) we obtain the energy of the system

$$\begin{aligned} E(l_x, l_y, l_z) = \frac{\hbar^2}{4m} \sum_{i=x,y,z} \frac{1}{l_i^2} + \frac{\omega_\perp^2}{4} \sum_{i=x,y} l_i^2 \\ + \frac{N}{4\sqrt{2}\pi^{3/2} l_x l_y l_z}\left(g + \frac{2}{3} g_d K\left(\frac{l_z}{l_x}, \frac{l_z}{l_y}\right)\right), \end{aligned} \tag{IV.3}$$

with the function

$$K(r_x, r_y) = \int_0^{2\pi} d\varphi \int_0^1 du \frac{(1 - u^2)\left[2r_y^2 - \left(r_x^2 + 2r_y^2\right)\cos^2\varphi\right] - u^2}{(1 - u^2)\left[r_y^2 + (r_x^2 - r_y^2)\cos^2\varphi\right] + u^2}. \tag{IV.4}$$

The full derivation of Eq. (IV.3) and the detail study of an analytical form of Eq. (IV.4) are presented in appendix B. A stable soliton solution corresponds to a minimum in the energy functional $E(l_x, l_y, l_z)$ at finite nonzero values of the soliton widths. In Fig. IV.2 we present the universal stability diagram as a function of the dimensionless parameters $g^* = gN/2\pi\hbar\omega_\perp l_\perp^3$, and $g_d^* = g_d N/2\pi\hbar\omega_\perp l_\perp^3$.

Interestingly, two different soliton regimes may be found, which differ remarkably in their properties and stability for growing $g_d > 0$. For sufficiently small $|g^*| < |g_c^*|$, with $|g_c^*| \simeq 1$, a soliton may be considered as purely 1D, i.e., $l_x = l_y \simeq l_\perp = \sqrt{\hbar/m\omega_\perp}$, whereas $l_z \gg l_\perp$. For such soliton, the DDI remains repulsive for any g_d^*. As a result, the soliton width l_z increases monotonically for growing g_d^*, until diverging at a critical value at which the soliton

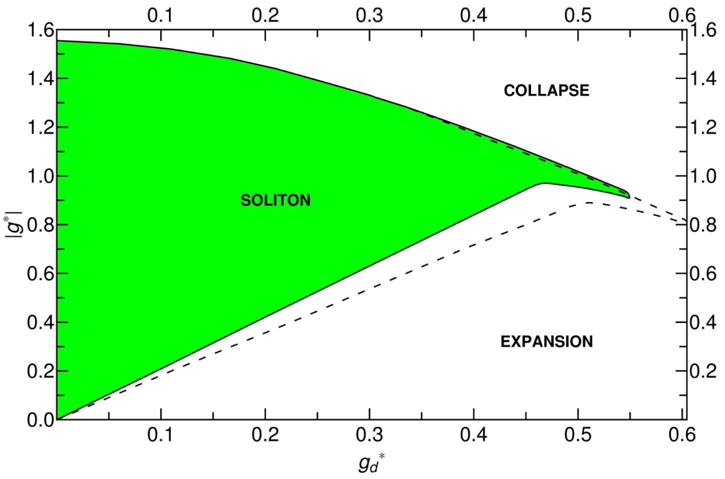

Figure IV.2: Universal stability diagram for a dipolar bright soliton in a single quasi-1D trap. Three regimes occur: stable soliton, instability against a 3D collapse and soliton expansion along the axis of the trap. The dashed line represents the stability boundary for a soliton dimer with $\Delta = 6l_\perp$.

delocalizes. The condition for soliton stability against the expansion may be then found analytically from Eq. (IV.3), $|g^*|/g_d^* > 2\pi/3$ (straight solid line in Fig. IV.1). In contrast, for $|g^*| > |g_c^*|$ the atomic cloud cannot be considered any more as 1D, since l_z becomes comparable with the transversal widths. As a result, a stable soliton solution occurs that clearly displays a 3D character. In this regime, the DDI interaction changes its character from repulsive to attractive at a finite $g_d^* > 0$ value, and hence for further growing g_d^* the soliton width decreases until the soliton becomes unstable against 3D collapse. Furthermore, we note that in the vicinity of $|g_c^*|$, the stability diagram presents an interesting reentrant character as a function of g_d, first expanding, then re-binding and finally collapsing (Fig. IV.3). Interestingly, contrary to the soliton-expansion transition, at which the soliton width smoothly diverges, the re-binding transition is first-order-like, since the soliton abruptly re-binds at a finite width.

IV.D

Soliton dimers

We assume in the following that a soliton in each tube is in the 1D regime discussed in Sec. IV.C (this condition is self-consistently verified). At the end of this section we briefly comment on the case of solitons in the 3D regime. In the 1D regime, the wavefunctions factorize $\Psi_j(\mathbf{r}) = \phi_j^\perp(x,y)\psi_j(z)$, with $\phi_j^\perp(x,y)$ the ground state wave function of the transverse harmonic oscilla-

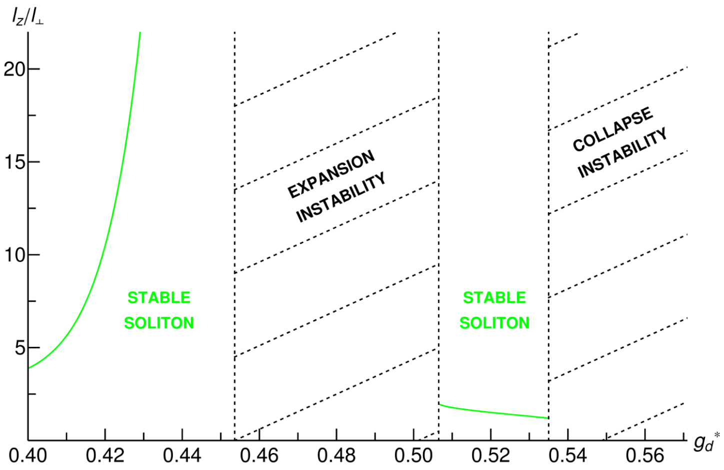

Figure IV.3: Reentrant character of the soliton stability in a single quasi-1D trap in the vicinity of g_c^*. Here, $|g^*| = 0.95$.

tor in a site j. Following the way presented in appendix A, we reduce the dimensionality of Eq. (IV.1) to arrive at the system of equations

$$\begin{aligned}\imath\hbar\partial_t\psi_j(z) = \Bigg[&-\frac{\hbar^2}{2m}\partial_z^2 + \frac{gN}{2\pi l_\perp^2}n_j(z)\\ &+\frac{g_d N}{3}\sum_{m=0}^{M-1}\int dk_z e^{\imath k_z z}\hat{n}_m(k_z)F_{m-j}(k_z)\Bigg]\psi_j(z),\end{aligned} \tag{IV.5}$$

with $\hat{n}_m(k_z)$ the Fourier transform of the axial wave function density $n_m(z) = \left|\psi_m(z)\right|^2$ in a site m and

$$\begin{aligned}F_q(k_z) = &\int\frac{dk_x dk_y}{\pi}\left(\frac{3k_y^2}{k_x^2+k_y^2+k_z^2}-1\right)\\ &\times e^{-\frac{1}{2}(k_x^2+k_y^2)l_\perp^2-\imath k_y q\Delta}.\end{aligned} \tag{IV.6}$$

For stable individual solitons the intersite DDI may result for $g_d > 0$ in a binding of two solitons in different quasi-1D tubes into a soliton dimer (Fig. IV.4). Such dimer resembles recently reported dimers of individual polar molecules. However, as discussed below, in the physics of the soliton dimer the interplay between intrasoliton interactions and intersoliton interactions leads to nontrivial effects, which do not occur in the case of molecular dimers due to the absence of onsite DDI.

Two solitons localized in neighboring quasi-1D tubes ($j = 0, 1$) and with a relative displacement z_r along the axis direction z (Fig. IV.4), experience an interaction potential

$$E_D(z_r) = \frac{g_d N}{3} \int dz\, n_1(z - z_r) \int dk_z e^{\imath k_z z} \hat{n}_0(k_z) F_1(k_z). \qquad \text{(IV.7)}$$

We calculate $E_D(z_r)$ evolving Eq. (IV.5) in imaginary time to obtain the ground state of the dimer $\psi_j^0(z)$ and then shifting the solitons to the distance z_r. Due to the anisotropy of the DDI the intersoliton potential is maximally attractive for $z_r = 0$, and becomes repulsive for large z_r (Fig. IV.4). Naturally, the binding potential $E_D(z_r)$ calculated for actual soliton wave-packets is significantly weaker than that expected for point-like particles $E_D^0(z_r) = g_d N(z_r^2 - 2\Delta^2)/(z_r^2 + \Delta^2)^{5/2}$. Nevertheless, we note that even for the case of the relatively small dipole moment of ^{52}Cr, which we employed in our calculations for Fig. IV.4, the energy scale of the binding remains significant (~ 100 Hz). Obviously, the binding would be stronger for condensates of atoms with larger dipole moment, such as dysprosium [217] and erbium [219], or in the case of polar molecules [179, 181, 183].

We now focus on the essential properties of the soliton dimer. First, following the imaginary time evolution of Eq. (IV.5), for a given $\Delta/l_\perp$, we compute the width l_z of the solitons forming the dimer as a function of g^* and g_d^* (see Fig. IV.5 (top)). Since we consider the 1D soliton regime, with an overall

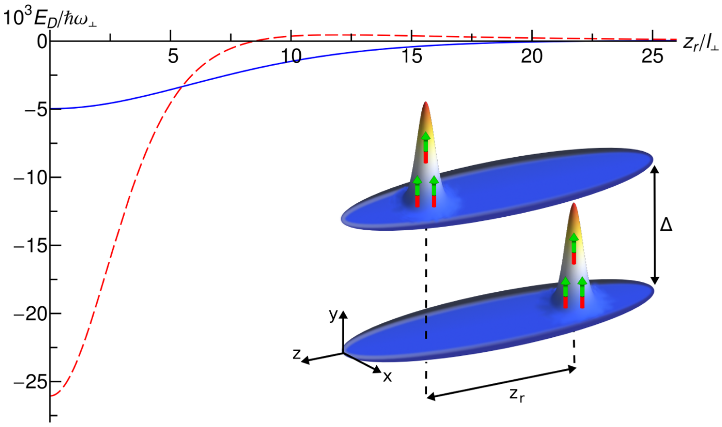

Figure IV.4: Intersoliton binding potential for the case of the soliton dimer. The red dashed line represents the potential calculated within the point-like approximation E_D^0. The blue solid line shows the actual potential computed numerically with Eq. (IV.7). Here, we consider the case of ^{52}Cr condensate ($\mu = 6\mu_B$, with μ_B the Bohr magneton), $a_{sc} = -7.1 a_0$ (with a_0 the Bohr radius), $N = 100$, $\Delta = 6 l_\perp = 512$ nm, and the lattice potential depth $s = 13.3 E_R$ (recoil energy). These parameters refer to $\omega_\perp = 26.7$ kHz and $(g^*, g_d^*) = (-0.88, 0.45)$. The inset depicts schematically the soliton dimer arrangement.

repulsive intrasoliton DDI, an increase of g_d results in a broadening of the solitons, and eventually to the instability of the individual solitons against expansion. Note, however, that the attractive intersoliton interactions, while providing the binding mechanism itself, induces a trapping of each soliton by its neighbor, which contributes to stabilization of each soliton against expansion. This increases the stability threshold found in Sec. IV.C for an individual soliton, as shown by the straight dashed line (at $|g^*|/g_d^* = 1.78$) in Fig. IV.2, obtained from a similar 3D variational calculation as that of the previous section.

The properties of the soliton dimer must be compared with those of intersite dimers formed by individual polar molecules. In the latter case, the localization of each molecular wave-packet is solely due to the attractive intersite DDI, which induce a mutual trapping of both molecules. This means, in particular, that for $g_d^* = 0$ each of the wave-packets delocalizes. Furthermore, owing to the absence of intrawave-packet repulsive DDI, an increase of g_d^* can only amplify localization and so the molecular dimer width decreases monotonically as a function of g_d^*, unlike the case of the soliton dimer. As a result, molecular dimers become stiffer (i.e., present growing excitation energies) for growing DDI.

In contrast, the elementary excitations of the soliton dimer present a more involved behavior that stems from the interplay between intra- and intersoliton DDI. We study the lowest-lying excitations by monitoring the real-time dynamics of the solitons following a small distortion of the ground state solution in the form $\psi_j(x,t=0) = \psi_j^{(0)} e^{-i(k_j x + \beta_j x^2)}$, corresponding to a perturbation of the soliton positions and their widths. Fig. IV.5 (bottom) shows the result of the Fourier transform of the position $\langle z(t) \rangle$ of one of the two oscillating solitons and hence the frequency of the dimer lowest-lying excitation (this is verified additionally by inspecting the Fourier transforms of soliton width and density oscillations). For sufficiently small DDI, and so for a small solitons widths, the lowest-lying excited mode of the dimer is associated exclusively to the motion of the center-of-mass of each soliton. In consequence, as g_d^* grows, so does the energy of dimer excitations, resembling the case of molecular dimers. In contrast to the molecular dimers, however, after reaching a certain critical value of g_d^* the soliton dimer becomes progressively softer (i.e., it exhibits decreasing excitation energies). This phenomenon arises since the soliton widths increase due to the repulsive intrasoliton DDI, and, as a result, the lowest-lying excitation becomes eventually an admixture of both position and width distortions. As discussed before, for a sufficiently large g_d^* the dimer becomes eventually unstable against expansion.

Finally, we stress that soliton dimers may exist as well in the 3D regime defined in Sec. IV.C, i.e., for $|g^*| > |g_c^*|$. As depicted in Fig. IV.2, the stability threshold against the soliton dimer collapse is basically the same as that for an individual soliton. Contrary to the 1D case, in the 3D regime the width of a soliton is relatively small $l_z \simeq l_\perp$ and so the binding potential between the two solitons, such as the one depicted in Fig. IV.4, becomes comparably deep as the point-like approximation E_D^0. Moreover, for $|g^*| > |g_c^*|$ the soliton width never becomes large enough to cause the mixing of position and width excitations. As a result, in the 3D regime, for growing g_d values the soliton dimer becomes only stiffer, up to the collapse threshold, similary to the case of molecular dimers.

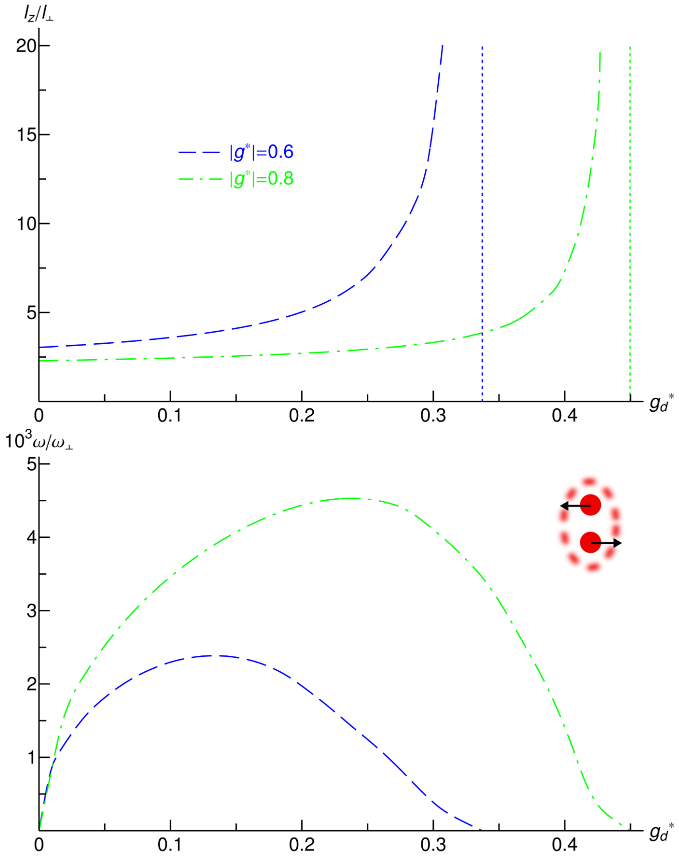

Figure IV.5: (top) Width of the soliton dimer as a function of g_d^* for $|g^*| = 0.6$ (blue dashed line) and $|g^*| = 0.8$ (green dot-dashed line), for the same parameters as in Fig. IV.4. The vertical dashed lines indicate the dimer expansion threshold. (bottom) Frequency of elementary excitations of the soliton dimer for the same parameters. The inset shows a scheme of the dimer elementary excitation mode.

IV.E

Soliton trimers

Interestingly, the DDI may lead to the formation of soliton molecules comprising of more than two solitons, in particular soliton trimers (Fig. IV.6). We note that trimers (and even more involved complexes) have been predicted as well for individual polar molecules [315, 316]. However, molecular trimers have been found to exist only in a rather narrow window of dipole moment orientations with respect to the trap axis, in the very vicinity of the magic angle, such that intrasite repulsion is minimized and intersite attraction is maximized. In particular, molecular trimers are precluded if the dipole orientation is aligned along the trap axis. Furthermore, as noted in Sec. IV.D, the formation of molecular bound states is handicapped by the fact that the intersite interactions do not only provide a binding between the molecules but are also indispensable for the localization of the individual molecular wave-packets themselves. This contrasts with the soliton case, where the existence of localized wavepackets is supported by intrasoliton interactions. As a result, as we discuss in this section, the interplay between inter- and intrasoliton interactions allows for stable soliton trimers for dipole moment orientations in which molecular trimers are absent.

In the following we consider for theoretical simplicity the case of dipoles oriented along the y axis (in the side-by-side configuration as that of the soli-

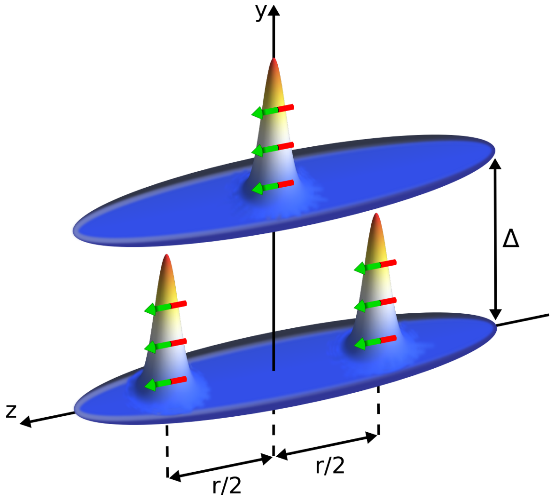

Figure IV.6: Scheme of the soliton trimer. The dipole moments are aligned in the head-to-tail configuration providing attractive intrasite and repulsive intersite dipolar interactions. In our work we mimick this scheme with qualitatively equivalent arrangement of dipoles aligned along the y axis (side-by-side configuration) but with $g_d^* < 0$ (see discussion in text).

ton dimer) but with $g_d < 0$. This may be achieved by means of a rotating magnetic field [271], or microwave dressing for polar molecules [269]. The results would be however qualitatively very similar to the case of dipoles oriented along the tubes, since both cases are characterized by repulsive intersite DDI and attractive intrasite DDI. Although the attractive intersite interactions seem naively to involve soliton fusion in the bottom tube, and hence to preclude the existence of the soliton trimer, such trimer results actually from a nontrivial interplay between intertube repulsion and intratube attraction. Namely, the single soliton in the upper tube provides a repulsive potential barrier that prevents the fusion of the two mutually-attracting solitons in the bottom tube, hence keeping the soliton trimer stable.

A major difference with respect to soliton dimers lies in the fact that now $g_d^* < 0$, and hence the intrasoliton interaction is attractive. In consequence, for growing $|g_d^*|$ the individual solitons shrink, i.e., the trimer is not unstable against the expansion of the individual solitons but rather against their collapse, as the solitons become eventually 3D for a sufficiently large $|g_d^*|$. As it has been shown for the soliton dimer, the threshold for the collapse instability is basically given by the intrasoliton physics. We have thus analyzed the stability of a soliton in a single quasi-1D trap for $g_d < 0$ (see Fig. IV.7), using the same 3D variational Gaussian ansatz discussed in Sec. IV.C. Naturally, soliton trimers may exist only within the stability region of individual solitons.

In the following we analyze the properties of trimers well within the 1D regime, i.e., far from the 3D collapse threshold, for which we can safely em-

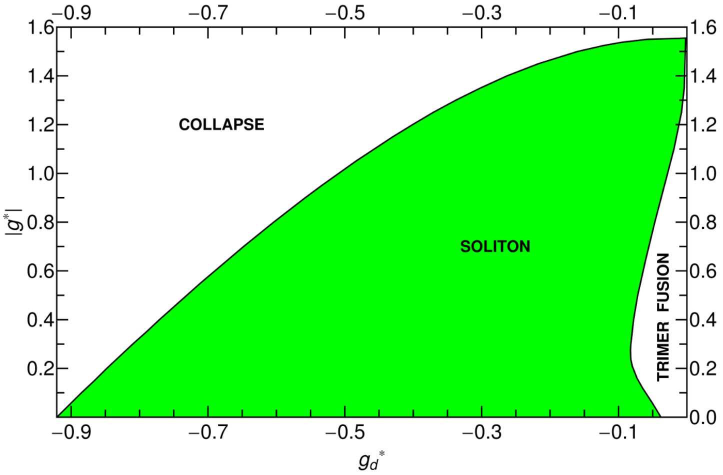

Figure IV.7: Universal stability diagram of a single dipolar bright soliton in a quasi-1D trap for $g_d^* < 0$. Two regimes occur: stable soliton and 3D instability against collapse. We indicate additionally the regime of the trimer instability against fusion (see discussion in text).

ploy the 1D GPEs (Eq. (IV.5)). In particular, after obtaining the ground state of the trimer configuration by means of the imaginary time evolution of these equations, we have computed the binding potential of the trimer $E_T(r)$ (Fig. IV.8) as a function of the distance r between the solitons in the bottom tube (Fig. IV.6). Crucially, at an intermediate distance r_{min}, $E_T(r)$ shows a local minimum that offers the possibility of a soliton trimer. A point-like approximation of the solitons would induce a binding

$$E_T^0(r) = g_d N \left[\frac{1}{r^3} + \frac{16(r^2 - 8\Delta^2)}{(r^2 + 4\Delta^2)^{5/2}} \right], \tag{IV.8}$$

resulting in an equilibrium position $r_{min}^0/\Delta \simeq 3.73$, independently of g_d. This approximation, however, differs significantly from the actual binding potential $E_T(r)$, proving again the relevance of the spatial extension of solitons. Specifically, as shown in Fig. IV.9 (top), the trimer size, understood as the actual equilibrium distance r_{min}, decreases with growing $|g_d^*|$ (whereas the binding energy increases). We also note that, as it may be expected, the soliton trimer is more loosely bound than the soliton dimer. For typical parameters of ^{52}Cr condensate, which we employed for the Fig. IV.8, the binding energy is of the order of 10Hz. We stress, however, that the binding will be certainly stronger in the case of more magnetic atoms (Dy, Er) or polar molecules.

Note that unlike the soliton dimer, the soliton trimer is related to a local

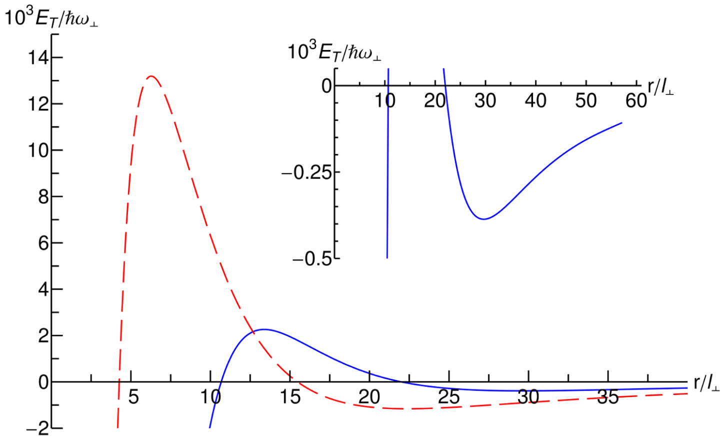

Figure IV.8: Soliton trimer potential energy. The red dashed line represents the potential E_T^0 obtained from the point-like approximation, whereas the blue solid line depicts the actual binding potential E_T calculated numerically integrating Eqs. (IV.5). We consider ^{52}Cr BEC (with $g_d < 0$) with $a_{sc} = -4.0 a_0$ and $N = 100$ atoms in every soliton, i.e., $(g^*, g_d^*) = (-0.50, -0.45)$. Here, $\Delta = 512$ nm, $s = 13.3 E_R$ and $\omega_\perp = 26.7$ kHz. The inset shows the potential energy minimum which sustains the trimer bound state.

minimum of the energy functional. In particular, the global energy minimum results from the fusion of the solitons in the bottom tube into a single soliton, which forms a tilted dimer with the top soliton. The trimer configuration of Fig. IV.6 is hence strictly speaking a metastable solution, which is separated from the fused solution by a potential barrier (Fig. IV.8). Macroscopic quantum tunneling through this barrier is negligible, and hence the metastable solution may be considered for all practical purposes as stable (as we have checked in real-time evolution). The potential barrier dissappears at a sufficiently small $|g_d^*|$, at which the soliton trimer becomes abruptly unstable against soliton fusion (see Fig. IV.7 and Fig. IV.9).

Finally, as in the case of the soliton dimers, we have analyzed the lowest-lying excitations of the soliton trimer. Since now $g_d < 0$, the solitons are always well localized. Hence, contrary to the dimer case, the lowest lying

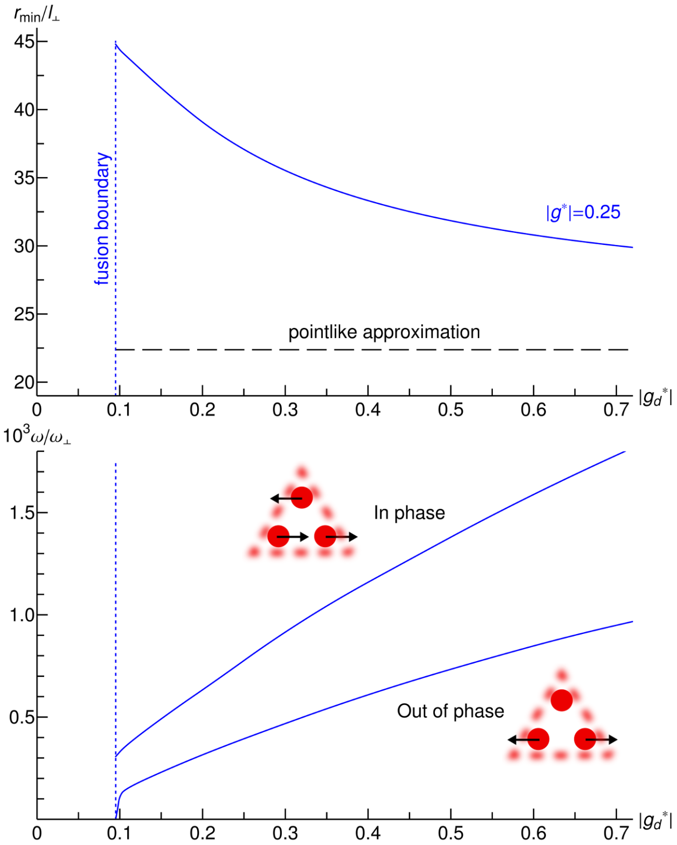

Figure IV.9: (top) Size of the soliton trimer as a function of g_d^* for $|g^*| = 0.25$ and the remaining lattice parameters as that in the Fig. IV.8. The dashed line indicates the result from the point-like approximation E_T^0. (bottom) Trimer elementary excitations for the same parameters. The insets show schemes of the trimer elementary excitation modes.

excitations are related solely to the solitons center of mass motion (without an excitation of the width of the solitons). We may hence define two different types of elementary excitations, characterized by an in-phase and an out-of-phase motion of the soliton pair in the bottom tube, respectively (Fig. IV.9 (bottom)). As in Sec. IV.D, we have probed these modes perturbing the soliton widths and positions of the trimer ground state, and monitoring the subsequent real-time dynamics given by Eq. (IV.5). After Fourier transforming the soliton positions, we obtain the lowest-lying excitations as a function of $|g_d^*|$. The results of the two excitation frequencies are depicted in Fig. IV.9 (bottom), which shows that for all $|g_d^*|$ the out-of-phase mode is always less energetic than the in-phase mode.

IV.F

Summary

In summary, intersite dipolar interactions support the formation of soliton molecules in a stack of quasi-1D tubes. The stability properties of quasi-1D solitons and intersite soliton molecules depend crucially on the interplay between dipolar and contact interactions, and the competition between intrasite and intersite effects. In particular, two different quasi-1D soliton regimes are possible: 1D solitons for which the intrasoliton DDI is always repulsive and that become eventually unstable against soliton delocalization, and 3D solitons, for which the DDI changes its character from repulsive to attractive for growing DDI, and that become eventually unstable against soliton collapse. We have shown that, contrary to the case of dimers of individual polar molecules, the interplay between intrasoliton interactions and intersoliton DDI leads to a nontrivial behavior of the lowest-lying excitations of soliton dimers. In the purely-1D regime a growing DDI render the dimer stiffer up to a maximum beyond which an increasing DDI softens the dimer due to the admixture between position and width excitations. Finally, we have shown that soliton trimers may be constructed for attractive intrasite and repulsive intersite DDI due to a subtle interplay between intratube attraction and intertube repulsion. Interestingly, these trimers occur in a regime in which trimers of individual polar molecules are not possible. The reported soliton molecules can be observed under realistic conditions within current experimental feasibilities. Moreover, we emphasize that the soliton binding mechanism described in this chapter can be straightforwardly generalized to engineer even more intricate soliton complexes comprising a larger number of solitons in more sites of an optical lattice.

⁂

V

Spontaneous self-assemblies of solitons in dipolar BECs

Intersite interactions play a crucial role in polar gases in optical lattices even in the absence of hopping. In this chapter we show that due to these long-range interactions a destabilized stack of quasi-one dimensional Bose-Einstein condensates develops a correlated modulational instability in the nonoverlapping sites. Interestingly, this density pattern may evolve spontaneously into soliton filaments or into a checkerboard soliton crystal that can be so created for the first time in ultracold gases. These self-assembled structures may be observed under realistic conditions within current experimental feasibilities.

V.A

Introduction

We have learned in the previous chapters of this thesis that nonlocal intersite dipolar interactions result in a rich variety of novel physical phenomena. In particular, in chapter IV we have seen that dipole-dipole coupling between nonoverlapping quasi-one-dimensional dipolar BECs give rise to dimers and trimers of solitons. Earlier, in section III.E we have come to know that the intersite interactions, even in the absence of hopping, crucially modify the elmentary excitations modes that acquire a collective character, being shared by all lattice sites.

As we discussed in Sec. II.C.7, quasi-one-dimensional geometries allow for the existence of BEC solitons and hence modulational instability in these systems leads to the formation of 1D patterns, so-called soliton trains, depicted in Fig. II.4. In contrast, according to discussion in Sec. II.C.5, dynamical instability in a BEC in two- and three-dimensional geometries is typically followed with a condensate collapse. In consequence, solitons patterns in higher dimensions, such as a 2D crystal of solitons, are fundamentally prevented in nonpolar BECs.

In this chapter we show that the destabilization of a dipolar BEC confined in a stack of nonoverlapping quasi-1D tubes may be followed by the spontaneous self-assembly of stable soliton filaments or a 2D checkerboard crystal of solitons, providing a route for the first realization of self-sustained 2D arrangements of BEC solitons. This dynamical self-assembly stems from the correlated character of the corresponding modulational instability. While for nondipolar condensates the instability in each lattice site would develop independently, the nonlocal dipolar interactions couple the nonoverlapping BECs to form an orderly density pattern shared among all sites. As we show, correlated modulational instability may be observable in current chromium [214], dysprosium [217] and erbium [219] experiments.

The dynamically formed soliton filaments, comprising of soliton dimers (see chapter IV), resemble dipolar chains of classical dipoles [324], as well as chains predicted for polar molecules [317, 318]. However, compared to the latter, soliton filamentation is expected to occur for smaller dipole moments due to the many-body character of each soliton. Remarkably, inverting the sign of the dipolar interactions results in the development of an anticorrelated density pattern which may be followed by the spontaneous formation of a stable crystal of solitons, composed of soliton trimers (see chapter IV). This 2D checkerboard crystal resembles the Wigner-like crystal predicted for polar molecules [325, 326]. However, contrary to the latter, it is dynamically formed and self-maintained by a nontrivial interplay between intratube attractive and intertube repulsive dipolar interactions.

The chapter is structured as follows. In Sec. V.B we introduce the considered model. In section V.C the spectrum of collective Bogoliubov excitations is examined and the early stage (linear regime) of the correlated modulational instability is considered. Section V.D is devoted to the phenomenon of spontaneous soliton filamentation and section V.E to the mechanism of dynamical formation of a soliton crystal. We conclude in Sec. V.F.

V.B

Model

We study below a dipolar BEC confined in a stack of quasi-1D tubes formed by an optical lattice (Fig. V.1). The lattice is assumed to be sufficiently deep to suppress intersite hopping. In each of the N_m lattice sites the xy-confinement is approximated by a harmonic potential with frequency $\omega_\perp$, whereas for simplicity we assume no confinement along the z direction. We consider atoms with a magnetic dipole moment μ (the results are equally valid for electric dipoles, such as polar molecules) oriented along y direction by an external magnetic field. The dipoles interact with each other via the dipole-dipole potential $V_d\left(\mathbf{r}-\mathbf{r}'\right) = g_d\left(1-3\cos^2\theta\right)/\left|\mathbf{r}-\mathbf{r}'\right|^3$, where $g_d = \mu_0\mu^2/4\pi$, with μ_0 being the vacuum permeability and θ the angle formed by the vector joining the two interacting particles and the dipole moment direction.

We assume the chemical potential much smaller than $\hbar\omega_\perp$ (this assumption is self-consistently verified in our calculations). Hence, we can factorize the BEC wave function at each site j, $\Psi_j(\mathbf{r}) = \phi_j(x,y)\psi_j(z)$, with $\phi_j(x,y)$ the ground-state wave function of the xy harmonic oscillator. Following the calculations presented in appendix A, we arrive at a system of N_m coupled 1D

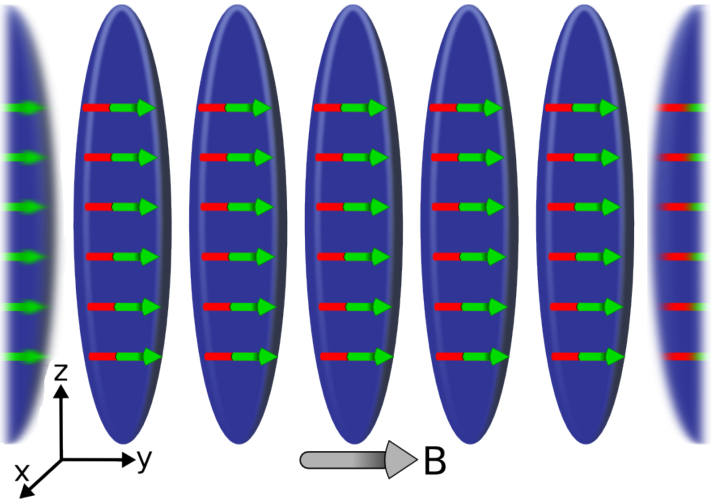

Figure V.1: Scheme of the stack of disjoint quasi-1D dipolar BECs.

Gross-Pitaevskii equations describing the BEC stack:

$$\imath\hbar\partial_t\psi_j(z) = \left[-\frac{\hbar^2}{2m}\partial_z^2 + \frac{g}{2\pi l_\perp^2}\left|\psi_j(z)\right|^2 \right.$$
$$\left. + \frac{g_d}{3}\sum_{m=0}^{N_m-1}\int\frac{dk_z}{2\pi}e^{\imath k_z z}\hat{n}_m(k_z)F_{m-j}(k_z)\right]\psi_j(z), \tag{V.1}$$

where $\hat{n}_m(k_z)$ is the Fourier transform of the axial density $n_m(z)$ at site m,

$$F_q(k_z) = \int\frac{dk_x dk_y}{\pi}\left(\frac{3k_y^2}{k_x^2+k_y^2+k_z^2} - 1\right)$$
$$\times\, e^{-\frac{1}{2}(k_x^2+k_y^2)l_\perp^2 - \imath k_y q\Delta}, \tag{V.2}$$

that we had already introduced in Eq. (IV.6) and $l_\perp = \sqrt{\hbar/m\omega_\perp}$ as the xy oscillator length, Δ as the lattice spacing, and $g = 4\pi a\hbar^2/m$. Note that for a fixed ratio $\Delta/l_\perp$ the physics of the system is governed by the values of g and g_d.

V.C

Linear regime: Bogoliubov modes

Starting from a homogeneous on-site linear density n_0 we are interested in the dynamics that follows the destabilization of the condensate after an abrupt change of the scattering length a. A substantial insight into the first

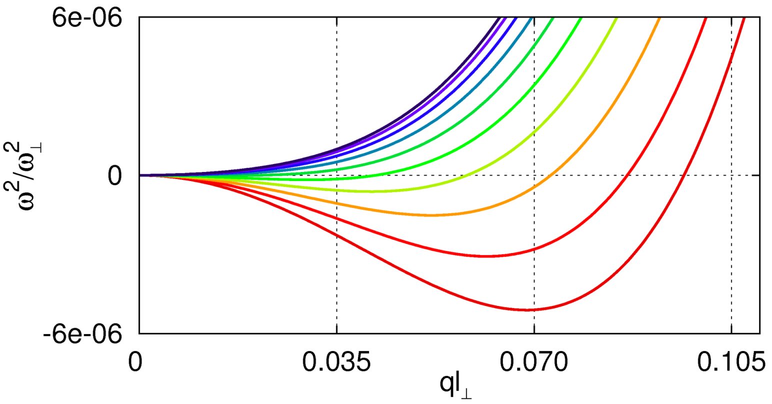

Figure V.2: Bogoliubov spectrum for a ^{52}Cr BEC ($\mu = 6\mu_B$, where μ_B is the Bohr magneton) with a density 10^{14} cm^{-3} and $a = -8.5a_0$ (a_0 is the Bohr radius), occupying $N_m = 10$ sites of a lattice with the intersite spacing $\Delta =$ 512 nm and a lattice depth of 13.3E$_R$ (recoil energy), which results in the $\omega_\perp = 2\pi\cdot 26.7$ kHz, and $l_\perp = 85.3$ nm. Here, $q_c = 0.07/l_\perp$.

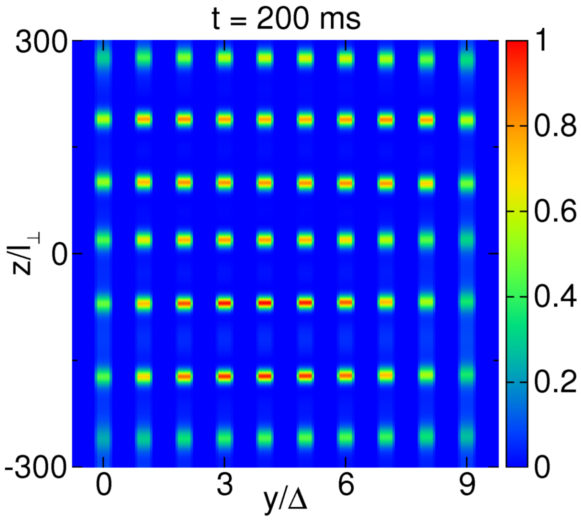

stages of the post-instability dynamics is provided by the analysis of the elementary excitations of the condensate. To this end we introduce a perturbation of the homogeneous solution, $\psi_j(z,t) = \left[\sqrt{n_0} + \chi_j(z,t)\right] e^{-\imath\mu_j t/\hbar}$, with $\chi_j(z,t) = u_j e^{\imath(zq-\omega t)} + v_j^* e^{-\imath(zq-\omega t)}$, where μ_j is the chemical potential in a site j, and q and ω are the z-momentum and the frequency of the elementary excitations, respectively. In appendix C we employ this ansatz into Eq.(V.1) and we derive the corresponding Bogoliubov-de Gennes equations yielding the excitation spectrum and the Bogoliubov coefficients u_j and v_j. Interestingly, even in absence of hopping, dipolar intersite interactions result in a collective character of the excitations that are shared by all sites. In consequence, the excitation spectrum acquires a band-like character [253] as depicted in Fig. V.2.

Modes with imaginary frequency are associated with dynamical instability. For nondipolar gases, intersite interactions are negligible and hence all transverse modes remain degenerated. As a result, modulational instability develops independently in each site and no correlated density pattern occurs during the post-instability dynamics. The situation dramatically changes for sufficiently large dipole moment, as the intersite interactions lift the degeneracy between the transverse modes. In particular, the most unstable mode becomes significantly more unstable than other modes, as shown in Fig. V.2, governing the BEC dynamics within the linear regime. Crucially, this most unstable mode is not only characterized by a z-momentum q_c (associated with the minimum of ω^2 in Fig. V.2) setting the modulational instability in each wire, but also by a transverse dependence along the y direction locking the density pattern between sites. As a result, during the first stages of the post-instability dynamics a correlated modulational instability develops. Interestingly, our numerical simulations predict that this phenomenon may be observed in existing chromium experiments [216] or even more pronouncedly

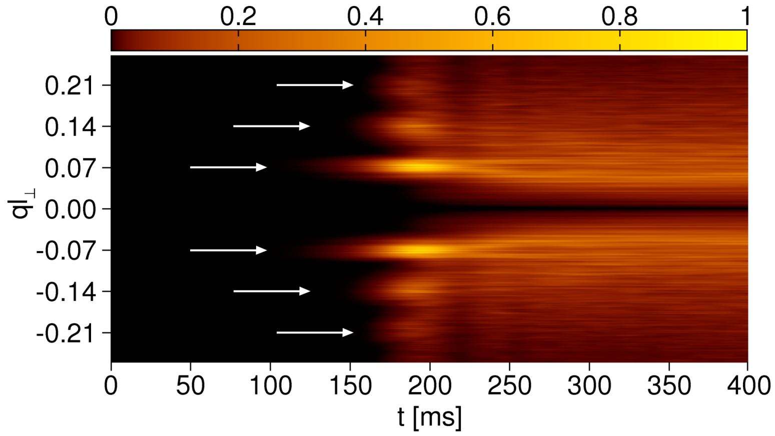

Figure V.3: (top) BEC wave function's density distribution (arb. unit) after 200 ms of time evolution for the same parameters as in Fig. V.2. For plotting purposes the y-width of the tubes has been magnified. (bottom) Dynamics of the Fourier transform of the associated column density $\Sigma(z,t)$ (arb. unit). The dominating $q=0$ peak has been removed for clarity and the remaining distribution has been normalized to the maximum. The arrows indicate the harmonics of q_c.

with recently condensed dysprosium [217] and erbium [219] atoms.

Fig. V.3 (top) depicts the case of a ^{52}Cr BEC destabilized by an abrupt change of $a>0$ into a sufficient $a<0$ by means of a Feshbach resonance. The numerical solution of Eq. (V.1) shows that despite the absence of inter-site hopping a correlated density pattern develops. As presented in Fig. V.3 (top) this instability pattern survives well into the nonlinear regime where the density modulation cannot be considered any more as a perturbation of the original homogeneous on-site BECs. In typical experiments the density alignements may be more easily monitored investigating the column density $\Sigma(z)=\sum n_m(z)$. Contrary to the uncorrelated case, for which $\Sigma(z)$ would show no clear structure, the correlated instability results in periodically modulated $\Sigma(z)$. Fig. V.3 (bottom) shows the dynamics of the Fourier transform of $\Sigma(z,t)$ which is clearly characterized by the appearance of harmonics of q_c (compare Fig. V.2 and Fig. V.3 (bottom)).

V.D

Filamentation

The density modulation depicted in Fig. V.3 (top) evolves into a correlated pattern of solitons. However, the solitons are created in an excited state, with both internal breathing excitation and center-of-mass motion. As a re-

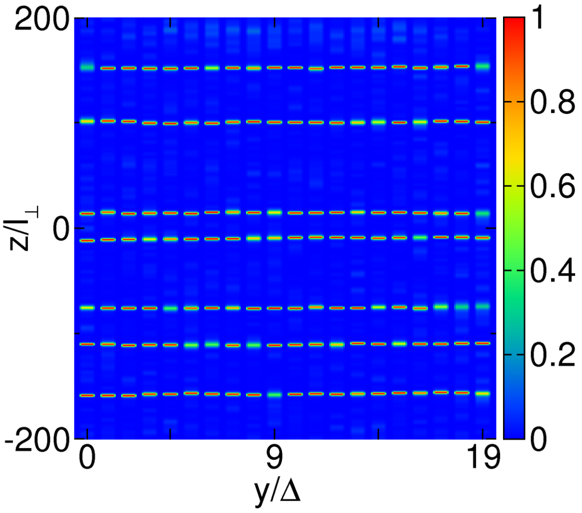

Figure V.4: Filamentation of solitons. Here, a snapshot of time evolution of the BEC density distribution (arb. unit) after 500 ms for, in particular, $N_m = 20$ lattice sites, $\mu = 18\mu_B$ and $a = -41.7a_0$. The remaining parameters are chosen as in the case of Fig. V.2.

sult, for insufficient dipolar interactions the correlated density modulation is destroyed during the subsequent nonlinear time evolution. Consequently, the positions of solitons at different sites become uncorrelated, not differing qualitatively from the case of nonpolar gases. Strong intersite interactions crucially change this picture as the correlated solitons in neighboring sites experience an attractive intersite potential. Approximating the solitons by Gaussians of width δ, such that $l_\perp \ll \delta, \Delta$, the binding energy for two solitons acquires the form

$$E_b = (-2g_d/\Delta^3)G(\delta/\Delta), \tag{V.3}$$

which differs from the binding energy between point-like solitons $(-2g_d/\Delta^3)$ by the regularization function

$$G(x) \simeq \frac{e^{1/4x^2}}{4\sqrt{2\pi}x^3}\left[(x^2+1)K_0\left(\frac{1}{4x^2}\right)+(x^2-1)K_1\left(\frac{1}{4x^2}\right)\right], \tag{V.4}$$

with K_n the modified Bessel function of second kind [327]. As a result of this intersite soliton attraction, and although the initial periodicity of the modulation (as that of Fig. V.3 (top)) is generally lost, self-assembled soliton filaments form spontaneously (Fig. V.4) when the center-of-mass kinetic energy of the solitons acquired in the post-instability dynamics cannot overcome the binding energy given by Eq. (V.3).

In order to analyze the dynamical filamentation quantitatively we introduce at this point the time-dependent dimer correlation function for sites m

and m'

$$G_{m,m'}(z,t) = \int dz'\, n_m(z',t) n_{m'}(z'+z,t) \tag{V.5}$$

and we define the normalized average dimer correlation

$$G^n(z,t) = G(z,t) / \int dz\, G(z,t), \tag{V.6}$$

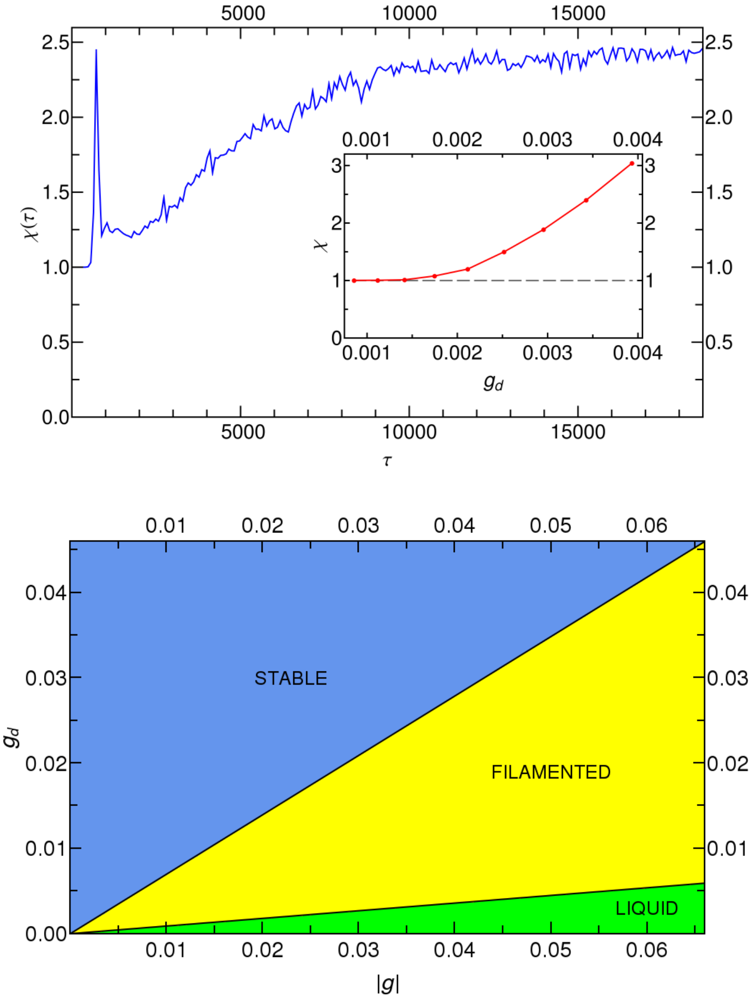

Figure V.5: (top) Function $\chi(\tau)$ for a typical case within the filamentation regime ($g = -0.019$, $g_d = 0.0034$, $\Delta = 6 l_\perp$). In particular, for the parameters that we employed in Fig. V.2 the time ($t = \tau/\omega_\perp$) that we here consider equals $t = 700$ ms. (inset) Time-averaged values of χ for long times, for different values of g_d and constant $g = -0.019$. (bottom) Phase diagram of the possible regimes for $g < 0$, $g_d > 0$.

with

$$G(z,t) = \frac{2}{N_m(N_m-1)} \sum_m \sum_{m'>m} G_{m,m'}(z,t). \tag{V.7}$$

A proper figure of merit describing the filamentation is provided by

$$\chi(t) = G^n(0,t)/\bar{G}^n(t), \tag{V.8}$$

where $\bar{G}^n(t) = \int dz\, G^n(z,t)^2$ is the mean value of $G^n(z,t)$. Such defined function $\chi(t)$ characterizes the tendency of the solitons at different sites to align into a filament.

In the following analysis we consider a simplified case of three lattice sites. Fig. V.5 (top) shows $\chi(t)$ for a typical case within the filamentation regime (see discussion below). The sharp initial peak indicates the formation of the correlated density pattern shared among all sites at the initial stage of the time evolution, as discussed in section V.C. Similarly to Fig. V.3, also here the pattern is quickly destroyed as the system enters the nonlinear regime. However, provided sufficently strong dipolar interactions, the intersite soliton binding E_b supports the formation of soliton filaments and in consequence $\chi(t)$ grows at larger times. Note that $\chi(t)$ eventually saturates remaining constant for times typically much longer than the usual experimental timescales.

In contrast, no filamentation occurs if the dipolar coupling is insufficient. In this case, at long times $\chi(t)$ averages to $\chi = 1$ indicating the absence of intersite soliton-soliton correlation. Hence, driving the g_d parameter from small to large values results in a transition from a nonfilamented into a filamented configuration (see the inset of Fig. V.5 (top)). Ultimately, for a sufficiently large g_d the repulsive on-site interactions compensate the attractive short-range interactions and the system remains stable.

As a result, we distinguish three distinct regimes of dynamics in a stack of 1D dipolar gases: (i) unstable uncorrelated (soliton liquid), (ii) unstable filamented, and (iii) stable. As shown in Fig. V.5 (bottom), for a fixed value of $\Delta/l_\perp$ these regimes are determined by the ratio $g_d/|g|$. For the considered case of three sites and $\Delta/l_\perp = 6$ the stability boundary line is given by $g_d/|g| = 0.70$, whereas the boundary line between the filamented and unstable nonfilamentated regimes occurs at $g_d/|g| = 0.09$. For the case of ^{52}Cr ($\mu = 6\mu_B$) the filamentation occurs for $5.2 < |a|/a_0 < 40.2$, whereas for ^{164}Dy ($\mu = 10\mu_B$) it occurs for $47.3 < |a|/a_0 < 367.0$.

We note that for a larger number of sites the system is more unstable due to the intersite attractive interactions [253]. Also, the boundary between filamented and unstable nonfilamented regimes is shifted towards larger g_d values due to the enhanced role of the string-like modes of the filaments. Hence, even though the qualitative results will not be affected, increasing the number of sites will in general reduce the filamentation regime.

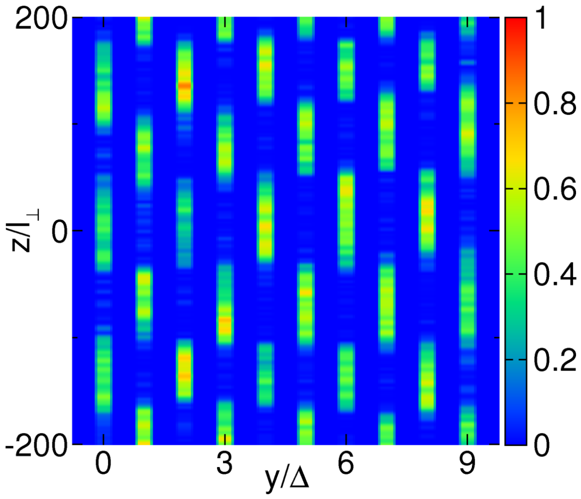

Figure V.6: Spontaneous crystallization of solitons in the case of negative g_d. Here, BEC density distribution (arb. unit) for $a = 306a_0$, $\mu = 36\mu_B$ and the remaining parameters such as in Fig. V.2.

V.E

Checkerboard soliton crystal

Interestingly, the sign of g_d may be inverted by means of transverse magnetic fields [271] or microwave dressing in the case of polar molecules [269]. Note that, although we consider this case for its theoretical simplicity, qualitatively the same results may be obtained orienting the dipoles along the tubes. In both of these cases the emerging instability is characterized by the most unstable Bogoliubov mode presenting a staggered y-dependence that results in an anticorrelated density pattern with maxima in a given site aligned with minima in the neighboring ones. Strikingly, for a sufficiently strong dipole moment, this anticorrelated structure formed at the initial stage of the post-instability dynamics seeds the formation of a permanent checkerboard soliton crystal in the nonlinear regime, as shown in Fig. V.6.

Remarkably, while purely repulsive interactions sustain 2D Wigner-like crystals proposed for polar molecules [325, 326], the crystal of solitons is self-maintained by a subtle interplay of dipolar intertube repulsion and intratube attraction. Due to the anticorrelated character of the density modulation, solitons in neighboring sites provide an effective potential barrier that prevents mutually attracting solitons in the same tube to come together, hence keeping the crystal stable.

In order to characterize quantitatively the dynamical formation of a soliton crystal, we employ the notation introduced in section V.D, defining the normalized averaged nearest-neighbor (NN) and next-to-nearest-neighbor (NNN) dimer correlations $G_\alpha^n(z,t) = G_\alpha(z,t)/\int dz\, G_\alpha(z,t)$, with $\alpha = NN, NNN$ and

$$G_{NN}(z,t) = \frac{1}{N_m - 1}\sum_m G_{m,m+1}(z,t), \tag{V.9}$$

$$G_{NNN}(z,t) = \frac{}{N_m - 2}\sum_m G_{m,m+2}(z,t), \tag{V.10}$$

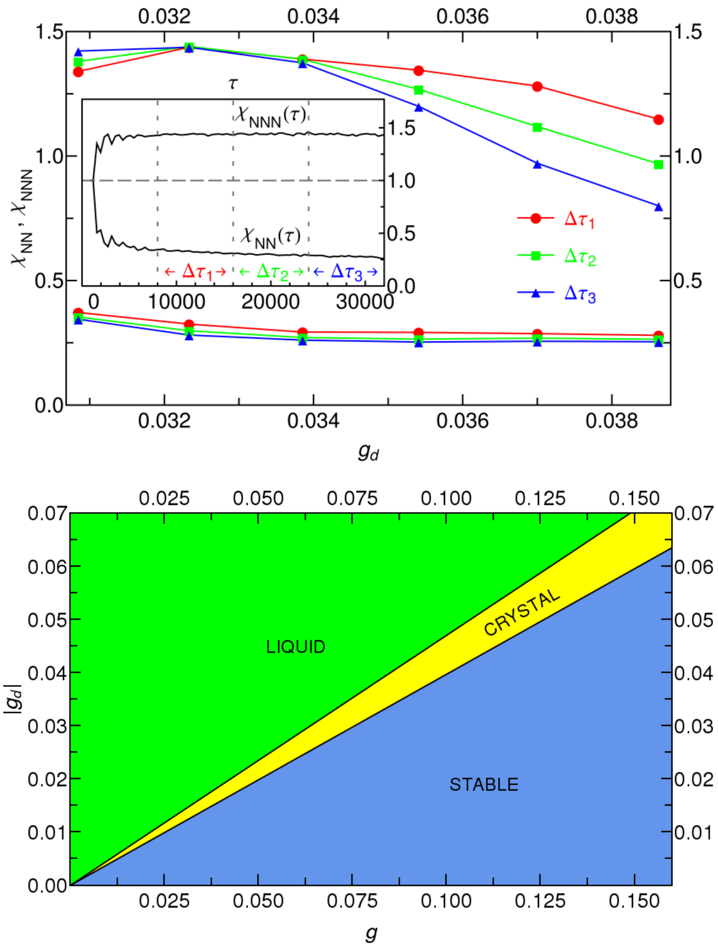

Figure V.7: (top) The inset shows a typical example of time evolution of $\chi_{NN}(\tau)$ and $\chi_{NNN}(\tau)$ within the soliton crystal regime ($g = 0.069$, $gd = -0.032$ and $\Delta = 6l_\perp$). We average $\chi_\alpha(\tau)$ within three different time intervals $\Delta\tau_{1,2,3}$, and we depict in the figure the corresponding averaged χ_α (●, ■, ▲) for different values of g_d and constant $g = 0.069$. Note that for $|g_d|/g > 0.47$, χ_{NNN} decreases in time, indicating destruction of the checkerboard crystal. In particular, for the parameters we employed in Fig. V.2, the time ($t = \tau/\omega_\perp$) that we here consider equals $t = 1200$ ms. (bottom) Phase diagram of the possible regimes for $g > 0$, $g_d < 0$.

and we introduce functions

$$\chi_{\alpha}(t) = G_{\alpha}^{n}(0,t)/\bar{G}_{\alpha}^{n}(t), \tag{V.11}$$

where $\bar{G}_{\alpha}^{n}(t) = \int dz\, G_{\alpha}^{n}(z,t)^2$ is the mean value of $G_{\alpha}^{n}(z,t)$. The checkerboard soliton arrangement is characterized by the NN anticorrelation ($\chi_{NN}(t) < 1$) and the NNN correlation ($\chi_{NNN}(t) > 1$). In the following we consider a particular case of four lattice sites. A generic example of $\chi_{NN}(t)$ and $\chi_{NNN}(t)$ time evolution within the crystalline regime (see discussion below) is depicted in the inset of Fig. V.7 (top).

As in the case of filamentation, the emergence of the soliton crystal is limited to a window of $|g_d|/g$ values. While for a weak dipolar coupling the system remains stable, a sufficiently large dipole moment value renders the attractive intratube interactions dominant and, in consequence, we observe the formation of the staggered soliton pattern. Note that this configuration, originating in the anticorrelated modulational instability emerging within the linear regime, is indeed a highly metastable state, as it maximizes NNN dipolar interactions. Crucially, however, our numerical simulations show that such soliton crystal state characterized by $\chi_{NN}(t) < 1$ coinciding with $\chi_{NNN}(t) > 1$ remains stable well beyond typical experimental timescales, being hence effectively permanent. Beyond a critical value of the dipolar coupling the NNN repulsion destroys the NNN anticorrelation and hence the crystal.

The instability properties of the soliton crystal may be studied by considering the average χ_{α} for different time windows, as depicted in Fig. V.7 (top). For all g_d values within the unstable regime the NN anticorrelation function $\chi_{NN}(t) < 1$ remains constant at all times. In contrast, depending on the value of the g_d parameter, $\chi_{NNN}(t)$ function shows two distinctive types of time dependence. Namely, while in the window of the crystallization regime $\chi_{NNN}(t)$ saturates at a value indicating NNN anticorrelation and so the emergence of a stable soliton crystal. Contrastingly, for large dipolar interactions the initially anticorrelated χ_{NNN}, which originates in the linear regime, decreases in time indicating destruction of the checkerboard pattern.

Hence, for negative g_d values we identify three distinct regimes depicted in Fig. V.7 (bottom): (i) a stable regime for small dipole values, (ii) an unstable regime intrinsically characterized by the dynamical formation of a checkerboard soliton crystal, and (iii) a strong dipolar interactions regime in which only nearest neighbor anticorrelation is preserved while the next-to-nearest neighbor correlation is lost (soliton liquid). In analogy to the filamentation phenomenon, for a fixed $\Delta/l_{\perp}$ value the regimes boundaries depend solely on the $|g_d|/g$ ratio. For $\Delta/l_{\perp} = 6$, the crystalliztion regime occurs for $0.40 < |g_d|/g < 0.47$, which for ^{52}Cr (^{164}Dy) requires $7.7 < a/a_0 < 9.1$ ($70.0 < a/a_0 < 82.9$).

V.F

Summary

In conclusion, the dipolar intersite interactions in a destabilized dipolar BEC confined in a stack of quasi-1D tubes induce an interesting dynamics characterized by the development of a correlated modulational instability in the nonoverlapping sites. For a sufficiently large dipole moment this density modulation seeds the spontaneous self-assembly of soliton filaments or a soliton checkerboard crystal, depending on the sign of the dipolar interactions. Contrary to filaments and crystals of individual molecules, filaments and crystals of solitons self-assemble spontaneously merely by simple destabilization of the condensate. Moreover, we expect that due to the many-body character of the constituent solitons the dipole moment necessary for observing these structures may be significantly reduced and that they may be attainable with partially polarized polar molecules or highly magnetic atoms, paving a promising route towards the first realization of 2D patterns of solitons in ultracold gases and, to the best of our knowledge, in nonlinear optics as well.

❧

VI

Faraday patterns in coupled quasi-1D dipolar BECs

We study Faraday patterns in quasi-one-dimensional dipolar Bose-Einstein condensates with parametrically driven dipolar interactions. We show that in the presence of a roton minimum in the excitation spectrum, the emergent Faraday waves differ substantially in two- and one-dimensional geometries, providing a clear example of the key role of confinement dimensionality in dipolar gases. Moreover, Faraday patterns constitute an excellent tool to study nonlocal effects in polar gases, as we illustrate for two parallel quasi-one-dimensional dipolar condensates. Nonlocal interactions between the condensates give rise to an excitation spectrum characterized by symmetric and antisymmetric modes, even in the absence of hopping. We show that this feature, absent in nondipolar gases, results in a critical driving frequency at which a marked transition occurs between correlated and anticorrelated Faraday patterns in the two condensates. Interestingly, at this critical frequency, the emergent Faraday pattern stems from a spontaneous symmetry-breaking mechanism.

VI.A

Introduction

In chapters IV and V we investigated the consequences of the anisotropy and long-range character of the dipole-dipole interactions in the context of soliton molecules and spontaneous formation of soliton self-assemblies, i.e., filaments and crystals. Yet, the wealth of phenomena originating in DDI extends to the domain of the so-called Faraday patterns (waves).

Faraday patterns constitute a paradigmatic example of pattern formation in periodically driven systems [328, 329] ranging from classical fluids [330] (see Fig. VI.1), through multimode lasers [331] and superfluid helium [332]. Interestingly, Faraday patterns may be observed in BECs by modulating the nonlinearity resulting from the interatomic interactions [333–338], as shown in recent experiments [339]. Faraday patterns in Bose-Einstein condensates may be directly linked to the spectrum of elementary excitations (see sec-

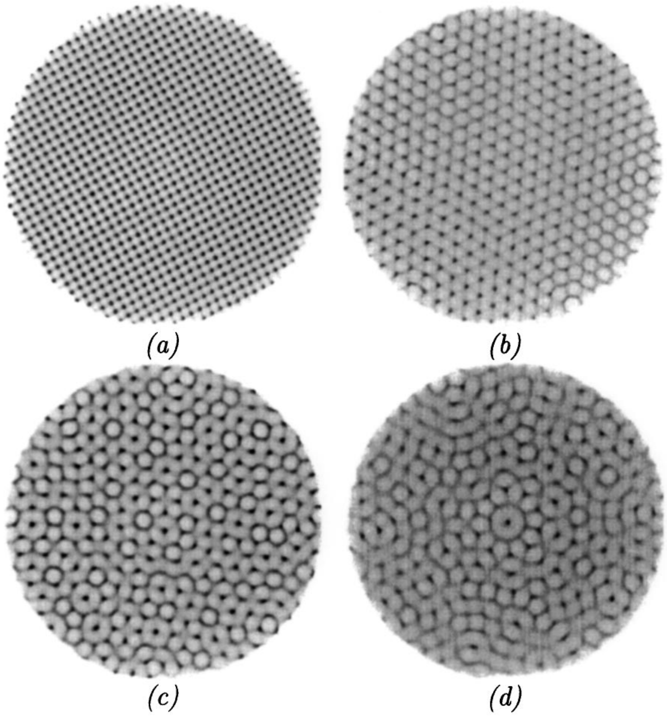

Figure VI.1: Faraday patterns on a surface of a classical fluid (here, silicon oil), subjected to oscillations of the vertical acceleration. Different frequencies of the oscillations result in different symmetries of the created density pattern: (a) square symmetry, (b) hexagonal symmetry, (c) 8-fold quasi-periodic, (d) 10-fold quasiperiodic. Reprinted from Phys. Rev. Lett. **78**, 4043 (1997).

tion II.C.8 and section III.E for the nondipolar and dipolar gases, respectively), and in this sense provide an excellent insight into fundamental properties of the condensates. In nondipolar gases the Faraday pattern selection is determined uniquely for each modulation frequency due to the monotonically growing character of the excitation energy [340]. Interestingly, this is no longer the case for dipolar BECs with a roton-like minimum in the excitation spectrum (see discussion in Sec. III.E). As a result, it has been shown that Faraday patterns in two-dimensional dipolar condensates present remarkable qualitative novel features [256]

In this chapter, we analyze quasi-one-dimensional dipolar condensates with periodically driven dipolar interactions. We demonstrate that Faraday patterns provide a clear example of the nontrivial role of confinement dimensionality in dipolar gases, showing that in the presence of a roton-like minimum in the excitation spectrum, Faraday patterns in a quasi-1D trap differ fundamentally with respect to the 2D case [256]. Moreover, Faraday patterns provide as well an excellent tool for a study of nonlocal effects in dipolar condensates, as we illustrate with two parallel quasi-1D BECs, in the absence of tunneling. The nonlocal dipolar interactions between both BECs lead to an unfolding of the excitation spectrum into symmetric and antisymmetric modes with respect to the transposition of the two condensates. We show that, as a consequence, at a critical driving frequency a transition between correlated (symmetric) and anticorrelated (antisymmetric) Faraday patterns in the two BECs occurs. For the critical driving the emergent Faraday pattern differs from one realization to another, resulting from a spontaneous symmetry-breaking mechanism.

The chapter is structured as follows. In Sec. VI.B we introduce the model for periodically driven quasi-1D dipolar condensates. Section VI.C is devoted to Faraday patterns in a single quasi-1D BEC, with a focus on the differences as compared to 2D condensates. Section VI.D is dedicated to the effects of the intercondensate dipolar interactions on the Faraday pattern selection in two parallel disjoint quasi-1D dipolar condensates. We conclude in section VI.E.

VI.B

Model

In the following, we consider quasi-1D dipolar BECs, either in a single trap (Sec. VI.C) or in two parallel traps (Sec. VI.D). Since the former case may be considered as a particular realization of the latter, we present in this section the general formalism for parallel quasi-1D BECs aligned along the z axis, and separated along the y axis by a distance Δ, as presented already, e.g., in Fig. IV.1. We assume the potential barrier separating both quasi-1D BECs sufficiently large to suppress any hopping between them. Each condensate experiences a strong harmonic confinement of frequency $\omega_\perp$ in the x-y plane and no confinement along the z direction. The atoms possess a magnetic dipole moment μ (the results are equally valid for electric dipoles) oriented by an external field along the y axis. In this chapter we employ dimensionless expressions, using units of frequency $\omega_\perp$ and length $l_\perp = \sqrt{\hbar/M\omega_\perp}$, with M the particle mass.

Due to the strong x-y confinement we assume that the system remains in the ground state of the x-y harmonic oscillator (this condition is self-consistently verified), and employ the nonlocal nonlinear Schrödinger formalism developed in appendix A for a stack of quasi-1D dipolar BECs, to obtain the coupled equations for the wave functions $\psi_j(z)$ in traps $j = 1, 2$:

$$\begin{aligned} i\partial_t \psi_j(z) = \Bigg[& -\frac{1}{2}\partial_z^2 + g n_j(z) \\ & + \frac{2\pi}{3} g_d \sum_m \int dk_z e^{ik_z z} \hat{n}_m(k_z) F_{m-j}(k_z) \Bigg] \psi_j(z). \end{aligned} \tag{VI.1}$$

Short-range interactions are characterized by the coupling constant $g = g^{3\mathrm{D}} n_0 / 2\pi\hbar\omega_\perp l_\perp^3$, where n_0 is the linear density, and $g^{3\mathrm{D}} = 4\pi a_{sc}\hbar^2/M$, with a_{sc} the s-wave scattering length. The DDI are determined by the coupling constant $g_d = g_d^{3\mathrm{D}} n_0 / 2\pi\hbar\omega_\perp l_\perp^3$, where $g_d^{3\mathrm{D}} = \mu_0\mu^2/4\pi$, with μ_0 the vacuum permeability. In Eq. (VI.1), $\hat{n}_m(k_z)$ is the Fourier transform of the linear density $n_m(z) = \left|\psi_m(z)\right|^2$, and

$$F_q(k_z) = \int_0^\infty dk \frac{k e^{-\frac{1}{2}k^2}}{k^2 + k_z^2} \left[\left(k^2 - 2k_z^2\right) J_0(kq\Delta) - 3k^2 J_2(kq\Delta) \right], \tag{VI.2}$$

derived in Eq. (A.16), with $J_n(x)$ as the Bessel functions of the first kind.

In the following we consider a parametric modulation of the dipole-dipole interactions

$$g_d(t) = \overline{g}_d(1 + 2\alpha\cos(2\omega t)), \tag{VI.3}$$

where α characterizes the modulation strength. Such modulation may be implemented with intensity oscillations of the polarizing electric field for the case of polar molecules, or with additional transverse magnetic fields, which lead to a precession of the dipole moment orientation, for the case of magnetic dipoles.

The modulation of g_d induces Faraday waves. With the aim of examining the growth of such patterns, we introduce the following ansatz for the wave functions:

$$\psi_j(z,t) = \psi_{j_H}\left(1 + A_j(t)\cos(qz)\right), \tag{VI.4}$$

which describes well the physics of the pattern in the linear regime, where the modulation is weak and we may consider each momentum component q of the pattern separately. In Eq. (VI.4), we introduce the complex amplitude $A_j(t) =$

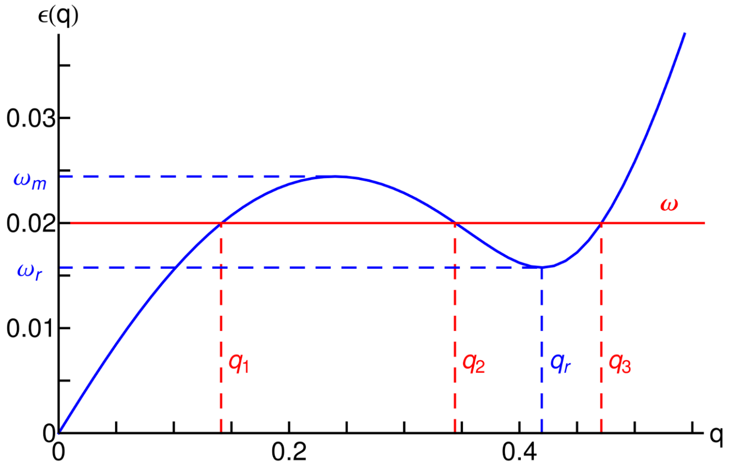

Figure VI.2: Excitation spectrum $\epsilon(q)$ of a single quasi-1D dipolar BEC, with $g = -0.1007$, $g_d = 0.0629$. Note the roton minimum at $\omega_r = \epsilon(q_r)$ and the maxon maximum at ω_m. For a driving frequency $\omega_r < \omega < \omega_m$ there are three possible momenta $q_{1,2,3}$ obeying the resonance condition $\epsilon(q) = \omega$.

$u_j(t)+iv_j(t)$, which determines the perturbation from the initial homogeneous solution $\psi_{jH} = \exp\{-i\overline{\mu}_j[t+(\Omega_j/\omega)\sin(2\omega t)]\}$, where $\Omega_j = \alpha(1-g/\overline{\mu}_j)$, and $\overline{\mu}_j = g + \frac{2\pi}{3}\overline{g}_d \sum F_{m-j}(0)$ is the chemical potential. Inserting Eqs. (VI.3) and (VI.4), into Eq. (VI.1), and linearizing in A_j we arrive at the system of equations describing the modulation dynamics

$$\frac{d^2u_j}{dt^2} + \frac{q^2}{2}\left[\left(\frac{q^2}{2}+2g\right)u_j + \frac{4\pi}{3}g_d(t)\sum_m u_m F_{|m-j|}(q)\right] = 0, \qquad \text{(VI.5)}$$

that we derive in detail in appendix D.

VI.C

Faraday Patterns in a single quasi-1D dipolar BEC

We consider in this section the case of a single condensate, being particularly interested in the differences between the emergent Faraday patterns in a quasi-1D trap and those predicted in Ref. [256] for a 2D condensate. By applying a similar Bogoliubov analysis as the one presented in Chapter V, and discussed in detail in appendix C, we obtain the spectrum of elementary excitations in the considered case (see Fig. VI.2):

$$\epsilon(q) = \sqrt{\frac{q^2}{2}\left(\frac{q^2}{2}+2g+\frac{4\pi}{3}g_dF_0(q)\right)} \qquad \text{(VI.6)}$$

where

$$F_0(q) = 1 + \frac{3}{2} q^2 e^{q^2/2} \mathrm{Ei}\left(-q^2/2\right), \tag{VI.7}$$

with $\mathrm{Ei}(x)$ the exponential integral function. Next, employing Eqs. (VI.5) and (VI.6), in accordance with the appendix D, we arrive at the corresponding Mathieu equation:

$$\frac{d^2u}{dt^2} + \left[\epsilon^2(q) + 2\omega^2 b(q,\omega,\alpha)\cos(2\omega t)\right] u = 0 \tag{VI.8}$$

with

$$b(q,\omega,\alpha) = \frac{2\pi}{3\omega^2} \bar{g}_d \alpha q^2 F_0(q). \tag{VI.9}$$

Following Floquet theorem [341], the solutions of Eq. (VI.8) are of the form $u(t) = e^{\tilde{\sigma}t} f(t)$ where $f(t) = f(t+\pi/\omega)$ and $\tilde{\sigma}(q,\omega,\alpha)$ is the Floquet characteristic exponent, which can be found numerically. If the real part $\sigma \equiv \mathrm{Re}(\tilde{\sigma}) > 0$, the homogeneous quasi-1D BEC becomes dynamically unstable and Faraday patterns emerge. The typical wave length of the pattern will be determined by the most unstable mode, i.e., that with the largest σ. In the limit of small driving amplitude, $\alpha \to 0$, the properties of the pattern are governed by momenta q obeying parametric resonances $\epsilon_n(q) = n\omega$.

Contrary to nondipolar BECs with a monotonic spectrum $\epsilon(q)$, dipolar gases may offer a more complex roton-maxon spectrum [211] (Fig. VI.2). As a consequence of this nonmonotonic character, for a specific range of ω, between the roton and maxon frequencies (ω_r and ω_m, respectively) there are three values $q_1 < q_2 < q_3$ satisfying the resonance condition $\epsilon(q) = \omega$. Figure VI.3 shows the stability diagram for a driving frequency in this particular window. As expected, for small amplitudes α, the three instability tongues (white regions) correspond exactly to $q_{1,2,3}$ (Fig. VI.2). This raises an interesting question about which of the three modes dominates the pattern formation. For a 2D geometry, Ref. [256] showed that when modulating dipole-dipole interactions, the most unstable mode corresponds to the intermediate momentum $q_2 < q_r$, with q_r the roton momentum. Crucially, as we show below, this is not the case in a quasi-1D dipolar condensate. This striking contrast between quasi-1D and 2D predictions illustrates once more the key role played by the trapping geometry in dipolar gases.

The problem of the most unstable mode is best understood employing a series expansion of the Floquet exponent with small parameter $b(q,\omega,\alpha)$ [335, 342, 343], which, for the first parametric resonance $\epsilon(q) = \omega$, yields $\sigma \simeq b(q,\omega,\alpha)/2 \propto q^2 F_0(q)$. Remarkably, in contrast to the 2D case, we find that the most unstable mode corresponds to the largest momentum $q_3 > q_r$ (solid line in Fig. VI.3). Fig. VI.4 depicts a momentum of the most unstable mode as a function of the driving frequency ω. The plot confirms that for all frequencies within the window $\omega_m < \omega < \omega_r$ the momentum characterizing the most unstable mode is larger than the roton momentum, contradicting the

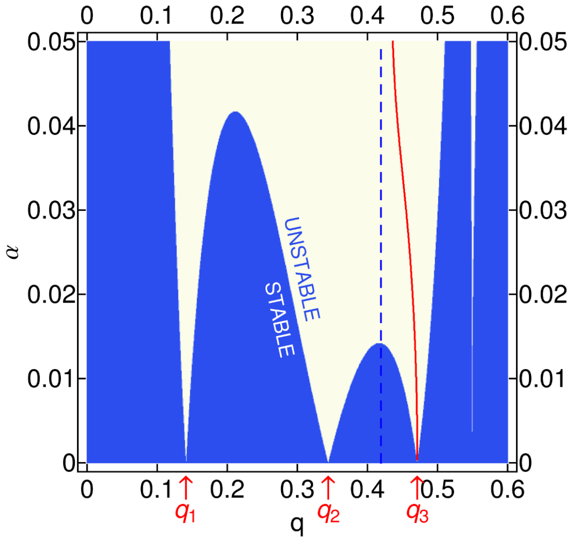

Figure VI.3: Stability diagram for the parameters of Fig. VI.2, as a function of the perturbation strength α and momentum q. The unstable region is depicted in white. The solid line indicates the most unstable mode, and the dashed line the roton momentum.

prediction for a 2D pancake geometry [256]. For $\omega < \omega_r$, alike in the 2D case, the observed modulations are dominated by higher resonances with q in the

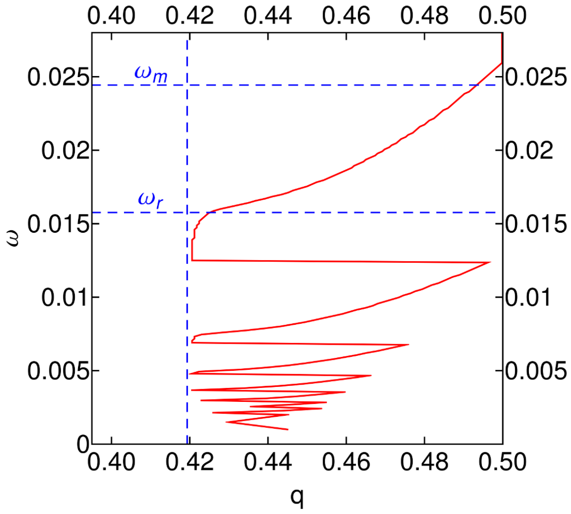

Figure VI.4: Most unstable momentum q as a function of the driving frequency ω for the parameters of Fig. VI.2, with $\alpha = 0.01$. The horizontal dashed lines indicate the roton and maxon frequencies ($\omega_{r,m}$), and the vertical line the roton momentum.

vicinity of q_r. However, unlike the 2D scenario, even in this regime the most unstable mode in a quasi-1D BEC is characterized by $q > q_r$. We emphasize that the different nature of the Faraday pattern reported here stems solely from the quasi-1D character of the condensate, which leads to a specific momentum dependence of $b(q,\omega,\alpha)$ that differs from that in 2D.

We have simulated numerically the time evolution of the nonlocal nonlinear Schrödinger equation (VI.1) with the parametrically driven nonlinearity, according to Eq. (VI.3). The emergent pattern has been examined by means of Fourier transform of the condensate density, which confirmed the results for the most unstable mode that we obtained within the Mathieu analysis.

VI.D

Faraday Patterns in two quasi-1D dipolar BECs

We now turn to the study of Faraday patterns in two parallel quasi-1D dipolar BECs. For nondipolar BECs, in the absence of hopping, each BEC behaves independently, and hence an experiment with two BECs reduces to two uncorrelated experiments with a single condensate. The situation is radically different in dipolar BECs, since, despite the absence of hopping, the nonlocal character of the dipolar potential gives rise to a coupling between the two BECs, with the strength of the intercondensate interactions governed by $F_1(k_z)$. These nonlocal interactions lead to a collective character of the elementary excitations that are shared among the two quasi-1D condensates,

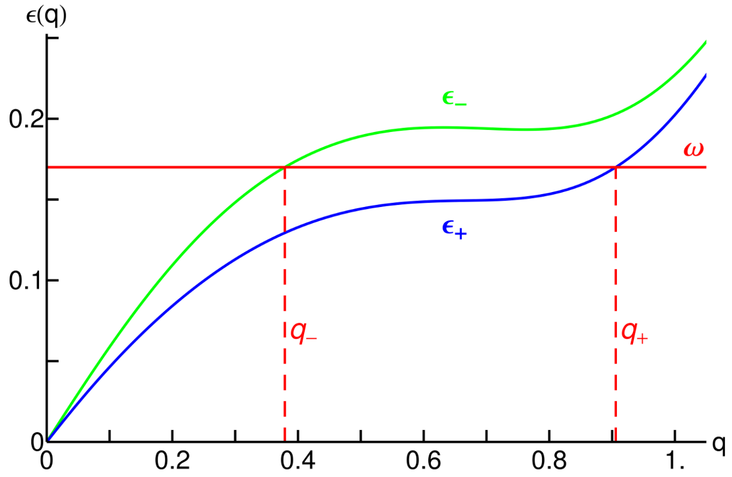

Figure VI.5: Elementary excitations of two parallel quasi-1D dipolar BECs, for $g = -0.0629$, $\overline{g}_d = 0.1749$, and $\Delta/l_\perp = 6$. Note the two branches of the elementary excitations $\epsilon_\pm(q)$, corresponding, respectively, to symmetric and antisymmetric modes with respect to the transposition of traps $j = 1 \leftrightarrow j = 2$.

alike the many tubes case discussed in Chapter V. Consequently, the excitation spectrum unfolds into two branches (see appendix C)

$$\epsilon_{\pm}(q) = \sqrt{\frac{q^2}{2}\left(\frac{q^2}{2} + 2g + \frac{4\pi}{3} g_d \left(F_0(q) \pm F_1(q)\right)\right)}, \tag{VI.10}$$

which correspond, respectively, to symmetric and antisymmetric states with respect to the transposition of traps $j = 1 \leftrightarrow j = 2$.

Interestingly, this implies that a periodic modulation of the dipolar interactions yields two different parametric resonances for each driving frequency $\omega = \epsilon_{\pm}(q_{\pm})$, even in the absence of the roton minimum (see Fig. VI.5). Note, that the patterns are characterized not only by their momentum $q_{\pm}$ but also by their symmetric $(+)$ or antisymmetric $(-)$ character. In analogy to Sec. VI.C, the double solution raises a fundamental question about which of these two modes is the most unstable, and hence provides the dominant Faraday pattern. We stress that this nontrivial physics stems directly from the intercondensate interactions, which lead to the splitting between the two branches in the spectrum, being a qualitatively new feature of dipolar condensates.

Similarly to the previous section, we employ Eqs. (VI.5) for $j = 1, 2$, and the spectra (VI.10). In turn, we obtain (see appendix D) two decoupled Mathieu equations for the symmetric and antisymmetric combinations $u_{\pm} = u_1 \pm$

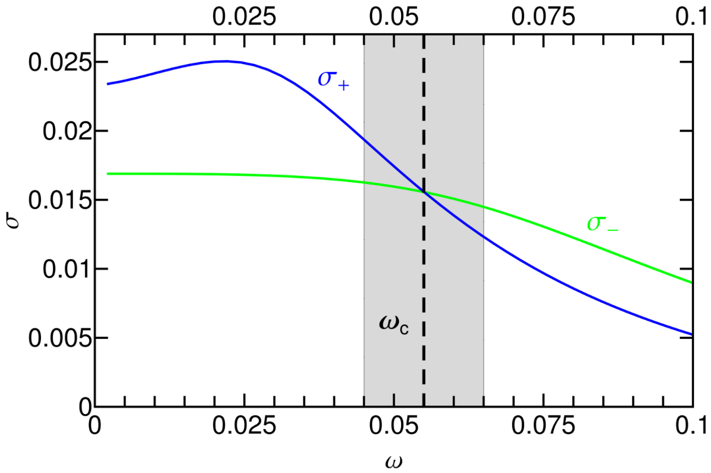

Figure VI.6: Real part $\sigma_{\pm}$ of the Floquet exponent, corresponding to the the first parametric resonance for the symmetric and antisymmetric excitation branches $\epsilon_{\pm}(q) = \omega$, as a function of the driving frequency ω. Note that at a critical frequency $\omega_c = 0.055$, both exponents are equal, $\sigma_+ = \sigma_-$, indicating a transition between the symmetric and the antisymmetric Faraday pattern. In the figure we employ $g = -0.0435$, $\overline{g}_d = 0.0437$, $\Delta = 6 l_{\perp}$, and $\alpha = 0.02$.

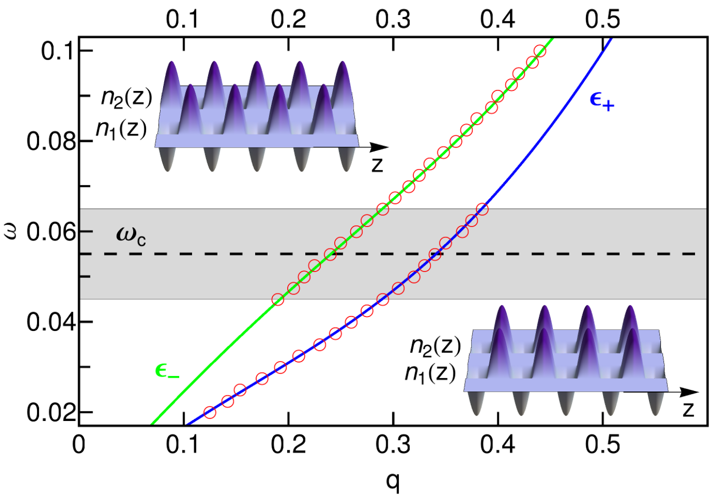

Figure VI.7: Analysis of the pattern selection as a function of the driving frequency ω, in the neighborhood of the critical frequency ω_c (for the same parameters as in Fig. VI.6). The solid lines represent the excitation branches. For each ω we indicate with a circle a momentum value where the numerical Fourier transform $\hat{n}_j(k_z)$ of the Faraday pattern shows a clear maximum. For ω well below (above) ω_c we observe a single peak at q_+ (q_-) indicating that a symmetric (antisymmetric) Faraday pattern emerges (see insets). In the vicinity of ω_c (shaded region), both modes are equally unstable and we observe the two corresponding peaks occurring simultaneously in the Fourier transform (see text).

u_2:

$$\frac{d^2u_\pm}{dt^2} + \left[\epsilon_\pm^2(q) + 2\omega^2 b_\pm(q,\omega,\alpha)\cos(2\omega t)\right]u_\pm = 0 \tag{VI.11}$$

with

$$b_\pm(q,\omega,\alpha) = \frac{2\pi}{3\omega^2}\overline{g}_d\alpha q^2(F_0(q) \pm F_1(q)), \tag{VI.12}$$

to which we apply the Floquet analysis employed in the study of Eq. (VI.8). As in the case of a single BEC, the first parametric resonances $\epsilon_\pm(q_\pm) = \omega$ are characterized by the Floquet exponent $\sigma_\pm \simeq b_\pm(q,\omega,\alpha)/2 \propto q^2(F_0(q) \pm F_1(q))$, and the emerging Faraday pattern is determined, for each driving frequency separately, by the mode with the largest σ. Remarkably, the involved momentum dependence of $F_0(q) \pm F_1(q)$ leads to an intricate relation between the Floquet exponents and the driving frequency ω, as presented in Fig. VI.6.

Crucially, the curves $\sigma_\pm(\omega)$ cross at a critical frequency ω_c. In consequence, we expect a distinct transition, as a function of the driving frequency ω, between the symmetric Faraday pattern for $\omega < \omega_c$ and the antisymmetric pattern for $\omega > \omega_c$. Such transition is marked by an abrupt change of the patterns from a maximum-maximum alignment (correlated patterns) to a maximum-minimum alignment (anticorrelated patterns), as depicted in the corresponding insets of Figs. VI.7 and VI.8. Moreover, for $\omega = \omega_c$ the patterns in both condensates exhibit a pronounced change of the wavelength of the modulation, from $l_+ = 2\pi/q_+(\omega_c)$ to $l_- = 2\pi/q_-(\omega_c)$.

This transition has been confirmed by means of direct numerical simulations of Eqs. (VI.1), with the parametric driving governed by Eq. (VI.3). As for a single condensate, we Fourier transform the density of each condensate to obtain the dominant momenta of the emergent Faraday patterns. The results, in the vicinity of the critical frequency ω_c, are depicted in Fig. VI.7, where, on top of the spectra $\epsilon_\pm$, for each driving frequency ω we indicate with a circle the momentum value where the numerically evaluated $\hat{n}_j(k_z)$ shows a marked maximum. We find that, in agreement with the results for $\sigma_\pm(\omega)$ presented in Fig. VI.6, for ω well below ω_c the pattern presents a single momentum component at q_+, being characterized by a correlation between the patterns in both quasi-1D BECs. In contrast, for ω well above ω_c a single momentum component q_- is observed, and the patterns in the two quasi-1D BECs are anticorrelated.

In order to quantify the transition between correlated and anticorrelated patterns we introduce the correlation coefficient

$$r = \frac{\int dz\, S_{n_1}(z) \cdot S_{n_2}(z)}{\sqrt{\int dz\, S_{n_1}^2(z)} \cdot \sqrt{\int dz\, S_{n_2}^2(z)}}, \tag{VI.13}$$

where $S_{n_j}(z) = n_j(z) - \overline{n_j}$, with $\overline{n_j}$ the average density in a trap j. Pattern correlation is then characterized by $r > 0$, whereas anticorrelation leads to $r < 0$. Fig. VI.8 illustrates the radically different time evolution of the correlation coefficient below and above the critical driving ω_c. Clearly, for frequencies sufficiently smaller (larger) than ω_c the system arrives at perfectly correlated (anticorrelated) pattern with $r = 1$ ($r = -1$).

An interesting scenario occurs for driving frequencies in the vicinity of the critical ω_c (shaded region in Figs. VI.6 and VI.7), where both the symmetric pattern with wavelength l_+ and the antisymmetric pattern with wavelength l_- are equally unstable. As a result, the Fourier transform of the density in each quasi-1D BEC shows a simultaneous appearance of both momentum peaks, q_+ and q_- (see Fig. VI.7).

Note that at $\omega = \omega_c$, not only $\epsilon_+(q_+) = \epsilon_-(q_-)$ but also $b_+(q_+, \omega, \alpha) = b_-(q_-, \omega, \alpha)$ and thus the two Mathieu equations (VI.11) for u_+ and u_- become identical. This symmetry is however spontaneously broken in experiments due to quantum and thermal fluctuations, which lead to different initial conditions (populations) for both modes, that change randomly from one realization to another. This spontaneous symmetry-breaking mechanism is best studied quantitatively by considering the relative weight of the momentum peaks at q_+ and q_- in the Fourier-transform of the density $\hat{n}(k_z)$. To this end, we

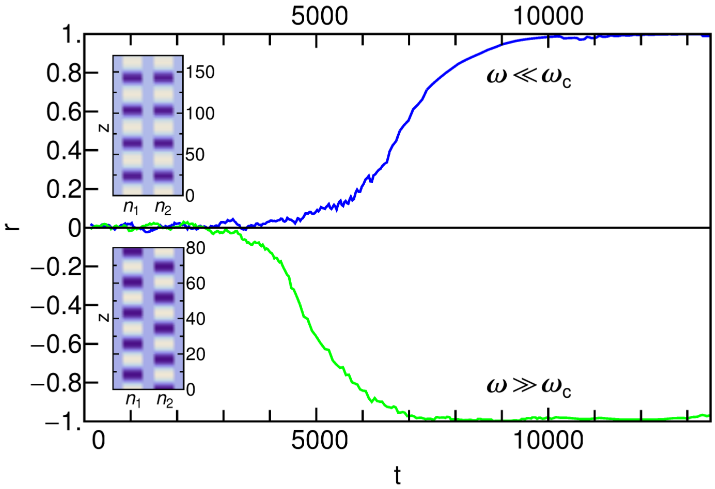

Figure VI.8: Correlation function $r(t)$ for the same parameters as in Fig. VI.7 ($\omega_c = 0.055$). The upper curve, which corresponds to $\omega = 0.025 < \omega_c$, approaches $r = 1$ indicating a perfectly correlated pattern in both quasi-1D traps. The lower curve, which corresponds to $\omega = 0.08 > \omega_c$, reaches $r = -1$ proving a perfect anticorrelation between the Faraday patterns in the two traps. The insets show the corresponding numerical results for the density distribution $n_j(z)$ for $t = 11000$, with the bright (dark) colors indicating density maxima (minima). Naturally, for sufficiently long times, well beyond the linear regime, the Faraday patterns and their correlations are eventually destroyed.

define the imbalance parameter

$$\chi(t) = \frac{\hat{n}(q_+,t) - \hat{n}(q_-,t)}{\hat{n}(q_+,t) + \hat{n}(q_-,t)}. \tag{VI.14}$$

For ω well below or above ω_c, once the pattern emerges, $\chi(t) = \pm 1$. In the vicinity of ω_c, however, the imbalance parameter $\chi(t)$ shows a clear periodicity with frequency 2ω (see Fig. VI.9). Note that these oscillations do not result from nonlinear competition, as they occur well within the linear regime. In fact, the 2ω oscillations of $\chi(t)$ originate in different, spontanously chosen, initial conditions for u_+ and u_-, which lead to their different time evolution that can be well approximated by $u_\pm(t) = (u_\pm^c \cos(\omega t) + u_\pm^s \sin(\omega t)) \exp(\sigma \omega t)$, where $u_\pm^{c/s}$ are the constants determined by the initial conditions. Furthermore, spontaneous symmetry-breaking leads to a different result for the imbalance $\chi(t)$ from one realization to another, what we have confirmed by considering small random differences in the initial conditions for our numerical simulations of Eqs. (VI.1).

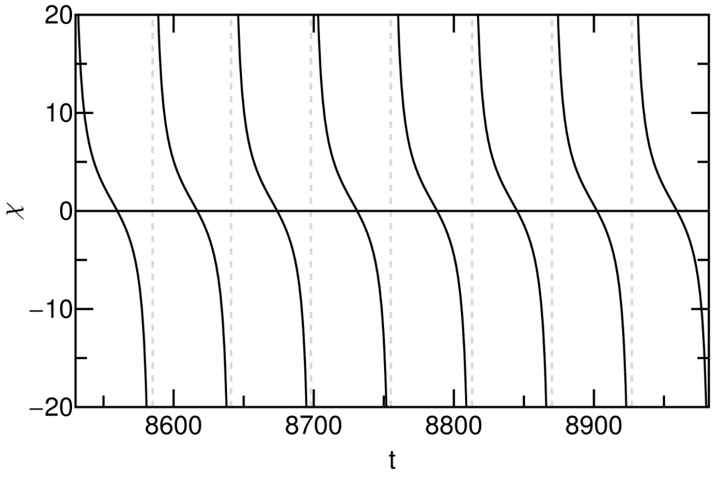

Figure VI.9: Population imbalance $\chi(t)$ between the two peaks at $q_{\pm}(\omega_c)$ for the critical driving $\omega = \omega_c$ (for the same parameters as Fig. VI.7). Note the 2ω periodicity ($T = \pi/\omega = 57.1$) that stems from a spontaneous symmetry breaking mechanism (see text).

VI.E

Summary

Faraday patterns in dipolar BECs are crucially dependent on the unique properties of the dipole-dipole interactions. In particular, due to the long-range anisotropic nature of the dipolar interactions, the character of the Faraday patterns depends strongly on the dimensionality of the condensates. We have shown that for periodically modulated dipolar interactions, Faraday patterns in 2D and 1D geometries differ substantially in the presence of a roton minimum in the excitation spectrum. Moreover, for parallel quasi-1D dipolar BECs, the intercondensate interactions lead, even in the absence of hopping, to an excitation spectrum characterized by symmetric and antisymmetric modes. This, in turn, gives rise at a critical driving frequency to a marked transition between correlated and anticorrelated Faraday patterns in the two condensates. Interestingly, at this transition point the Faraday pattern selection stems from a spontaneous symmetry breaking mechanism.

❧

VII

Roton confinement in trapped dipolar BECs

Roton excitations constitute a key feature of dipolar gases, connecting these systems with superfluid helium. We show that the density dependence of the excitations spectrum results in a spatial roton confinement, which becomes particularly relevant in pancake dipolar condensates with large aspect ratios. We demonstrate that this confinement is crucial for the understanding of the dynamics following roton instability. We also show that an arrest of the instability can be employed to create a trapped roton gas, which is revealed by confined density modulations. Roton confinement is expected to play a key role in the ongoing experiments. In particular we discuss local susceptibility against density perturbations, which we illustrate for the case of a vortex lattice.

VII.A

Introduction

In the chapters IV, V and IV we have focused on a stack of quasi-one-dimensional dipolar condensates, which can be created with a two-dimensional optical lattice. In the following we will study a single pancake dipolar condensate. Such quasi-two-dimensional geometry can be considered as an example of a single layer in a stack of pancake condensates, which can be created with a one-dimensional optical lattice (see Fig. II.1, discussion in chapter III, and, e.g., Refs. [250–254, 260]).

In particular, in section III.E we have broadly discussed the spectrum of elementary excitations in a dipolar gas and we have strongly stressed the peculiarity of its roton-maxon form, which contrast distinctively with the dispersion of the elementary excitations in a nonpolar gas (see section II.C.8). As we have learned, when the dispersion minimum reaches zero energy, the BEC becomes unstable against intermediate (finite) momentum excitations and the roton instability develops [211, 239, 249]. Interestingly, this type of instability features novel type of phenomena that are absent in the usual phonon instability in nonpolar (see Sec. II.C.5 and Sec. II.C.8) and dipolar (see Sec. III.C and Sec. III.D) gases.

In Sec. III.E we have also pointed out that the presence of the roton in the dispersion relation establishes a direct link between dipolar gases and physics of superfluid helium [276–278, 281–283]. Notably, a deep roton minimum in helium leads to intriguing effects related to density modulations close to defects, boundaries, and vortex cores [290–294], a phenomenon whose counterpart is also anticipated in a dipolar BEC [227, 240, 344].

In He the roton properties may be controlled by means of pressure [345–347]. Similarly, the roton minimum in a dipolar BEC depends on contact and dipolar interactions, being particularly sensitive to density. In this chapter we demonstrate that this density dependence leads to a spatial roton confinement in the trap center, due to the inhomogeneous density profile, which is particularly relevant for pancake BECs with large aspect ratios. This roton confinement, which has been hinted in recent numerical calculations [236, 241], resembles the one of rotons around a vortex line in He [348], although in that case the confinement results from a spatially-dependent Doppler shift. In Sec. VII.B we show that the roton confinement is well described within the local-density approximation (LDA), which allows for a simple analytical derivation of the localized roton wave functions. Furthermore, in Sec. VII.C we demonstrate that the roton confinement is crucial for the understanding of roton instability in a pancake trap after an abrupt quench of the scattering length. Interestingly, the associated modulational instability, post-collapse dynamics and atom losses present a nontrivial dependence on the excitations prior to the destabilization. Moreover, in Sec. VII.D we show that arresting the roton instability allows for the creation of a trapped gas of rotons, which is revealed by density modulations confined in the trap center. Finally, in Sec. VII.E we discuss other consequences of roton localization, and in particular we focus on local susceptibility against density perturbations, which leads to vortex lattices with spatially-varying vortex-core profiles. We conclude in Sec. VII.F.

VII.B

Analytical model

We consider in this chapter a dipolar BEC of N bosons of mass m and (electric or magnetic) dipole moment d oriented along z. The BEC is loaded in a harmonic trap $V_t(\mathbf{r})$ of frequencies ω in the xy plane and $\omega_z = \lambda\omega$ along z. We assume a pancake-like confinement with $\lambda \gg 1$. The BEC wave function $\psi(\mathbf{r},t)$ is determined by the time-dependent nonlocal Gross-Pitaevskii equation (III.5),

$$i\hbar\frac{\partial}{\partial t}\psi(\mathbf{r},t) = \left[-\frac{\hbar^2\nabla^2}{2m} + V_t(\mathbf{r}) + g|\psi(\mathbf{r},t)|^2\right]\psi(\mathbf{r},t) + \int d^3r' V_{dd}(\mathbf{r}-\mathbf{r}')|\psi(\mathbf{r}',t)|^2\psi(\mathbf{r},t), \tag{VII.1}$$

where $g = 4\pi\hbar^2 aN/m$ characterizes the short-range interactions, a is the s-wave scattering length, $V_{dd}(\mathbf{r}) = \frac{Nd^2}{r^3}(1-3\cos^2\theta)$ is the DDI potential introduced in Eq. (III.1), θ is the angle between $\mathbf{r}$ and the z axis, and the wave function satisfies the normalization condition $\int d^3r|\psi(\mathbf{r},t)|^2 = 1$.

We first consider $\omega = 0$, briefly summarizing the results of Ref. [211] that we discussed in Sec. III.E. There, the ground-state wave function is $\psi_0(z)\exp(-i\mu t/\hbar)$, where μ is the chemical potential and $\psi_0(z)$ fulfills a 1D local GPE with a regularized coupling constant $g+g_d$, with $g_d = 8\pi d^2/3$. Assuming a transverse Thomas-Fermi profile (see Sec. II.C.4) we obtain $\mu = (g+g_d)n_0$, with n_0 as the peak density. The dispersion relation for excitations with in-plane momentum $\mathbf{q}$ is obtained after linearizing around the ground-state solution (see Sec.III.D). Interestingly, the dispersion may present a roton-like minimum at intermediate q values. Under proper conditions the spectrum is well approximated by:

$$\epsilon_h^2(q,\mu) = E(q)^2 - G(\beta)E(q)\mu + \hbar^2\omega_z^2, \tag{VII.2}$$

where $E(q) \equiv \hbar^2q^2/2m$ and $G(\beta) \equiv \frac{(\beta-2)(5\beta+2)}{3(1+\beta)(2\beta+1)}$, with $\beta \equiv g_d/g$ (compare with Eq. (III.15)). The roton minimum results (for a certain regime of β and $\mu/\hbar\omega_z$) from the term proportional to μ, which reduces the excitation energy if $\beta > 2$.

For $\omega > 0$, the spectrum may be evaluated for each $\rho = \sqrt{x^2+y^2}$ using LDA. We begin computing from Eq. (VII.1) the 3D ground-state profile $n_0(\mathbf{r}) = |\psi_0(\mathbf{r})|^2$ and we extract for each ρ the corresponding z-profile, $n_0^{1D}(z) = n_0(\mathbf{r})/n_0^{2D}(\boldsymbol{\rho})$, with $n_0^{2D}(\boldsymbol{\rho}) = \int dz\, n_0(\mathbf{r})$. We then calculate the local chemical potential $\mu_l(\rho)$. Solving the 1D Bogoliubov-de Gennes equations (see Eqns. (III.9)-(III.10)) we obtain the local spectrum $\epsilon(q,\rho)$, which can be approximated with $\epsilon_h(q,\mu_l(\rho))$. Note that in nonpolar BECs interactions (and hence density) play a crucial role for collective excitations with small momenta (see Fig. II.5), for which LDA fails. This is because LDA may be legitimately employed only if $qR \gg 1$ (with R the Thomas-Fermi radius in the xy plane [349]), but in this case the spectrum is only weakly density dependent. The situation is crucially different for polar gases and the roton minimum, which occurs at $q_r l_z \simeq 1$ [211], with $l_z^2 = \hbar/m\omega_z$. Hence, $q_r R \gg 1$ for $\lambda \gg 1$, and LDA may be safely used to evaluate the roton minimum, which- crucially- remains very sensitive to the local density.

In particular, since $\mu_l(\rho)$ decreases with ρ, in the trap center the roton energy is lowest, $E_0/\hbar\omega_z \simeq \sqrt{1-(G\mu_l(0))/2\hbar\omega_z)^2}$. For larger ρ the roton minimum becomes shallower, and eventually disappears. The dispersion presents thus a minimum both in momentum, at $q_r l_z \simeq \sqrt{G(\beta)\mu_l(0)/\hbar\omega_z}$, and in space, at $\rho = 0$ (Fig. VII.1). Hence, remarkably, an inhomogeneous density profile in

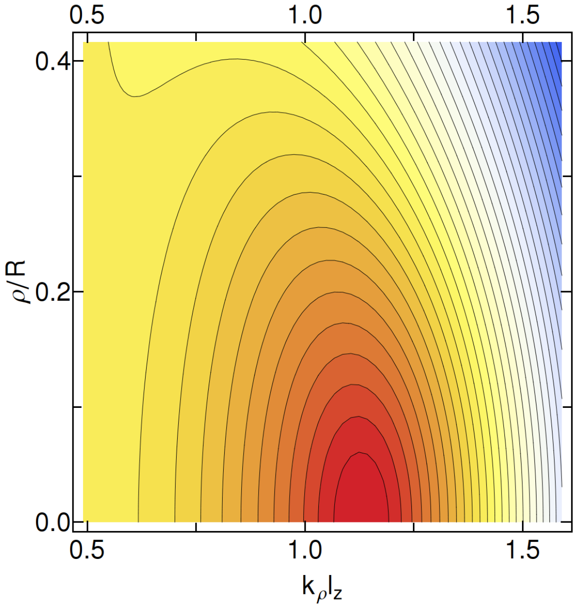

Figure VII.1: Elementary excitations spectrum $\epsilon(q,\rho)$ of a BEC, calculated within the local density approximation (see see text). Here, we consider an erbium BEC with $N = 2\times10^5$ atoms, $\omega_z = 2\pi \times 1$ kHz and $\lambda = 40$. Note the existence of a deep minimum (dark red region) in both position space and momentum space that leads to the roton confinement.

a dipolar BEC results in the spatial *roton confinement*.

Around the roton minimum

$$\epsilon(q,\rho) \simeq \frac{\hbar^2(q-q_r)^2}{2m_*} + \frac{1}{2}m_*\omega_*^2\rho^2, \tag{VII.3}$$

which, interestingly, resembles the Rashba model for a trapped BEC in the presence of spin-orbit coupling [350, 351]. Rotons possess an effective mass $m_* \equiv m\sqrt{1/(q_r l_z)^2 - 1/4}$, and are confined by an effective harmonic potential with frequency $\omega_* \equiv \omega_z \frac{m q_r l_z^2}{m_* R\sqrt{2}}$. Roton localization is hence characterized by the harmonic length $l_* \equiv \sqrt{\hbar/m_*\omega_*} = 2^{1/4}(R/q_r)^{1/2}$. Note that $l_*/R \sim \sqrt{l_z/R}$. Hence roton confinement is particularly significant for large $\lambda \gg 1$. Moreover, we find that if $\lambda \gg 1$ then $q_r l_* \sim \sqrt{R/l_z} \gg 1$, justifying the use of LDA.

To calculate the lowest-lying roton states we quantize Eq. (VII.3), and move to momentum space, where the Rashba-like dispersion $\sim (q-q_r)^2$ acts as a ring-like potential [350]. The roton wave functions are of the form $\phi_{n,s}(q)e^{is\varphi}/\sqrt{q}$, which obey

$$\left[\frac{E_{n,s}}{\hbar\omega_*} - \frac{s^2-\frac{1}{4}}{2(ql_*)^2}\right]\phi_{n,s} = \left[-\frac{1}{2l_*^2}\frac{d^2}{dq^2} + \frac{l_*^2}{2}(q-q_r)^2\right]\phi_{n,s}. \tag{VII.4}$$

For $q_r l_* \gg 1$, we may expand around $q \simeq q_r$, obtaining the eigenenergies $E_{n,s}/\hbar\omega_* = (s^2 - 1/4)/(2(q_r l_*)^2) + n + 1/2$, which are characterized by the angular momentum s around the Rashba-like ring, and the radial harmonic excitations with frequency ω_*. The lowest roton states are given by $n = 0$, being of the form $\psi_s(\rho) \sim e^{-\rho^2/2l_*^2} J_s(q_r\rho)$, with J_s the Bessel function.

VII.C

Local modulational instability and collapse

The localized roton states are crucial in the BEC dynamics following roton instability in pancake traps [352]. We consider a stable BEC prepared with an initial scattering length $a_i > a_c$, with a_c the critical value for the onset of roton instability. We are interested in the dynamics after an abrupt quench to $a_f < a_c$, where the roton energy becomes imaginary. Figs. VII.2 and VII.3 show the results of our simulations of Eq. (VII.1) for an erbium BEC.

Although the most unstable mode is $\psi_0(\rho)$, other modes with low s may contribute to the modulational instability due to the small energy differences between these levels. As a nontrivial consequence of that, the density pattern that develops after the quench is crucially influenced by the initial (thermal or quantum) population of those excitations which are exponentially amplified during the destabilization. This dependence is mimicked in our numerics by considering small random deviations $\delta\psi(\mathbf{r})$ from the ground state ψ_0

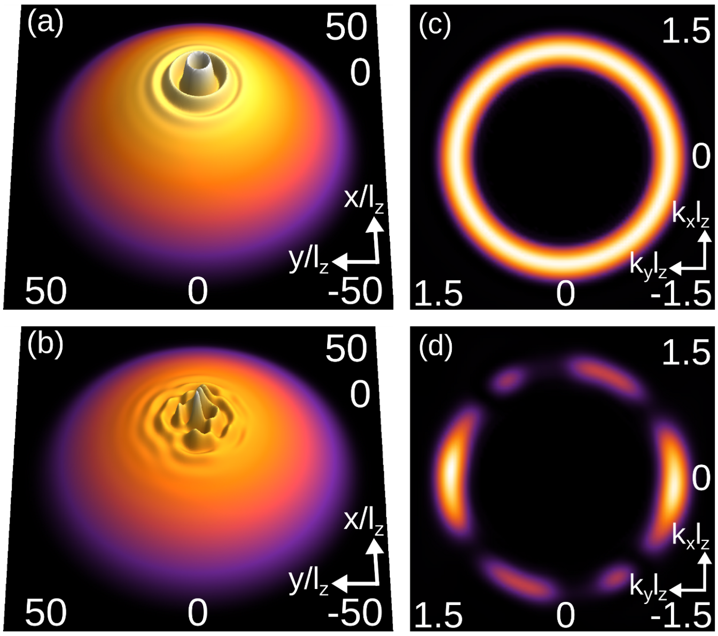

Figure VII.2: Roton instability for 10^5 Erbium atoms, with $\omega_z = 2\pi \times 450.0$Hz and $\lambda = 30$, $a_i = a_c = 8.49a_0$ and $a_f = 0$ (see text). We consider a small initial seeding $\psi(\mathbf{r}, t = 0) = \psi_0(\mathbf{r})e^{i\phi(\mathbf{r})}$, with a random $\phi(\mathbf{r})$ homogeneously distributed with $|\phi(\mathbf{r})|/\pi < \xi$. ($a$) Concentric rings ($s = 0$) formed after $t = 19$ms for small initial fluctuations ($\xi = 10^{-10}$). (b) Modulational instability after $t = 15.5$ms consisting of several s states for large initial fluctuations ($\xi = 10^{-6}$). (c) and (d) show the momentum distribution of (a) and (b), respectively (the large peak at $k = 0$ is suppressed for clarity of the figures).

(which is calculated for $a = a_i$) in the form: $\psi(\mathbf{r}, t = 0) = \psi_0(\mathbf{r}) + \delta\psi(\mathbf{r})$, with different amplitudes (see the caption of Fig. VII.2). Even though this allows us to discuss the possible collapse scenarios, the actual amplitude of the initial fluctuations depends on a_i and on temperature, T, and its analysis lies beyond the scope of this thesis. If for a_i the spectrum is weakly (or not) rotonized, for $k_B T \ll \mu_l(0)$ (k_B is the Boltzmann constant) the population of the dominant unstable modes for $a = a_f$ is negligible (corresponding to our simulations with small noise amplitude). In contrast, the initial population of unstable modes may be significant for $k_B T \sim E_0$, if for a_i the roton depth, E_0, approaches zero (corresponding to our simulations with large noise amplitude).

For a small initial population of the unstable modes, the modulation instability proceeds at a sufficiently slow pace such that the most unstable mode $\psi_0(\rho)$ dominates. As a result, a localized pattern of concentric rings develops (Fig. VII.2a), $n(\rho, t) - n_0(\rho) \sim \sqrt{n_0(\rho)}\, \Re(\psi_0(\rho))$, with a localization length in excellent agreement with the expected l_* (Fig. VII.3c). We note that similar concentric rings in a pancake dipolar BEC have been discussed in Ref. [353]. In that case, however, the ring structure was not localized and did not result from roton confinement but from dynamically unstable phonon modes. The corresponding momentum distribution of the pattern that we observe is characterized by the appearance of a ring, given by the Rashba-like dispersion (Fig. VII.2c). In contrast, for larger initial fluctuations the pattern growth is too fast to select the most unstable mode only and the created density pattern results from a (shot-to-shot dependent) linear combination of modes with different s. As a consequence, the formed pattern is characterized by a superposition of eccentric collapse centers (Fig. VII.2b). In this case, the corresponding momentum distribution presents a ring-like structure as well, but with an azimuthal modulation arising from the linear combination of various s states (Fig. VII.2d).

Similarly to other collapse scenarios in cold gases (see Sec. II.C.5 and Sec. III.C, and references therein), three-body losses play here a crucial role

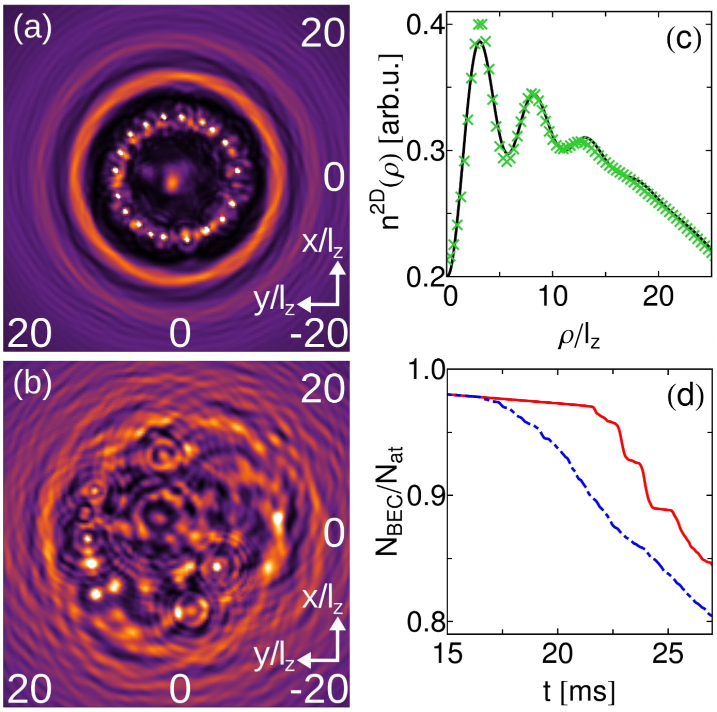

Figure VII.3: (a) and (b) depict the post-collapse dynamics after $t = 23$ ms for Fig. VII.2a and after $t = 19.5$ ms for Fig. VII.2b, respectively. (c) Radial density $n_0^{2D}(\rho)$ (see text) (green crosses) and theoretical prediction assuming $\psi_0(\rho)$ on top of the TF profile (black solid line). (d) Remnant BEC fraction for the case in Fig. VII.2a (red solid line) and for the case in Fig. VII.2b (blue dashed line). Compare with Fig. III.5 presenting the d-wave pattern.

as well. We included the losses in our simulations of Eq. (VII.1) by adding a term $-i\hbar\frac{L_3}{2}N^2|\psi(\mathbf{r},t)|^4\psi(\mathbf{r},t)$ (see discussion in Sec. III.C and Eq. (III.7)), with a loss rate $L_3 = 10^{-28}\text{cm}^{-6}\text{s}^{-1}$. When the collapse proceeds, the three-body losses become relevant at the density maxima, arresting the collapse and preventing singularities of the wave function [354]. As a result, the particles are expelled from the collapse center(s) and the BEC explodes. The global (phonon-like) collapse studied in dipolar chromium and erbium BECs [216, 219] results in a large decrease of the atom number and in a d-wave pattern in TOF (see Fig. III.5). The pattern formation discussed above leads to a a very different collapse dynamics. Concentric rings as those of Fig. VII.2a are followed by a sequential collapse (and azimuthal instability) of the rings, starting from the inner (denser) ones towards the outer ones (Fig. VII.3a). As a result, the atom number decreases in time in a step-like manner (red solid line in Fig. VII.3d). For the case of large initial fluctuations, the superimposed eccentric collapse centers (Fig. VII.2b) lead to a complex post-collapse behavior with characteristic mutually interfering jets expelled out of each local collapse center (Fig. VII.3b). In this case the atom decrease is smooth, lacking the step-like behavior of the previous case (blue dashed line in Fig. VII.3d). In both scenarios the locality of the collapse has two main consequences. First, TOF pictures lack the d-wave symmetry (post-collapse TOF pictures are to a large extent dominated by the central $q = 0$ peak, with the additional weak ring feature discussed above). Second, only a small number of atoms is lost during the collapse, compared to the large losses observed in global collapses. Therefore, the roton local collapse may be distinguished from the phonon global collapse by both the atom losses and the post-collapse TOF images, even without accessing the in-situ dynamics.

VII.D

Confined roton gas

Interestingly, roton instability may be employed to create a confined roton gas. As discussed above, an initially stable BEC may be driven into roton instability by quenching $a < a_c$. The pattern formation shown in Figs. VII.2a and VII.2b, may be alternatively understood as the growth of roton population. At this initial stage of the collapse, roton population is much lower than N, and hence we may neglect condensate depletion or roton-roton interactions. Once the roton gas is populated we return to the stable regime with a quench up, $a > a_c$ [354]. Since both m_* and ω_* do not vary significantly at the instability threshold, the created rotons are expected to remain confined in the trap center also for the final stable configuration. As shown in Fig. VII.4, the density pattern remains localized at the trap center, revealing the confinement of the created roton gas [355]. We recall that the density modulations remain confined due to the locality of the dispersion. Therefore,

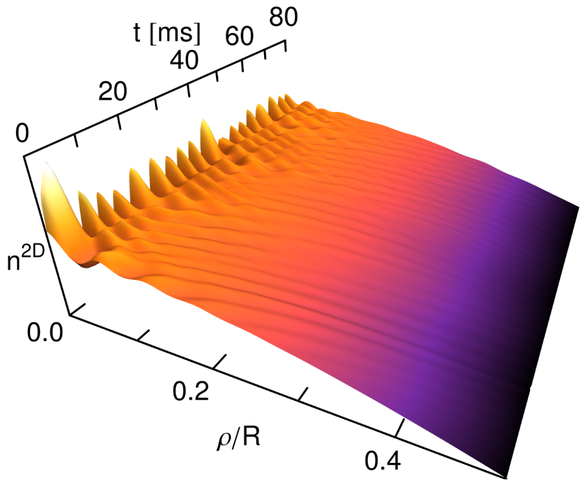

Figure VII.4: Evolution of a radial density cut for the case of Fig. VII.2a, but arresting the collapse after $t \simeq 16$ms with a quench up to $a = 8.55a_0$. A trapped roton gas is revealed by a confined density modulation at the trap center.

the rotons (density modulations) may be deconfined by further increasing a, above the value where the roton minimum disappears.

VII.E

Spatially dependent susceptibility

A deep roton minimum induces in the vicinity of a perturbation a large susceptibility against the formation of density modulations with the roton wavelength. This well-known effect in helium [290–294] is also relevant in dipolar BECs [240]. The dependence of the roton depth on the BEC density leads to a spatially dependent susceptibility, which we illustrate for the relevant case of vortices [356]. Vortex cores present a crater-like shape for a deep roton minimum [227, 240], absent for a shallow or inexistent roton minimum. Hence, vortices at different positions in a trapped BEC present a different core profile. This is particularly evident in a vortex lattice (Fig. VII.5), where the crater-like modulations of the cores at the trap center disappear for vortices close to the BEC boundary. Note however that the vortex lattice still presents a triangular Abrikosov geometry, since the energy scale resulting from the density oscillations is overwhelmed by the Coulomb-like vortex-vortex repulsion. Note also, that contrary to He [294], density oscillations cannot exist far from the vortex core, due to enhanced instability [227].

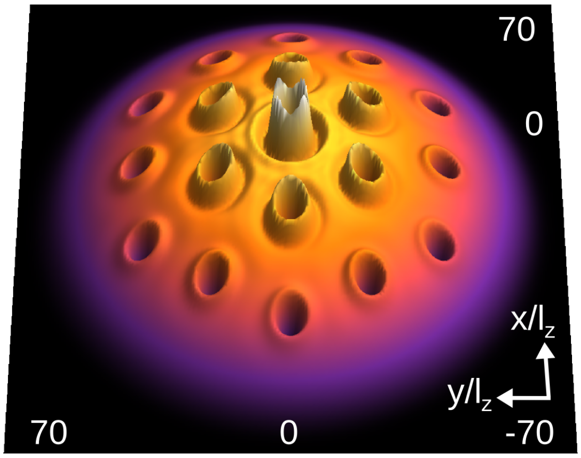

Figure VII.5: Vortex lattice for a BEC of $N = 1 \times 10^5$ Er atoms and the same trap as in Fig. VII.1, at the threshold of the roton instability. The lattice is generated by rotating the trap with a frequency 0.3ω.

VII.F

Summary

In summary, inhomogeneous trapping in pancake dipolar BECs with large aspect ratios leads to spatial roton confinement, which is crucial for the understanding of roton instability. The roton-like dispersion has not yet been observed experimentally, being currently a major goal pursued by several groups. Roton confinement is expected to play a key role in these experiments, since harmonic traps are typically employed and large aspect ratios are required to study the roton dispersion. In addition to the local susceptibility discussed above [356], roton confinement should be carefully considered when measuring the critical superfluid velocity, performing Bragg scattering [357] or analyzing finite temperature physics, which may be very interesting since the thermal roton cloud is expected to localize in the trap center.

❧

VIII

Conclusions and Outlook

In summary, in this thesis we have extensively studied novel phenomena arising in a dipolar Bose-Einstein condensate in an optical lattice. We have shown how the presence of the long-range and anisotropic dipole-dipole interactions fundamentally modifies the physics of the considered systems.

In particular, in chapter IV, we have demonstrated that in a stack of non-overlapping quasi-one-dimensional dipolar condensates the inherently non-local dipolar interactions give rise to intertube bound states of solitons. A detailed analysis of stability and properties of a soliton dimer and a soliton trimer has been presented and it has been found that such soliton complexes may be observed within current experimental feasibilities.

Next, in chapter V, we have considered a destabilization of the stack and we have discovered that for a sufficiently large dipole moment it may be followed by the development of a correlated modulational instability that stems from the dipolar intertube coupling, even in the absence of intersite hopping. Interestingly, in the considered quasi-one-dimensional condensates, this instability can evolve into stable soliton filaments or soliton crystal, depending on the sign of the dipole-dipole interactions. A thorough study of this phenomenon has revealed that it is well feasible under realistic experimental conditions.

Furthermore, in chapter VI, it has been shown that the physics of Faraday patterns in a dipolar condensate crucially depends on the dimensionality of the setup. We have also demonstrated that the intertube dipolar interactions lead to an unprecedented crossover between correlated and anticorrelated patterns in the case of two lattice sites with a quasi-one-dimensional dipolar condensate.

Finally, in chapter VII, we have investigated a trapped dipolar condensate in a two-dimensional geometry and we have found that the density dependence of the elementary excitations spectrum results in the confinement of the excitations in the trap center. It has been found that this novel phenomenon is of the utmost importance for the understanding of dynamics that follows the roton instability. Moreover, we have demonstrated that an arrest of this instability opens a realistic possibility of creation of confined roton gas and we have discussed how the roton confinement gives rise to the spatially dependent susceptibility against perturbations of the condensate density.

The findings of this thesis motivate further research. In particular, the results of chapter IV allow to think about interesting scattering scenarios of the soliton molecules. Furthermore, as recently suggested for nondipolar solitons, such scattering process can be employed to create mesoscopic entangled states of solitons. The role of dipole-dipole interactions in this method has not yet been addressed and remains unclear. Another possible extension of the presented work on dimers and trimers is a study on more exotic compounds such as, e.g., soliton hexamers. Moreover, in the proceedings of chapter V we have observed that a symmetry of the soliton crystal changes when varying the strength of interactions. This intriguing transition (crossover), which we have have not fully examined, offers an exciting possibility of studies on solid-solid transition. In chapter VI we have addressed possible scenarios for the Faraday patterns when the overall dipolar coupling is modulated. Interestingly, the presence of the lattice brings about the idea when the dipolar coupling is kept constant and intertube distance (the lattice spacing) is periodically modulated, which experimentally is perfectly feasible. In this case, contrary to the one considered in this thesis, the intratube dipolar interactions are kept constant while only the intertube dipolar interactions vary. Based on this premise we expect new interesting physics of the Faraday patterns. Lastly, in chapter VII we have considered zero temperature situation and we have shown that, under certain conditions, the condensate elementary excitations are confined in the trap center. For finite temperatures we expect that the thermally populated roton excitations (thermal cloud), in contrast with the case of nondipolar condensate, should be also localized around the condensate density maximum. Moreover, the locality of the condensate spectrum may be probed by a measurement of the response of the BEC against an external perturbation, e.g., an additional lattice, which is characterized by a certain length scale. We expect then that the response signal, which- as it is clear from our results- will strongly depend on the position in the cloud, should reach its maximum for the length scale corresponding to the roton wavelength, providing a route for its experimental measurement. Finally, the reported possibility of creation of a confined roton gas opens an interesting perspective towards the controlled study of fundamental roton properties, such as, e.g., roton-roton interactions, which should be also addressed.

❧

A

Dimensionally reduced GPE

We begin with fully three-dimensional GPE describing a dipolar Bose-Einstein condensate (BEC) confined in a two-dimensional optical lattice, forming a stack of parallel, nonoverlapping lattice sites, as depicted in Fig. IV.1. A wave function in a site j of the lattice is then described by

$$\imath\hbar\partial_t\Psi_j(\mathbf{r},t) = \Bigg[-\frac{\hbar^2}{2M}\nabla^2 + U(\mathbf{r}) + g|\Psi_j(\mathbf{r},t)|^2 + \sum_m \int d^3\mathbf{r}'\, V_d(\mathbf{r}-\mathbf{r}')|\Psi_m(\mathbf{r}',t)|^2\Bigg]\Psi_j(\mathbf{r},t), \tag{A.1}$$

where $U(\mathbf{r})$ is an external potential and $g = 4\pi a_{sc}\hbar^2/M$, with a_{sc} as the scattering length and M the particle mass. The dipole-dipole potential

$$V_d\left(\mathbf{r}-\mathbf{r}'\right) = g_d\left(1-3\cos^2\theta\right)/\left|\mathbf{r}-\mathbf{r}'\right|^3 \tag{A.2}$$

is characterized by $g_d = \mu_0\mu^2/4\pi$, with μ as the particle dipole moment, μ_0 as the vacuum permeability, and θ being the angle formed by the vector joining the two interacting particles and the dipole moment direction.

We now assume that the energy scale associated with the chemical potential μ_j is much smaller than that of the confinement in each lattice site $\hbar\omega_\perp$. Hence, we can factorize the BEC wave function

$$\Psi_j(\mathbf{r}) = \phi_j^\perp(x,y)\,\psi_j(z), \tag{A.3}$$

with $\phi_j^{\perp}(x,y)$ the ground-state wave function of the xy harmonic oscillator, and in consequence

$$\phi_j^{\perp}(x,y) = \frac{1}{\sqrt{\pi} l_{\perp}} \exp\left(-\frac{x^2}{2l_{\perp}^2}\right) \exp\left(-\frac{(y-j\Delta)^2}{2l_{\perp}^2}\right), \tag{A.4}$$

with $l_{\perp}$ as the xy oscillator length and Δ as the distance between the parallel condensates. Employing Eqs. (A.3) and (A.4) to Eq. (A.1), and integrating it with respect to x and y, we arrive at

$$\imath\hbar\partial_t \psi_j(z,t) = \left[-\frac{\hbar^2}{2M}\partial_z^2 + U(z) + \frac{g}{2\pi l_{\perp}^2}\left|\psi_j(z,t)\right|^2 + \mathcal{V}_d(z,t)\right]\psi_j(z,t), \tag{A.5}$$

where we have introduced the dipolar mean-field potential

$$\mathcal{V}_d(z,t) = \int dx \int dy \sum_m \int d^3\mathbf{r}'\, V_d(\mathbf{r}-\mathbf{r}')|\Psi_m(\mathbf{r}',t)|^2\, |\phi_j^{\perp}(x,y)|^2. \tag{A.6}$$

Following the idea presented in Ref. [210], we now apply the convolution theorem,

$$\int d^3\mathbf{r}'\, V_d(\mathbf{r}-\mathbf{r}')|\Psi_m(\mathbf{r}',t)|^2 = \int \frac{d^3\mathbf{k}}{(2\pi)^3} e^{\imath\mathbf{k}\mathbf{r}}\, \hat{V}_d(\mathbf{k})\widehat{|\Psi_m(\mathbf{k},t)|}^2, \tag{A.7}$$

and we rewrite Eq. (A.6) in the following form

$$\mathcal{V}_d(z,t) = \int dx \int dy \sum_m \int \frac{d^3\mathbf{k}}{(2\pi)^3} e^{\imath\mathbf{k}\mathbf{r}}\, \hat{V}_d(\mathbf{k})\hat{n}_m(\mathbf{k},t)\, n_j^{\perp}(x,y), \tag{A.8}$$

where $\hat{V}_d(\mathbf{k})$ is the Fourier transform of the dipole-dipole potential Eq. (A.2), $\hat{n}_m(\mathbf{k},t)$ is the Fourier transform of the density $n_m(\mathbf{r},t) = |\Psi_m(\mathbf{r},t)|^2$, and $n_j^{\perp}(x,y) = |\phi_j^{\perp}(x,y)|^2$. Performing the integration of Eq. (A.8) with respect to x and y we arrive at

$$\mathcal{V}_d(z,t) = \sum_m \int \frac{d^3\mathbf{k}}{(2\pi)^3} e^{\imath k_z z}\, \hat{V}_d(\mathbf{k})\, \hat{n}_m(\mathbf{k},t)\, \hat{n}_j^{\perp *}(k_x,k_y) \tag{A.9}$$

$$= \sum_m \int \frac{dk_z}{2\pi} e^{\imath k_z z} \hat{n}_m(k_z,t) \int \frac{dk_x k_y}{(2\pi)^2}\, \hat{V}_d(\mathbf{k})\, \hat{n}_m^{\perp}(k_x,k_y)\, \hat{n}_j^{\perp *}(k_x,k_y). \tag{A.10}$$

Next, we employ the ansatz (A.4) to calculate the density in Fourier space,

$$\hat{n}_m^{\perp}(k_x,k_y) = \exp\left(-\frac{l_{\perp}^2}{4}(k_x^2+k_y^2) - \imath k_y m\Delta\right), \tag{A.11}$$

and, by applying the expansion of a plane wave in the basis of spherical waves, we derive the momentum representation of the dipole-dipole potential (for the particular geometry that we consider throughout this thesis, as depicted, e.g., in Fig. IV.1)

$$\hat{V}_d(\mathbf{k}) = \frac{4\pi}{3} g_d \left(\frac{3k_y^2}{\mathbf{k}^2} - 1 \right). \tag{A.12}$$

Inserting Eqs. (A.11) and (A.12) into Eq. (A.10), we obtain

$$\mathcal{V}_d(z,t) = \frac{g_d}{3} \sum_m \int \frac{dk_z}{2\pi} e^{\imath k_z z} \hat{n}_m(k_z) F_{m-j}(k_z), \tag{A.13}$$

where

$$\begin{aligned} F_q(k_z) = & \int \frac{dk_x dk_y}{\pi} \left(\frac{3k_y^2}{k_x^2 + k_y^2 + k_z^2} - 1 \right) \\ & \times \exp\left(-\frac{1}{2} \left(k_x^2 + k_y^2 \right) l_\perp^2 - \imath k_y q \Delta \right). \end{aligned} \tag{A.14}$$

Eq. (A.14) does not have an analytical form and hence solving Eq. (A.5) requires numerical integration of $F_q(k_z)$. However, introducing polar coordinates,

$$k_x = k_\rho \cos\phi, \qquad k_y = k_\rho \sin\phi, \tag{A.15}$$

it is possible to simplify Eq. (A.14) and rewrite $F_q(k_z)$ in terms of the Bessel functions of the first kind $J_n(x)$:

$$\begin{aligned} F_q(k_z) = & \frac{1}{\pi} \int_0^{2\pi} d\phi \int_0^\infty dk_\rho k_\rho \left(\frac{2k_\rho^2 - 3k_\rho^2 \cos^2\phi - k_z^2}{k_\rho^2 + k_z^2} \right) \exp\left(-\frac{1}{2} k_\rho^2 l_\perp^2 - \imath k_\rho q \Delta \sin\phi \right) \\ = & \frac{1}{\pi} \int_0^\infty dk_\rho k_\rho \left(\frac{\frac{1}{2}k_\rho^2 - k_z^2}{k_\rho^2 + k_z^2} \right) \exp\left(-\frac{1}{2} k_\rho^2 l_\perp^2 \right) \int_0^{2\pi} d\phi \exp\left(-\imath k_\rho q \Delta \sin\phi \right) \\ & - \frac{3}{2\pi} \int_0^\infty dk_\rho k_\rho \frac{k_\rho^2}{k_\rho^2 + k_z^2} \exp\left(-\frac{1}{2} k_\rho^2 l_\perp^2 \right) \int_0^{2\pi} d\phi \cos(2\phi) \exp\left(-\imath k_\rho q \Delta \sin\phi \right) \\ = & \int_0^\infty dk_\rho k_\rho \frac{\exp\left(-\frac{1}{2} k_\rho^2 l_\perp^2 \right)}{k_\rho^2 + k_z^2} \left[\left(k_\rho^2 - 2k_z^2 \right) J_0\left(k_\rho q \Delta \right) - 3k_\rho^2 J_2\left(k_\rho q \Delta \right) \right]. \end{aligned} \tag{A.16}$$

◆

B

Analytical expressions for the energy functional

We begin with the full three-dimensional GPE (A.1) introduced in appendix A,

$$\begin{aligned}\imath\hbar\partial_t\Psi_j(\mathbf{r},t) = \bigg[&-\frac{\hbar^2}{2M}\nabla^2 + U(\mathbf{r}) + g|\Psi_j(\mathbf{r},t)|^2 \\ &+ \sum_m \int d^3\mathbf{r}'\, V_d(\mathbf{r}-\mathbf{r}')|\Psi_m(\mathbf{r}',t)|^2 \bigg] \Psi_j(\mathbf{r},t), \end{aligned} \tag{B.1}$$

and we consider a single condensate described by the anisotropic gaussian ansatz

$$\Psi(\mathbf{r},t) = \frac{1}{\pi^{3/4}} \frac{1}{\left(l_x l_y l_z\right)^{1/2}} \exp\left(-\frac{x^2}{2l_x^2} - \frac{y^2}{2l_y^2} - \frac{z^2}{2l_z^2} \right), \tag{B.2}$$

to compute the energy functional

$$E = E^{kin} + E^{trap} + E^{contact} + E^d. \tag{B.3}$$

Employing Eqs. (B.1) and (B.2), a straightforward integration results in the following expressions:

$$E^{kin} = -\frac{\hbar^2}{2M} \int d^3\mathbf{r}\, \Psi^*(\mathbf{r},t)\nabla^2\Psi(\mathbf{r},t) = \frac{\hbar^2}{4M} \sum_{i=x,y,z} \frac{1}{l_i^2}, \tag{B.4}$$

$$E^{trap} = -\frac{\hbar^2}{2M}\int d^3\mathbf{r}\,\Psi^*(\mathbf{r},t)U(\mathbf{r})\Psi(\mathbf{r},t) = \frac{M}{4}\sum_{i=x,y,z}\omega_i^2 l_i^2, \tag{B.5}$$

$$E^{contact} = -\frac{g}{2}\int d^3\mathbf{r}\,\Psi^*(\mathbf{r},t)|\Psi(\mathbf{r},t)|^2\Psi(\mathbf{r},t) = \frac{g}{4\sqrt{2}\pi^{3/2}l_x l_y l_z}. \tag{B.6}$$

The dipolar term E^d in the energy functional calls for more involved calculations. In the following, we present the derivation of the full analytical expression for E^d. Similarly to calculations presented in appendix A, we first reexpress E^d in the momentum representation:

$$\begin{aligned} E^d =& \frac{1}{2}\int d^3\mathbf{r}\,\Psi^*(\mathbf{r},t)\int d^3\mathbf{r}'\,V_d\left(\mathbf{r}-\mathbf{r}'\right)|\Psi(\mathbf{r}',t)|^2\Psi(\mathbf{r},t) \\ =& \frac{1}{2}\int\frac{d^3\mathbf{k}}{(2\pi)^3}\hat{n}^2(\mathbf{k})\hat{V}_d(\mathbf{k}), \end{aligned} \tag{B.7}$$

where, employing Eq. (B.2),

$$\hat{n}(\mathbf{k}) = \int d^3\mathbf{r}\,e^{-\imath\mathbf{kr}}|\Psi(\mathbf{r},t)|^2 = \exp\left(-\frac{k_x^2 l_x^2}{4} - \frac{k_y^2 l_y^2}{4} - \frac{k_z^2 l_z^2}{4}\right). \tag{B.8}$$

Writing Eq. (B.7) explicitly, i.e., together with Eq. (B.8) and $\hat{V}_d(\mathbf{k})$ defined in Eq. (A.12), and introducing new integration variables $q_i = k_i l_i/\sqrt{2}$ we arrive at:

$$E^d = \frac{g_d\sqrt{2}}{6\pi^2 l_x l_y l_z}\int d^3\mathbf{q}\,e^{-\mathbf{q}^2}\left(\frac{\frac{2q_y^2}{l_y^2} - \frac{q_x^2}{l_x^2} - \frac{q_z^2}{l_z^2}}{\frac{q_x^2}{l_x^2} + \frac{q_y^2}{l_y^2} + \frac{q_z^2}{l_z^2}}\right). \tag{B.9}$$

Next, introducing spherical coordinates,

$$q_x = q\sin\theta\cos\phi, \qquad q_y = q\sin\theta\sin\phi, \qquad q_z = q\cos\theta, \tag{B.10}$$

and integrating out the q dependence we obtain:

$$\begin{aligned} E^d =& \frac{g_d}{12\sqrt{2}\pi^{3/2}l_x l_y l_z}\int_0^{2\pi} d\varphi\int_0^{\pi} d\theta\,\sin\theta\left[\frac{\sin^2\theta\left(-x\cos^2\varphi + 2y\sin^2\varphi\right) - \cos^2\theta}{\sin^2\theta\left(x\cos^2\varphi + y\sin^2\varphi\right) + \cos^2\theta}\right] \\ =& \frac{g_d}{6\sqrt{2}\pi^{3/2}l_x l_y l_z}\int_0^{2\pi} d\varphi\int_0^{1} du\left\{\frac{\left(1-u^2\right)\left[2y-(x+2y)\cos^2\varphi\right] - u^2}{\left(1-u^2\right)\left[y+(x-y)\cos^2\varphi\right] + u^2}\right\} \qquad \text{(B.11)} \\ =& \frac{g_d}{6\sqrt{2}\pi^{3/2}l_x l_y l_z}K\left(\sqrt{x},\sqrt{y}\right), \qquad \text{(B.12)} \end{aligned}$$

with $x = (l_z/l_x)^2$ and $y = \left(l_z/l_y\right)^2$, and function $K\left(\sqrt{x}, \sqrt{y}\right)$ that we had introduced in Eq. (IV.4), in Section IV.C. We now notice that the integral with respect to φ, of the form present in Eq. (B.11), has the following analytical form:

$$\int_0^{2\pi} d\varphi \frac{A + B\cos^2\varphi}{C + D\cos^2\varphi} = 2\pi\left[\frac{A}{C}\sqrt{\frac{C}{C+D}} - \frac{B}{D}\left(\sqrt{\frac{C}{C+D}} - 1\right)\right], \tag{B.13}$$

and hence

$$E^d = \frac{g_d}{3\sqrt{2\pi}l_x l_y l_z}\left\{-\frac{x+2y}{x-y} - (1+2y)\mathscr{I}_1 + 2y\mathscr{I}_2 + \frac{x+2y}{x-y}\mathscr{I}_3\right\} \tag{B.14}$$

where:

$$\mathscr{I}_1 = \int_0^1 du \frac{u^2}{\sqrt{\left[u^2(1-x)+x\right]\left[u^2(1-y)+y\right]}} \tag{B.15}$$

$$\mathscr{I}_2 = \int_0^1 du \frac{1}{\sqrt{\left[u^2(1-x)+x\right]\left[u^2(1-y)+y\right]}} \tag{B.16}$$

$$\mathscr{I}_3 = \int_0^1 du \sqrt{\frac{u^2(1-y)+y}{u^2(1-x)+x}}. \tag{B.17}$$

In order to integrate Eqs. (B.15)-(B.17), it is necessary to correctly specify the mutual relations between l_x, l_y and l_z. In Chapter IV we consider solitons localized in an one-dimensional condensate aligned along the z axis, as depicted in Fig. IV.1, and thus it is justified to consider in the following $l_z > l_{x,y}$. Furthermore, the positive sign of the dipolar coupling, i.e., $g_d > 0$, leads effectively to $l_y > l_x$. We refer to this case by denoting the corresponding integrals with the plus sign, i.e, $\mathscr{I}_{1,2,3}^{(+)}$:

$$\mathscr{I}_1^{(+)} = \frac{1}{y-1}\sqrt{\frac{y}{x-1}}\left[F\left(a^{(+)}(x); b^{(+)}(x,y)\right) - E\left(a^{(+)}(x); b^{(+)}(x,y)\right)\right], \tag{B.18}$$

$$\mathscr{I}_2^{(+)} = \frac{1}{\sqrt{y(x-1)}}F\left(a^{(+)}(x); b^{(+)}(x,y)\right), \tag{B.19}$$

$$\mathscr{I}_3^{(+)} = \sqrt{\frac{y}{x-1}}E\left(a^{(+)}(x); b^{(+)}(x,y)\right), \tag{B.20}$$

where:

$$a^{(+)}(x) = \arcsin\sqrt{1-\frac{1}{x}}, \qquad b^{(+)}(x,y) = \sqrt{\frac{x(y-1)}{y(x-1)}}. \tag{B.21}$$

In contrast, for negative dipolar coupling, i.e., $g_d < 0$, the size of the condensate in the x direction is larger than in the y direction, and so $l_x > l_y$. We refer to this case by denoting the corresponding integrals with the minus sign, i.e, $\mathscr{I}^{(-)}_{1,2,3}$:

$$\mathscr{I}^{(-)}_1 = \frac{1}{x-1}\sqrt{\frac{x}{y-1}}\left[F\Big(a^{(-)}(y);b^{(-)}(x,y)\Big) - E\Big(a^{(-)}(y);b^{(-)}(x,y)\Big)\right], \tag{B.22}$$

$$\mathscr{I}^{(-)}_2 = \frac{1}{\sqrt{x(y-1)}}F\Big(a^{(-)}(y);b^{(-)}(x,y)\Big), \tag{B.23}$$

$$\mathscr{I}^{(-)}_3 = \frac{\sqrt{x(y-1)}}{x-1}\left[E\Big(a^{(-)}(y);b^{(-)}(x,y)\Big) - \frac{y-x}{x(y-1)}F\Big(a^{(-)}(y);b^{(-)}(x,y)\Big)\right]. \tag{B.24}$$

where:

$$a^{(-)}(y) = \arcsin\sqrt{1-\frac{1}{y}}, \qquad b^{(-)}(x,y) = \sqrt{\frac{y(x-1)}{x(y-1)}}. \tag{B.25}$$

In Eqs. (B.18)-(B.24), $F(a;b)$ is the elliptic integral of the first kind [327],

$$F(a;b) = \int_0^a d\alpha\,\frac{1}{\sqrt{1-b^2\sin^2\alpha}}, \tag{B.26}$$

and $E(a;b)$ is the elliptic integral of the second kind,

$$E(a;b) = \int_0^a d\alpha\,\sqrt{1-b^2\sin^2\alpha}. \tag{B.27}$$

Eqs. (B.4)-(B.6) and Eq. (B.14), together with the analytical form of Eqs. (B.18)-(B.24), offer a convenient way of minimization of the energy functional (B.3), which we employ to compute the stability diagrams in Figs. IV.2 and IV.7, in Chapter IV.

❧

C

Bogoliubov-de Gennes equations

We begin with Eqs. (A.5) and (A.13) derived in appendix A

$$\imath\hbar\partial_t\psi_j(z,t) = \Big[-\frac{\hbar^2}{2M}\partial_z^2 + \frac{g}{2\pi l_\perp^2}\left|\psi_j(z,t)\right|^2 + \frac{g_d}{3}\sum_m\int\frac{dk_z}{2\pi}e^{\imath k_z z}\hat{n}_m(k_z)F_{m-j}(k_z)\Big]\psi_j(z,t), \tag{C.1}$$

where we have assumed no external potential $U(z) = 0$, and we employ the Bogoliubov ansatz for the wave function of the condensate,

$$\psi_j(z,t) = \left(\sqrt{n_0} + \chi_j(z,t)\right)e^{-\imath\mu_j t/\hbar}, \tag{C.2}$$

where n_0 is the axial density, μ_j is the chemical potential in a site j, and

$$\chi_j(z,t) = u_j e^{\imath(zq-\omega t)} + v_j^* e^{-\imath(zq-\omega t)} \tag{C.3}$$

is a perturbation of the homogeneous solution, with q and ω as the z momentum component and the frequency of the elementary excitations, respectively. Inserting the ansatz (C.2) into Eq. (C.1) and linearizing in the perturbation amplitude we obtain the following terms:

$$\begin{aligned} &\imath\hbar\partial_t\psi_j(z,t) \\ &= \left[\mu_j\sqrt{n_0} + e^{\imath(zq-\omega t)}u_j\left(\mu_j+\hbar\omega\right) + e^{-\imath(zq-\omega t)}v_j^*\left(\mu_j-\hbar\omega\right)\right]e^{-\imath\mu_j t/\hbar}, \end{aligned} \tag{C.4}$$

$$-\frac{\hbar^2}{2M}\partial_z^2\psi_j(z,t) = \frac{\hbar^2q^2}{2M}\left[u_j e^{\imath(zq-\omega t)} + v_j^* e^{-\imath(zq-\omega t)}\right]e^{-\imath\mu_j t/\hbar}, \tag{C.5}$$

$$\begin{aligned} &\frac{g}{2\pi l_\perp^2}\left|\psi_j(z,t)\right|^2\psi_j(z,t) \\ &= \frac{gn_0}{2\pi l_\perp^2}\left[\sqrt{n_0} + e^{\imath(zq-\omega t)}\left(2u_j+v_j\right) + e^{-\imath(zq-\omega t)}\left(2v_j^*+u_j^*\right)\right]e^{-\imath\mu_j t/\hbar}, \end{aligned} \tag{C.6}$$

$$\begin{aligned} &\frac{g_d}{3}\sum_m\int\frac{dk_z}{2\pi}e^{\imath k_z z}\hat{n}_m(k_z)F_{m-j}(k_z)\psi_j(z,t) \\ &= \frac{g_d n_0}{3}\left\{e^{\imath(zq-\omega t)}\left[u_j\sum_m F_{m-j}(0) + \sum_m F_{m-j}(q)(u_m+v_m)\right]\right. \\ &\quad\left. + e^{-\imath(zq-\omega t)}\left[v_j^*\sum_m F_{m-j}(0) + \sum_m F_{m-j}(q)\left(u_m^*+v_m^*\right)\right]\right\}e^{-\imath\mu_j t/\hbar}. \end{aligned} \tag{C.7}$$

Collecting Eqs. (C.4)-(C.7) and utilizing linear independence of $e^{\imath(zq-\omega t)}$, and $e^{-\imath(zq-\omega t)}$, we arrive at the system of equations

$$\left\{\begin{aligned} &\mu_j = \frac{gn_0}{2\pi l_\perp^2} + \frac{g_d n_0}{3}\sum_m F_{m-j}(0) && \text{(C.8)} \\ &0 = -u_j\left(\mu_j+\hbar\omega\right) + \frac{\hbar^2q^2}{2M}u_j + \frac{gn_0}{2\pi l_\perp^2}\left(2u_j+v_j\right) \\ &\quad + \frac{g_d n_0}{3}\left[u_j\sum_m F_{m-j}(0) + \sum_m F_{m-j}(q)(u_m+v_m)\right] && \text{(C.9)} \\ &0 = -v_j^*\left(\mu_j-\hbar\omega\right) + \frac{\hbar^2q^2}{2M}v_j^* + \frac{gn_0}{2\pi l_\perp^2}\left(2v_j^*+u_j^*\right) \\ &\quad + \frac{g_d n_0}{3}\left[v_j^*\sum_m F_{m-j}(0) + \sum_m F_{m-j}(q)\left(u_m^*+v_m^*\right)\right]. && \text{(C.10)} \end{aligned}\right.$$

Inserting Eq. (C.8) into Eqs. (C.9) and (C.10) we arrive at the final form of the Bogoliubov-de Gennes equations describing the considered setup:

$$\begin{cases} 0 = -u_j\left(-\dfrac{gn_0}{2\pi l_\perp^2} + \hbar\omega - \dfrac{\hbar^2 q^2}{2M}\right) + \dfrac{gn_0}{2\pi l_\perp^2} v_j \\ \qquad + \dfrac{g_d n_0}{3}\displaystyle\sum_m F_{m-j}(q)(u_m + v_m) & \text{(C.11)} \\ 0 = -v_j^*\left(-\dfrac{gn_0}{2\pi l_\perp^2} - \hbar\omega - \dfrac{\hbar^2 q^2}{2M}\right) + \dfrac{gn_0}{2\pi l_\perp^2} u_j^* \\ \qquad + \dfrac{g_d n_0}{3}\displaystyle\sum_m F_{m-j}(q)\left(u_m^* + v_m^*\right) & \text{(C.12)} \end{cases}$$

In general, i.e., for an arbitrary number of condensates, the system of Eqs. (C.11) and (C.12) calls for numerical solutions, as those presented in Fig. V.2. It is instructive, however, to calculate the spectrum analyticaly for a small system, which amounts to rewriting Eqs. (C.11) and (C.12) in a matrix form and demanding the determinant of the matrix to vanish. In particular, for a single condensate we obtain the following spectrum of elementary excitations:

$$\hbar^2\omega^2 = \frac{\hbar^2 q^2}{2M}\left[\frac{\hbar^2 q^2}{2M} + \frac{gn_0}{\pi l_\perp^2} + \frac{2}{3l_\perp^2}F_0(ql_\perp)g_d n_0\right] \tag{C.13}$$

where

$$F_0(x) = 1 + \frac{3}{2}x^2 e^{x^2/2}\mathrm{Ei}\left(-x^2/2\right), \tag{C.14}$$

is a particular case of Eq. (A.14), with Ei(x) the exponential integral function [327]. An example of the spectrum (C.13) is presented in Fig. VI.2. For two condensates, proceeding like in the latter case, we arrive at the following result:

$$\hbar^2\omega_\pm^2 = \frac{\hbar^2 q^2}{2M}\left[\frac{\hbar^2 q^2}{2M} + \frac{gn_0}{\pi l_\perp^2} + \frac{2}{3l_\perp^2}\Big(F_0(ql_\perp) \pm F_1(ql_\perp)\Big)g_d n_0\right], \tag{C.15}$$

with clearly unfolded branches of the Bogoliubov spectrum, depicted, e.g., in Figs. V.2 and VI.5.

❧

D

Derivation of the Mathieu equations

We begin with Eqs. (A.5) and (A.13) derived in appendix A. Employing the units of frequency $\omega_\perp$ and $l_\perp = \sqrt{\hbar/M\omega_\perp}$, with M as the particle mass, and assuming no external potential $U(\mathbf{r}) = 0$, we arrive at:

$$i\partial_t\psi_j(z) = \Bigg[-\frac{1}{2}\partial_z^2 + gn_j(z) \\ + \frac{2\pi}{3}g_d\sum_m\int dk_z e^{ik_z z}\hat{n}_m(k_z)F_{|m-j|}(k_z)\Bigg]\psi_j(z), \tag{D.1}$$

with $g = g^{3\mathrm{D}}n_0/2\pi\hbar\omega_\perp l_\perp^3$ and $g_d = g_d^{3\mathrm{D}}n_0/2\pi\hbar\omega_\perp l_\perp^3$, where n_0 is the linear density and $g^{3\mathrm{D}} = 4\pi a_{sc}\hbar^2/M$, and $g_d^{3\mathrm{D}} = \mu_0\mu^2/4\pi$, as defined in the full three-dimensional case in appendix A. In the following we consider a parametric modulation of the dipolar coupling,

$$g_{d_j}(t) = \overline{g}_d(1 + 2\alpha_j\cos(2\omega_j t)), \tag{D.2}$$

together with the ansatz for the wave function:

$$\psi_j(z,t) = \psi_{j_H}\left(1 + A_j(t)\cos(qz)\right), \tag{D.3}$$

where the homogeneous solution is given by

$$\psi_{j_H} = \exp\{-i\overline{\mu}_j[t + (\Omega_j/\omega_j)\sin(2\omega_j t)]\}, \tag{D.4}$$

with $\overline{\mu}_j = g + \frac{2\pi}{3}\overline{g}_d \sum_m F_{|m-j|}(0)$ determined by Eq. (C.8), and $\Omega_j = \alpha(1-g/\overline{\mu}_j)$. Inserting Eq. (D.3) into Eq. (D.1), and linearizing in A_j we arrive at:

$$\begin{aligned}\imath\cos(qz)\frac{d}{dt}A_j = & -\left(1+A_j\cos(qz)\right)\left(1+2\Omega_j\cos(2\omega_j t)\right)\overline{\mu}_j \\ & +\frac{1}{2}q^2A_j\cos(qz)+g\left[1+\left(2A_j+A_j^*\right)\cos(qz)\right] \\ & +\frac{2\pi}{3}g_{d_j}(t)\Bigg[\left(1+A_j\cos(qz)\right)\sum_m F_{m-j}(0) \\ & \qquad +\cos(qz)\sum_m\left(A_m+A_m^*\right)F_{m-j}(q)\Bigg], \end{aligned} \tag{D.5}$$

and utilizing the explicit expression for $\overline{\mu}_j$, we find:

$$\begin{aligned}\imath\frac{d}{dt}A_j = & \frac{1}{2}q^2A_j+g\left(A_j+A_j^*\right) \\ & +\frac{2\pi}{3}\overline{g}_d\left(1+2\alpha_j\cos(2\omega_j t)\right)\sum_m\left(A_m+A_m^*\right)F_{m-j}(q). \end{aligned} \tag{D.6}$$

Next, decomposing the amplitude $A_j = u_j + \imath v_j$ and separating real and imaginary terms in Eq. (D.6) we obtain:

$$\left\{\begin{aligned} & \frac{d}{dt}u_j = \frac{1}{2}q^2v_j, && \text{(D.7)} \\ & \frac{d}{dt}v_j = -\frac{1}{2}q^2u_j-2gu_j-\frac{4\pi}{3}g_{d_j}(t)\sum_m u_mF_{m-j}(q), && \text{(D.8)} \end{aligned}\right.$$

and in consequence, combining Eqs. (D.7)-(D.8),

$$\frac{d^2}{dt^2}u_j+\left(\frac{q^2}{2}\right)\left[\left(\frac{q^2}{2}+2g\right)u_j+\frac{4\pi}{3}g_{d_j}(t)\sum_m u_mF_{m-j}(q)\right]=0. \tag{D.9}$$

In the case of a single dipolar BEC, Eq. (D.9) reads:

$$\frac{d^2}{dt^2}u+\left[\omega_q^2+\frac{4\pi}{3}\overline{g}_d\alpha q^2F_0(q)\cos(2\omega t)\right]u=0, \tag{D.10}$$

where we find the dimensionless form of Eq. (C.13) describing the Bogoliubov elementary excitations spectrum in a single condensate:

$$\omega_q^2=\frac{q^2}{2}\left(\frac{q^2}{2}+2g+\frac{4\pi}{3}\overline{g}_dF_0(q)\right). \tag{D.11}$$

Eq. (D.10) acquires the form of the Mathieu equation [358]. For two dipolar condensates, with $\omega_1 = \omega_2$ and $\alpha_1 = \alpha_2$, Eq. (D.10) reads:

$$\begin{cases} \dfrac{d^2}{dt^2}u_1 + \omega_q^2 u_1 + \dfrac{2\pi}{3}\overline{g}_d q^2 F_1(q) u_2 \\ \qquad\qquad + \dfrac{4\pi}{3}\overline{g}_d \alpha q^2 (F_0 u_1 + F_1 u_2)\cos(2\omega t) = 0 & \text{(D.12)} \\ \dfrac{d^2}{dt^2}u_2 + \omega_q^2 u_2 + \dfrac{2\pi}{3}\overline{g}_d q^2 F_1(q) u_1 \\ \qquad\qquad + \dfrac{4\pi}{3}\overline{g}_d \alpha q^2 (F_1 u_1 + F_0 u_2)\cos(2\omega t) = 0. & \text{(D.13)} \end{cases}$$

We now notice that by introducing new variables $u_\pm = u_1 \pm u_2$ it is possible to decouple the two Eqs. (D.12) and (D.13) to the following form:

$$\frac{d^2}{dt^2}u_+ + \left[\left(\omega_q^2 + \frac{2\pi}{3}\overline{g}_d q^2 F_1(q)\right) + \frac{4\pi}{3}\overline{g}_d \alpha q^2 \Big(F_0(q) + F_1(q)\Big)\cos(2\omega t)\right] u_+ = 0, \tag{D.14}$$

$$\frac{d^2}{dt^2}u_- + \left[\left(\omega_q^2 - \frac{2\pi}{3}\overline{g}_d q^2 F_1(q)\right) + \frac{4\pi}{3}\overline{g}_d \alpha q^2 \Big(F_0(q) - F_1(q)\Big)\cos(2\omega t)\right] u_- = 0, \tag{D.15}$$

to find again the dimensionless form of the Bogolibov spectrum (C.15) for two condensates:

$$\omega_{q\pm}^2 = \omega_q^2 \pm \frac{2\pi}{3}\overline{g}_d q^2 F_1(q) \tag{D.16}$$

$$= \frac{q^2}{2}\left[\frac{q^2}{2} + 2g + \frac{4\pi}{3} g_d \Big(F_0(q) \pm F_1(q)\Big)\right]. \tag{D.17}$$

Finally, we can write the equations describing the pattern dynamics for two condensates in a compact Mathieu-like form:

$$\frac{d^2}{dt^2}u_\pm + \left[\omega_{q\pm}^2 + \frac{4\pi}{3}\overline{g}_d \alpha q^2 \Big(F_0(q) \pm F_1(q)\Big)\cos(2\omega t)\right] u_\pm = 0. \tag{D.18}$$

⁂

Bibliography

[1] S. N. Bose, "Plancks Gesetz und Lichtquantenhypothese," Z. Phys. **26**, 178 (1924).

[2] A. Einstein, "Quantentheorie des einatomigen idealen Gases," Sitzber. Kgl. Preuss. Akad. Wiss. , 3 (1925).

[3] M. H. Anderson, J. R. Ensher, M. R. Matthews, C. E. Wieman, and E. A. Cornell, "Observation of Bose-Einstein condensation in a dilute atomic vapor," Science **269**, 198 (1995).

[4] C. C. Bradley, C. A. Sackett, J. J. Tollett, and R. G. Hulet, "Evidence of Bose-Einstein condensation in an atomic gas with attractive interactions," Phys. Rev. Lett. **75**, 1687 (1995).

[5] K. B. Davis, M. O. Mewes, M. R. Andrews, N. J. van Druten, D. S. Durfee, D. M. Kurn, and W. Ketterle, "Bose-Einstein condensation in a gas of sodium atoms," Phys. Rev. Lett. **75**, 3969 (1995).

[6] F. Dalfovo, S. Giorgini, L. P. Pitaevskii, and S. Stringari, "Theory of Bose-Einstein condensation in trapped gases," Rev. Mod. Phys. **71**, 463 (1999).

[7] A. J. Leggett, "Bose-Einstein condensation in the alkali gases: Some fundamental concepts," Rev. Mod. Phys. **73**, 307 (2001).

[8] I. Bloch, J. Dalibard, and W. Zwerger, "Many-body physics with ultracold gases," Rev. Mod. Phys. **80**, 885 (2008).

[9] C. J. Pethick and H. Smith, *Bose-Einstein condensation in dilute gases* (Cambridge University Press, 2002).

[10] L. P. Pitaevskii and S. Stringari, *Bose-Einstein Condensation* (Clarendon Press, Oxford, 2003).

[11] M. Ueda, *Fundamentals and Frontiers of Bose-Einstein Condensation* (World Scientific, 2010).

[12] T. W. Hänsch and A. L. Schawlow, “Cooling of gases by laser radiation,” Opt. Commun. **13**, 68 (1975).

[13] D. J. Wineland and W. M. Itano, “Laser cooling of atoms,” Phys. Rev. A **20**, 1521 (1979).

[14] C. J. Foot, *Atomic Physics* (Oxford University Press, 2005).

[15] P. Meystre, *Atom Optics* (Springer, 2001).

[16] P. D. Lett, R. N. Watts, C. I. Westbrook, W. D. Phillips, P. L. Gould, and H. J. Metcalf, “Observation of atoms laser cooled below the doppler limit,” Phys. Rev. Lett. **61**, 169 (1988).

[17] J. Dalibard and C. Cohen-Tannoudji, “Laser cooling below the doppler limit by polarization gradients: simple theoretical models,” J. Opt. Soc. Am. B **6**, 2023 (1989).

[18] H. J. Metcalf and P. van der Straten, *Laser Cooling and Trapping* (Springer, 1999).

[19] E. Arimondo and G. Orriols, “Nonabsorbing atomic coherences by coherent two-photon transitions in a three-level optical pumping,” Lettere Al Nuovo Cimento Series 2 **17**, 333 (1976).

[20] G. Alzetta, A. Gozzini, L. Moi, and G. Orriols, “An experimental method for the observation of r.f. transitions and laser beat resonances in oriented na vapour,” Il Nuovo Cimento B Series 11 **36**, 5 (1976).

[21] A. Aspect, E. Arimondo, R. Kaiser, N. Vansteenkiste, and C. Cohen-Tannoudji, “Laser cooling below the one-photon recoil energy by velocity-selective coherent population trapping,” Phys. Rev. Lett. **61**, 826 (1988).

[22] A. Aspect, E. Arimondo, R. Kaiser, N. Vansteenkiste, and C. Cohen-Tannoudji, “Laser cooling below the one-photon recoil energy by velocity-selective coherent population trapping: theoretical analysis,” J. Opt. Soc. Am. B **6**, 2112 (1989).

[23] M. Kasevich and S. Chu, “Laser cooling below a photon recoil with three-level atoms,” Phys. Rev. Lett. **69**, 1741 (1992).

[24] J. Reichel, F. Bardou, M. B. Dahan, E. Peik, S. Rand, C. Salomon, and C. Cohen-Tannoudji, “Raman cooling of cesium below 3 nK: New approach inspired by Lévy flight statistics,” Phys. Rev. Lett. **75**, 4575 (1995).

[25] W. Ketterle and N. J. V. Druten, “Evaporative cooling of trapped atoms,” Adv. At., Mol., Opt. Phys. **37**, 181 (1996).

[26] H. F. Hess, “Evaporative cooling of magnetically trapped and compressed spin-polarized hydrogen,” Phys. Rev. B **34**, 3476 (1986).

[27] N. Masuhara, J. M. Doyle, J. C. Sandberg, D. Kleppner, T. J. Greytak, H. F. Hess, and G. P. Kochanski, “Evaporative cooling of spin-polarized atomic hydrogen,” Phys. Rev. Lett. **61**, 935 (1988).

[28] K. Davis, M.-O. Mewes, and W. Ketterle, “An analytical model for evaporative cooling of atoms,” Applied Physics B **60**, 155 (1995).

[29] K. B. Davis, M.-O. Mewes, M. A. Joffe, M. R. Andrews, and W. Ketterle, “Evaporative cooling of sodium atoms,” Phys. Rev. Lett. **74**, 5202 (1995).

[30] W. Petrich, M. H. Anderson, J. R. Ensher, and E. A. Cornell, “Stable, tightly confining magnetic trap for evaporative cooling of neutral atoms,” Phys. Rev. Lett. **74**, 3352 (1995).

[31] D. E. Pritchard, K. Helmerson, and A. G. Martin, *Atomic Physics 11*, edited by S. Haroche, J. C. Gay, and G. Grynberg (World Scientific, Singapore, 1989).

[32] T. W. Hijmans, O. J. Luiten, I. D. Setija, and J. T. M. Walraven, “Optical cooling of atomic hydrogen in a magnetic trap,” J. Opt. Soc. Am. B **6**, 2235 (1989).

[33] J. T. M. Walraven, *Quantum Dynamics of Simple Systems*, edited by G. L. Oppo and S. M. Barnett (Institute of Physics Publ., London, 1996).

[34] E. L. Raab, M. Prentiss, A. Cable, S. Chu, and D. E. Pritchard, “Trapping of neutral sodium atoms with radiation pressure,” Phys. Rev. Lett. **59**, 2631 (1987).

[35] H. Metcalf, “Magneto-optical trapping and its application to helium metastables,” J. Opt. Soc. Am. B **6**, 2206 (1989).

[36] T. Bergeman, G. Erez, and H. J. Metcalf, “Magnetostatic trapping fields for neutral atoms,” Phys. Rev. A **35**, 1535 (1987).

[37] R. Grimm, M. Weidemüller, and Y. B. Ovchinnikov, “Optical dipole traps for neutral atoms,” Adv. At., Mol., Opt. Phys. **42**, 95 (2000).

[38] M. D. Barrett, J. A. Sauer, and M. S. Chapman, “All-optical formation of an atomic Bose-Einstein condensate,” Phys. Rev. Lett. **87**, 010404 (2001).

[39] M. Greiner, *Ultracold quantum gases in three-dimensional optical lattice potentials*, Ph.D. thesis, Ludwi-Maximilians-Universität München (2003).

[40] I. Bloch, "Ultracold quantum gases in optical lattices," Nat. Phys. **1**, 23 (2005).

[41] M. Greiner and S. Folling, "Condensed-matter physics: Optical lattices," Nature **453**, 736 (2008).

[42] I. Bloch, "Exploring quantum matter with ultracold atoms in optical lattices," J. Phys. B: At. Mol. Opt. Phys. **38**, 629 (2005).

[43] O. Morsch and M. Oberthaler, "Dynamics of Bose-Einstein condensates in optical lattices," Rev. Mod. Phys. **78**, 179 (2006).

[44] M. Lewenstein, A. Sanpera, V. Ahufinger, B. Damski, A. Sen(De), and U. Sen, "Ultracold atomic gases in optical lattices: mimicking condensed matter physics and beyond," Advances in Physics **56**, 243 (2007).

[45] K. Huang, *Statistical Mechanics* (Wiley, 1987).

[46] A. J. Legget, *Quantum Liquids: Bose Condensation and Cooper Pairing in Condensed-Matter Systems* (Oxford University Press, 2006).

[47] C. Cohen-Tannoudji, *Poincaré Seminar 2003*, edited by J. Dalibard and V. Rivasseau (Birkhäuser, 2004).

[48] K. Sacha, *Kondensat Bosego-Einsteina* (Instytut Fizyki im. M. Smoluchowskiego, 2004).

[49] J. Reichel and V. Vuletic, eds., *Atom chips* (Wiley, 2011).

[50] V. Bagnato, D. E. Pritchard, and D. Kleppner, "Bose-Einstein condensation in an external potential," Phys. Rev. A **35**, 4354 (1987).

[51] V. Bagnato and D. Kleppner, "Bose-Einstein condensation in low-dimensional traps," Phys. Rev. A **44**, 7439 (1991).

[52] W. Ketterle and N. J. van Druten, "Bose-Einstein condensation of a finite number of particles trapped in one or three dimensions," Phys. Rev. A **54**, 656 (1996).

[53] D. S. Petrov, M. Holzmann, and G. V. Shlyapnikov, "Bose-Einstein condensation in quasi-2D trapped gases," Phys. Rev. Lett. **84**, 2551 (2000).

[54] D. S. Petrov, G. V. Shlyapnikov, and J. T. M. Walraven, "Regimes of quantum degeneracy in trapped 1D gases," Phys. Rev. Lett. **85**, 3745 (2000).

[55] A. Görlitz, J. M. Vogels, A. E. Leanhardt, C. Raman, T. L. Gustavson, J. R. Abo-Shaeer, A. P. Chikkatur, S. Gupta, S. Inouye, T. Rosenband, and W. Ketterle, "Realization of Bose-Einstein condensates in lower dimensions," Phys. Rev. Lett. **87**, 130402 (2001).

[56] F. Schreck, L. Khaykovich, K. L. Corwin, G. Ferrari, T. Bourdel, J. Cubizolles, and C. Salomon, "Quasipure Bose-Einstein condensate immersed in a Fermi sea," Phys. Rev. Lett. **87**, 080403 (2001).

[57] D. S. Petrov, D. M. Gangardt, and G. V. Shlyapnikov, "Low-dimensional trapped gases," J. Phys. IV France **116**, 5 (2004).

[58] J. Esteve, J.-B. Trebbia, T. Schumm, A. Aspect, C. I. Westbrook, and I. Bouchoule, "Observations of density fluctuations in an elongated Bose gas: Ideal gas and quasicondensate regimes," Phys. Rev. Lett. **96**, 130403 (2006).

[59] U. Al Khawaja, J. O. Andersen, N. P. Proukakis, and H. T. C. Stoof, "Low dimensional Bose gases," Phys. Rev. A **66**, 013615 (2002).

[60] M. Greiner, I. Bloch, O. Mandel, T. W. Hänsch, and T. Esslinger, "Exploring phase coherence in a 2D lattice of Bose-Einstein condensates," Phys. Rev. Lett. **87**, 160405 (2001).

[61] S. Burger, F. S. Cataliotti, C. Fort, P. Maddaloni, F. Minardi, and M. Inguscio, "Quasi-2D Bose-Einstein condensation in an optical lattice," EPL (Europhysics Letters) **57**, 1 (2002).

[62] A. Posazhennikova, "Colloquium: Weakly interacting, dilute Bose gases in 2D," Rev. Mod. Phys. **78**, 1111 (2006).

[63] M. D. Landau and E. M. Lifshitz, *Quantum Mechanics* (Pergamon, London, 1959).

[64] Y. Castin, *Coherent atomic matter waves*, edited by R. Kaiser, C. Westbrrok, and F. David, Les Houches Session LXII (Springer, 2001).

[65] J. J. Sakurai, *Modern Quantum Mechanics* (Addison Wesley, 1993).

[66] H. Feshbach, "A unified theory of nuclear reactions," II. Ann. Phys. **19**, 287 (1962).

[67] S. Inouye, M. R. Andrews, J. Stenger, H. J. Miesner, D. M. Stamper-Kurn, and W. Ketterle, "Observation of Feshbach resonances in a Bose-Einstein condensate," Nature **392**, 151 (1998).

[68] M. Theis, G. Thalhammer, K. Winkler, M. Hellwig, G. Ruff, R. Grimm, and J. H. Denschlag, "Tuning the scattering length with an optically induced Feshbach resonance," Phys. Rev. Lett. **93**, 123001 (2004).

[69] D. M. Bauer, M. Lettner, C. Vo, G. Rempe, and S. Durr, "Control of a magnetic Feshbach resonance with laser light," Nat. Phys. **5**, 339 (2009).

[70] C. Chin, R. Grimm, P. Julienne, and E. Tiesinga, "Feshbach resonances in ultracold gases," Rev. Mod. Phys. **82**, 1225 (2010).

[71] H. S. Friedrich, *Theoretical Atomic Physics* (Springer, 2006).

[72] L. Khaykovich, F. Schreck, G. Ferrari, T. Bourdel, J. Cubizolles, L. D. Carr, Y. Castin, and C. Salomon, "Formation of a matter-wave bright soliton," Science **296**, 1290 (2002).

[73] K. E. Strecker, G. B. Partridge, A. G. Truscott, and R. G. Hulet, "Formation and propagation of matter-wave soliton trains," Nature **417**, 150 (2002).

[74] E. A. Donley, N. R. Claussen, S. L. Cornish, J. L. Roberts, E. A. Cornell, and C. E. Wieman, "Dynamics of collapsing and exploding Bose-Einstein condensates," Nature **412**, 295 (2001).

[75] C. A. Regal, M. Greiner, and D. S. Jin, "Observation of resonance condensation of fermionic atom pairs," Phys. Rev. Lett. **92**, 040403 (2004).

[76] E. A. Donley, N. R. Claussen, S. T. Thompson, and C. E. Wieman, "Atom-molecule coherence in a Bose-Einstein condensate," Nature **417**, 529 (2002).

[77] T. Köhler, K. Góral, and P. S. Julienne, "Production of cold molecules via magnetically tunable Feshbach resonances," Rev. Mod. Phys. **78**, 1311 (2006).

[78] N. N. Bogoliubov, "On the theory of superfluidity," J. Phys. USSR **11**, 23 (1947).

[79] Strictly speaking, this statement is not true due to the quantum depletion of the condensate, i.e., the decrease in the condensate fraction produced by the interactions between atoms [6]. If, however, the previously discussed condition $na_{sc}^3 \ll 1$ holds, the condensate depletion $\hat{\Psi}'(\mathbf{r})$ from the Eq. (II.16) is negligible and, in the zero order perturbative treatment, can be legitimately omitted. Therefore, here we can safely claim that all N particles are in the condensate and replace $\hat{\Psi}(\mathbf{r})$ with $\Psi(\mathbf{r})$. See, e.g., Ref. [6] for results beyond the zero order approximation.

[80] E. P. Gross, "Structure of a quantized vortex in boson systems," Nuovo Cimento **20**, 454 (1961).

[81] L. P. Pitaevskii, "Vortex lines in an imperfect Bose gas," Sov. Phys. JETP **13**, 451 (1961).

[82] Y. Kagan, A. E. Muryshev, and G. V. Shlyapnikov, "Collapse and Bose-Einstein condensation in a trapped Bose gas with negative scattering length," Phys. Rev. Lett. **81**, 933 (1998).

[83] J. M. Gerton, D. Strekalov, I. Prodan, and R. G. Hulet, "Direct observation of growth and collapse of a Bose-Einstein condensate with attractive interactions," Nature **408**, 692 (2000).

[84] J. L. Roberts, N. R. Claussen, S. L. Cornish, E. A. Donley, E. A. Cornell, and C. E. Wieman, "Controlled collapse of a Bose-Einstein condensate," Phys. Rev. Lett. **86**, 4211 (2001).

[85] H. Saito and M. Ueda, "Intermittent implosion and pattern formation of trapped Bose-Einstein condensates with an attractive interaction," Phys. Rev. Lett. **86**, 1406 (2001).

[86] H. Saito and M. Ueda, "Mean-field analysis of collapsing and exploding Bose-Einstein condensates," Phys. Rev. A **65**, 033624 (2002).

[87] C. C. Bradley, C. A. Sackett, and R. G. Hulet, "Bose-Einstein condensation of lithium: Observation of limited condensate number," Phys. Rev. Lett. **78**, 985 (1997).

[88] C. A. Sackett, C. C. Bradley, M. Welling, and R. G. Hulet, "Bose-Einstein condensation of lithium," Appl. Phys. B **65**, 433 (1997).

[89] A. Gammal, T. Frederico, and L. Tomio, "Critical number of atoms for attractive Bose-Einstein condensates with cylindrically symmetrical traps," Phys. Rev. A **64**, 055602 (2001).

[90] V. M. Pérez-García, H. Michinel, and H. Herrero, "Bose-Einstein solitons in highly asymmetric traps," Phys. Rev. A **57**, 3837 (1998).

[91] C. Mora and Y. Castin, "Extension of Bogoliubov theory to quasicondensates," Phys. Rev. A **67**, 053615 (2003).

[92] J. O. Andersen, U. Al Khawaja, and H. T. C. Stoof, "Phase fluctuations in atomic Bose gases," Phys. Rev. Lett. **88**, 070407 (2002).

[93] K. V. Kheruntsyan, D. M. Gangardt, P. D. Drummond, and G. V. Shlyapnikov, "Pair correlations in a finite-temperature 1D Bose gas," Phys. Rev. Lett. **91**, 040403 (2003).

[94] R. Desbuquois, L. Chomaz, T. Yefsah, J. Leonard, J. Beugnon, C. Weitenberg, and J. Dalibard, "Superfluid behaviour of a two-dimensional Bose gas," Nature Physics **8**, 645 (2012).

[95] W. Hansel, P. Hommelhoff, T. W. Hansch, and J. Reichel, "Bose-Einstein condensation on a microelectronic chip," Nature **413**, 498 (2001).

[96] H. Ott, J. Fortagh, G. Schlotterbeck, A. Grossmann, and C. Zimmermann, "Bose-Einstein condensation in a surface microtrap," Phys. Rev. Lett. **87**, 230401 (2001).

[97] P. G. Drazin and R. S. Johnson, *Solitons: An Introduction* (Cambridge University Press, 1989).

[98] Y. S. Kivshar and B. A. Malomed, "Dynamics of solitons in nearly integrable systems," Rev. Mod. Phys. **61**, 763 (1989).

[99] T. Dauxois and M. Peyrard, *Physics of Solitons* (Cambridge University Press, 2006).

[100] G. Agrawal, ed., *Nonlinear Fiber Optics* (Academic Press, 2006).

[101] Y. V. Kartashov, B. A. Malomed, and L. Torner, "Solitons in nonlinear lattices," Rev. Mod. Phys. **83**, 247 (2011).

[102] A. Hasegawa and F. Tappert, "Transmission of stationary nonlinear optical pulses in dispersive dielectric fibers. I. Anomalous dispersion," App. Phys. Lett. **23**, 142 (1973).

[103] L. F. Mollenauer, R. H. Stolen, and J. P. Gordon, "Experimental observation of picosecond pulse narrowing and solitons in optical fibers," Phys. Rev. Lett. **45**, 1095 (1980).

[104] S. Maneuf, R. Desailly, and C. Froehly, "Stable self-trapping of laser beams: Observation in a nonlinear planar waveguide," Optics Comm. **65**, 193 (1988).

[105] M. Segev, B. Crosignani, A. Yariv, and B. Fischer, "Spatial solitons in photorefractive media," Phys. Rev. Lett. **68**, 923 (1992).

[106] G. C. Duree, J. L. Shultz, G. J. Salamo, M. Segev, A. Yariv, B. Crosignani, P. Di Porto, E. J. Sharp, and R. R. Neurgaonkar, "Observation of self-trapping of an optical beam due to the photorefractive effect," Phys. Rev. Lett. **71**, 533 (1993).

[107] W. E. Torruellas, Z. Wang, D. J. Hagan, E. W. VanStryland, G. I. Stegeman, L. Torner, and C. R. Menyuk, "Observation of two-dimensional spatial solitary waves in a quadratic medium," Phys. Rev. Lett. **74**, 5036 (1995).

[108] X. Liu, L. J. Qian, and F. W. Wise, "Generation of optical spatiotemporal solitons," Phys. Rev. Lett. **82**, 4631 (1999).

[109] A. A. Kanashov and A. M. Rubenchik, "On diffraction and dispersion effect on three wave interaction," Physica D **4**, 122 (1981).

[110] B. A. M. Torner, D. Mihalache, F. Wise, and Lluis, "Spatiotemporal optical solitons," J. Opt. B: Quantum Semiclass. Opt. **7**, R53 (2005).

[111] S. Minardi, F. Eilenberger, Y. V. Kartashov, A. Szameit, U. Röpke, J. Kobelke, K. Schuster, H. Bartelt, S. Nolte, L. Torner, F. Lederer, A. Tünnermann, and T. Pertsch, "Three-dimensional light bullets in arrays of waveguides," Phys. Rev. Lett. **105**, 263901 (2010).

[112] V. F. Zakharov and A. B. Shabat, "Exact theory of two-dimensional self-focusing and one-dimensional self-modulation of wave in nonlinear media," JETP **34**, 62 (1972).

[113] W. Zhang, D. F. Walls, and B. C. Sanders, "Atomic soliton in a traveling wave laser beam," Phys. Rev. Lett. **72**, 60 (1994).

[114] P. A. Ruprecht, M. J. Holland, K. Burnett, and M. Edwards, "Time-dependent solution of the nonlinear Schrödinger equation for Bose-condensed trapped neutral atoms," Phys. Rev. A **51**, 4704 (1995).

[115] W. P. Reinhardt and C. W. Clark, "Soliton dynamics in the collisions of Bose-Einstein condensates: an analogue of the Josephson effect," J. Phys. B: At. Mol. Opt. Phys. **30**, L785 (1997).

[116] A. D. Jackson, G. M. Kavoulakis, and C. J. Pethick, "Solitary waves in clouds of Bose-Einstein condensed atoms," Phys. Rev. A **58**, 2417 (1998).

[117] T. F. Scott, R. J. Ballagh, and K. Burnett, "Formation of fundamental structures in Bose-Einstein condensates," J. Phys. B: At. Mol. Opt. Phys. **31**, L329 (1998).

[118] R. Dum, J. I. Cirac, M. Lewenstein, and P. Zoller, "Creation of dark solitons and vortices in Bose-Einstein condensates," Phys. Rev. Lett. **80**, 2972 (1998).

[119] A. E. Muryshev, H. B. van Linden van den Heuvell, and G. V. Shlyapnikov, "Stability of standing matter waves in a trap," Phys. Rev. A **60**, R2665 (1999).

[120] Ł. Dobrek, M. Gajda, M. Lewenstein, K. Sengstock, G. Birkl, and W. Ertmer, "Optical generation of vortices in trapped Bose-Einstein condensates," Phys. Rev. A **60**, R3381 (1999).

[121] P. O. Fedichev, A. E. Muryshev, and G. V. Shlyapnikov, "Dissipative dynamics of a kink state in a Bose-condensed gas," Phys. Rev. A **60**, 3220 (1999).

[122] T. Busch and J. R. Anglin, "Motion of dark solitons in trapped Bose-Einstein condensates," Phys. Rev. Lett. **84**, 2298 (2000).

[123] L. D. Carr, M. A. Leung, and W. P. Reinhardt, "Dynamics of the Bose-Einstein condensate: quasi-one-dimension and beyond," J. Phys. B: At. Mol. Opt. Phys. **33**, 3983 (2000).

[124] Y. S. Kivshar, T. J. Alexander, and S. K. Turitsyn, "Nonlinear modes of a macroscopic quantum oscillator," Phys. Lett. A **278**, 225 (2001).

[125] J. Denschlag, J. E. Simsarian, D. L. Feder, C. W. Clark, L. A. Collins, J. Cubizolles, L. Deng, E. W. Hagley, K. Helmerson, W. P. Reinhardt, S. L. Rolston, B. I. Schneider, and W. D. Phillips, "Generating solitons by phase engineering of a Bose-Einstein condensate," Science **287**, 97 (2000).

[126] S. Burger, K. Bongs, S. Dettmer, W. Ertmer, K. Sengstock, A. Sanpera, G. V. Shlyapnikov, and M. Lewenstein, "Dark solitons in Bose-Einstein condensates," Phys. Rev. Lett. **83**, 5198 (1999).

[127] H. Saito and M. Ueda, "Dynamically stabilized bright solitons in a two-dimensional Bose-Einstein condensate," Phys. Rev. Lett. **90**, 040403 (2003).

[128] F. K. Abdullaev, J. G. Caputo, R. A. Kraenkel, and B. A. Malomed, "Controlling collapse in Bose-Einstein condensates by temporal modulation of the scattering length," Phys. Rev. A **67**, 013605 (2003).

[129] H. Sakaguchi and B. A. Malomed, "Two-dimensional solitons in the Gross-Pitaevskii equation with spatially modulated nonlinearity," Phys. Rev. E **73**, 026601 (2006).

[130] W. H. Zurek, "Causality in condensates: Gray solitons as relics of BEC formation," Phys. Rev. Lett. **102**, 105702 (2009).

[131] B. Damski and W. H. Zurek, "Soliton creation during a Bose-Einstein condensation," Phys. Rev. Lett. **104**, 160404 (2010).

[132] E. Witkowska, P. Deuar, M. Gajda, and K. Rzążewski, "Solitons as the early stage of quasicondensate formation during evaporative cooling," Phys. Rev. Lett. **106**, 135301 (2011).

[133] V. Tikhonenko, J. Christou, B. Luther-Davies, and Y. S. Kivshar, "Observation of vortex solitons created by the instability of dark soliton stripes," Opt. Lett. **21**, 1129 (1996).

[134] A. V. Mamaev, M. Saffman, and A. A. Zozulya, "Propagation of dark stripe beams in nonlinear media: Snake instability and creation of optical vortices," Phys. Rev. Lett. **76**, 2262 (1996).

[135] B. P. Anderson, P. C. Haljan, C. A. Regal, D. L. Feder, L. A. Collins, C. W. Clark, and E. A. Cornell, "Watching dark solitons decay into vortex rings in a Bose-Einstein condensate," Phys. Rev. Lett. **86**, 2926 (2001).

[136] T. Tsuzuki, "Nonlinear waves in the Pitaevskii-Gross equation," J. Low Temp. Phys **4**, 441 (1971).

[137] P. G. Kevrekidis, D. J. Frantzeskakis, and R. Carreto-Gonzáles, eds., *Emergent Nonlinear Phenomena in Bose-Einstein Condensates* (Springer, 2008).

[138] J. P. Gordon, "Interaction forces among solitons in optical fibers," Opt. Lett. **8**, 596 (1983).

[139] K. Tai, A. Hasegawa, and A. Tomita, "Observation of modulational instability in optical fibers," Phys. Rev. Lett. **56**, 135 (1986).

[140] U. Al Khawaja, H. T. C. Stoof, R. G. Hulet, K. E. Strecker, and G. B. Partridge, "Bright soliton trains of trapped Bose-Einstein condensates," Phys. Rev. Lett. **89**, 200404 (2002).

[141] L. D. Carr and J. Brand, "Spontaneous soliton formation and modulational instability in Bose-Einstein condensates," Phys. Rev. Lett. **92**, 040401 (2004).

[142] A. I. Streltsov, O. E. Alon, and L. S. Cederbaum, "Swift loss of coherence of soliton trains in attractive Bose-Einstein condensates," Phys. Rev. Lett. **106**, 240401 (2011).

[143] B. J. Dąbrowska-Wüster, S. Wüster, and M. J. Davis, "Dynamical formation and interaction of bright solitary waves and solitons in the collapse of Bose-Einstein condensates with attractive interactions," New J. Phys. **11**, 053017 (2009).

[144] K. E. Strecker, G. B. Partridge, A. G. Truscott, and R. G. Hulet, "Bright matter wave solitons in Bose-Einstein condensates," New J. Phys. **5**, 73 (2003).

[145] P. Leboeuf, N. Pavloff, and S. Sinha, "Solitonic transmission of Bose-Einstein matter waves," Phys. Rev. A **68**, 063608 (2003).

[146] L. D. Carr and J. Brand, "Pulsed atomic soliton laser," Phys. Rev. A **70**, 033607 (2004).

[147] M. I. Rodas-Verde, H. Michinel, and V. M. Pérez-García, "Controllable soliton emission from a Bose-Einstein condensate," Phys. Rev. Lett. **95**, 153903 (2005).

[148] G. Lenz, P. Meystre, and E. M. Wright, "Nonlinear atom optics," Phys. Rev. Lett. **71**, 3271 (1993).

[149] S. L. Rolston and W. D. Phillips, "Nonlinear and quantum atom optics," Nature **416**, 219 (2002).

[150] A. D. Cronin, J. Schmiedmayer, and D. E. Pritchard, "Optics and interferometry with atoms and molecules," Rev. Mod. Phys. **81**, 1051 (2009).

[151] M.-O. Mewes, M. R. Andrews, D. M. Kurn, D. S. Durfee, C. G. Townsend, and W. Ketterle, "Output coupler for Bose-Einstein condensed atoms," Phys. Rev. Lett. **78**, 582 (1997).

[152] I. Bloch, T. W. Hänsch, and T. Esslinger, "Atom laser with a cw output coupler," Phys. Rev. Lett. **82**, 3008 (1999).

[153] E. W. Hagley, L. Deng, M. Kozuma, J. Wen, K. Helmerson, S. L. Rolston, and W. D. Phillips, "A well-collimated quasi-continuous atom laser," Science **283**, 1706 (1999).

[154] S. Inouye, T. Pfau, S. Gupta, A. P. Chikkatur, A. Gorlitz, D. E. Pritchard, and W. Ketterle, "Phase-coherent amplification of atomic matter waves," Nature **402**, 641 (1999).

[155] M. Kozuma, Y. Suzuki, Y. Torii, T. Sugiura, T. Kuga, E. W. Hagley, and L. Deng, "Phase-coherent amplification of matter waves," Science **286**, 2309 (1999).

[156] A. P. Chikkatur, Y. Shin, A. E. Leanhardt, D. Kielpinski, E. Tsikata, T. L. Gustavson, D. E. Pritchard, and W. Ketterle, "A continuous source of Bose-Einstein condensed atoms," Science **296**, 2193 (2002).

[157] V. Y. F. Leung, A. G. Truscott, and K. G. H. Baldwin, "Nonlinear atom optics with bright matter-wave soliton trains," Phys. Rev. A **66**, 061602 (2002).

[158] N. P. Robins, C. Figl, M. Jeppesen, G. R. Dennis, and J. D. Close, "A pumped atom laser," Nat. Phys. **4**, 731 (2008).

[159] N. Veretenov, Y. Rozhdestvensky, N. Rosanov, V. Smirnov, and S. Fedorov, "Interferometric precision measurements with Bose-Einstein condensate solitons formed by an optical lattice," Eur. Phys. J. D **42**, 455 (2007).

[160] N. G. Parker, A. M. Martin, S. L. Cornish, and C. S. Adams, "Collisions of bright solitary matter waves," J. Phys. B: At. Mol. Opt. Phys. **41**, 045303 (2008).

[161] T. P. Billam, S. L. Cornish, and S. A. Gardiner, "Realizing bright-matter-wave-soliton collisions with controlled relative phase," Phys. Rev. A **83**, 041602 (2011).

[162] A. D. Martin and J. Ruostekoski, "Quantum dynamics of atomic bright solitons under splitting and recollision, and implications for interferometry," New J. Phys. **14**, 043040 (2012).

[163] C. Weiss and Y. Castin, "Creation and detection of a mesoscopic gas in a nonlocal quantum superposition," Phys. Rev. Lett. **102**, 010403 (2009).

[164] A. I. Streltsov, O. E. Alon, and L. S. Cederbaum, "Scattering of an attractive Bose-Einstein condensate from a barrier: Formation of quantum superposition states," Phys. Rev. A **80**, 043616 (2009).

[165] M. Lewenstein and B. A. Malomed, "Entanglement generation by collisions of quantum solitons in the Born approximation," New J. Phys. **11**, 113014 (2009).

[166] A. I. Streltsov, O. E. Alon, and L. S. Cederbaum, "Efficient generation and properties of mesoscopic quantum superposition states in an attractive Bose-Einstein condensate threaded by a potential barrier," J. Phys. B: At. Mol. Opt. Phys. **42**, 091004 (2009).

[167] B. Gertjerenken, T. P. Billam, C. L. Blackley, C. R. Le Sueur, L. Khaykovich, S. L. Cornish, and C. Weiss, "Entangling two distinguishable matter-wave bright solitons via collisions," (2012), arXiv:1301.0718 .

[168] A. L. Fetter and J. D. Walecka, *Quantum Theory of Many-particle Systems* (McGraw-Hill, 1971).

[169] M. D. Landau and E. M. Lifshitz, *Statistical Physics, Part 2* (Butterworth-Heinemann, 1980).

[170] A. A. Abrikosov, L. P. Gorkov, and I. E. Dzyaloshinski, *Methods of quantum field theory in statistical physics* (Dover Publications, 1975).

[171] A. L. Fetter, "Nonuniform states of an imperfect Bose gas," Annals of Physics **70**, 67 (1972).

[172] G. V. Shlyapnikov, "Ultracold Quantum Gases, Part 1, Bose-Einstein condensed gases," (2009), notes to the course taught in École de Physique des Houches 2009, Ultracold Quantum Gases of Atoms and Molecules, and in Van der Waals-Zeeman Institute, University of Amsterdam.

[173] P. G. De Gennes, "Boundary effects in superconductors," Rev. Mod. Phys. **36**, 225 (1964).

[174] A. L. Fetter, "Ground state and excited states of a confined condensed Bose gas," Phys. Rev. A **53**, 4245 (1996).

[175] A. L. Fetter and A. A. Svidzinsky, "Vortices in a trapped dilute Bose-Einstein condensate," J. Phys.: Condens. Matter **13**, R135 (2001).

[176] A. Brunello, F. Dalfovo, L. Pitaevskii, and S. Stringari, "How to measure the Bogoliubov quasiparticle amplitudes in a trapped condensate," Phys. Rev. Lett. **85**, 4422 (2000).

[177] J. M. Vogels, K. Xu, C. Raman, J. R. Abo-Shaeer, and W. Ketterle, "Experimental observation of the Bogoliubov transformation for a Bose-Einstein condensed gas," Phys. Rev. Lett. **88**, 060402 (2002).

[178] D. DeMille, "Quantum computation with trapped polar molecules," Phys. Rev. Lett. **88**, 067901 (2002).

[179] J. Deiglmayr, A. Grochola, M. Repp, K. Mörtlbauer, C. Glück, J. Lange, O. Dulieu, R. Wester, and M. Weidemüller, "Formation of ultracold polar molecules in the rovibrational ground state," Phys. Rev. Lett. **101**, 133004 (2008).

[180] K.-K. Ni, S. Ospelkaus, M. H. G. de Miranda, A. Pe'er, B. Neyenhuis, J. J. Zirbel, S. Kotochigova, P. S. Julienne, D. S. Jin, and J. Ye, "A high phase-space-density gas of polar molecules," Science **322**, 231 (2008).

[181] K.-K. Ni, S. Ospelkaus, D. Wang, G. Quéméner, B. Neyenhuis, M. H. G. de Miranda, J. L. Bohn, J. Ye, and D. S. Jin, "Dipolar collisions of polar molecules in the quantum regime," Nature **464**, 1324 (2010).

[182] L. D. Carr, D. DeMille, R. V. Krems, and J. Ye, "Cold and ultracold molecules: science, technology and applications," New J. Phys. **11**, 055049 (2009).

[183] S. Ospelkaus, K.-K. Ni, G. Quéméner, B. Neyenhuis, D. Wang, M. H. G. de Miranda, J. L. Bohn, J. Ye, and D. S. Jin, "Controlling the hyperfine state of rovibronic ground-state polar molecules," Phys. Rev. Lett. **104**, 030402 (2010).

[184] S. Ospelkaus, K.-K. Ni, D. Wang, M. H. G. de Miranda, B. Neyenhuis, G. Quéméner, P. S. Julienne, J. L. Bohn, D. S. Jin, and J. Ye, "Quantum-state controlled chemical reactions of ultracold potassium-rubidium molecules," Science **327**, 853 (2010).

[185] W. Li, T. Pohl, J. M. Rost, S. T. Rittenhouse, H. R. Sadeghpour, J. Nipper, B. Butscher, J. B. Balewski, V. Bendkowsky, R. Löw, and T. Pfau, "A homonuclear molecule with a permanent electric dipole moment," Science **334**, 1110 (2011).

[186] M. H. G. de Miranda, A. Chotia, B. Neyenhuis, D. Wang, G. Quemener, S. Ospelkaus, J. L. Bohn, J. Ye, and D. S. Jin, "Controlling the quantum stereodynamics of ultracold bimolecular reactions," Nat. Phys. **7**, 502 (2011).

[187] M. Zeppenfeld, B. G. U. Englert, R. Glockner, A. Prehn, M. Mielenz, C. Sommer, L. D. van Buuren, M. Motsch, and G. Rempe, "Sisyphus cooling of electrically trapped polyatomic molecules," Nature **491**, 570 (2012).

[188] A. Chotia, B. Neyenhuis, S. A. Moses, B. Yan, J. P. Covey, M. Foss-Feig, A. M. Rey, D. S. Jin, and J. Ye, "Long-lived dipolar molecules and Feshbach molecules in a 3D optical lattice," Phys. Rev. Lett. **108**, 080405 (2012).

[189] C.-H. Wu, J. W. Park, P. Ahmadi, S. Will, and M. W. Zwierlein, "Ultracold fermionic Feshbach molecules of ^{23}Na^{40}K," Phys. Rev. Lett. **109**, 085301 (2012).

[190] T. Takekoshi, M. Debatin, R. Rameshan, F. Ferlaino, R. Grimm, H.-C. Nägerl, C. R. Le Sueur, J. M. Hutson, P. S. Julienne, S. Kotochigova, and E. Tiemann, "Towards the production of ultracold ground-state rbcs molecules: Feshbach resonances, weakly bound states, and the coupled-channel model," Phys. Rev. A **85**, 032506 (2012).

[191] D. Tong, S. M. Farooqi, J. Stanojevic, S. Krishnan, Y. P. Zhang, R. Côté, E. E. Eyler, and P. L. Gould, "Local blockade of Rydberg excitation in an ultracold gas," Phys. Rev. Lett. **93**, 063001 (2004).

[192] R. Heidemann, U. Raitzsch, V. Bendkowsky, B. Butscher, R. Löw, and T. Pfau, "Rydberg excitation of Bose-Einstein condensates," Phys. Rev. Lett. **100**, 033601 (2008).

[193] T. F. Gallagher and P. Pillet, "Dipole-Dipole interactions of Rydberg atoms," Adv. At., Mol., Opt. Phys. **56**, 161 (2008).

[194] V. Bendkowsky, B. Butscher, J. Nipper, J. P. Shaffer, R. Low, and T. Pfau, "Observation of ultralong-range Rydberg molecules," Nature **458**, 1005 (2009).

[195] G. Pupillo, A. Micheli, M. Boninsegni, I. Lesanovsky, and P. Zoller, "Strongly correlated gases of Rydberg-dressed atoms: Quantum and classical dynamics," Phys. Rev. Lett. **104**, 223002 (2010).

[196] H. Weimer, M. Müller, I. Lesanovsky, P. Zoller, and H. P. Büchler, "A Rydberg quantum simulator," Nat. Phys. **6**, 382 (2010).

[197] N. Henkel, R. Nath, and T. Pohl, “Three-dimensional roton excitations and supersolid formation in Rydberg-excited Bose-Einstein condensates,” Phys. Rev. Lett. **104**, 195302 (2010).

[198] P. Schausz, M. Cheneau, M. Endres, T. Fukuhara, S. Hild, A. Omran, T. Pohl, C. Gross, S. Kuhr, and I. Bloch, “Observation of spatially ordered structures in a two-dimensional Rydberg gas,” Nature **491**, 87 (2012).

[199] T. Peyronel, O. Firstenberg, Q.-Y. Liang, S. Hofferberth, A. V. Gorshkov, T. Pohl, M. D. Lukin, and V. Vuletic, “Quantum nonlinear optics with single photons enabled by strongly interacting atoms,” Nature **488**, 57 (2012).

[200] R. Löw, H. Weimer, J. Nipper, J. B. Balewski, B. Butscher, H. P. Büchler, and T. Pfau, “An experimental and theoretical guide to strongly interacting Rydberg gases,” J. Phys. B: At. Mol. Opt. Phys. **45**, 113001 (2012).

[201] B. Groh and S. Dietrich, “Long-ranged orientational order in dipolar fluids,” Phys. Rev. Lett. **72**, 2422 (1994).

[202] B. Groh and S. Dietrich, “Spatial structures of dipolar ferromagnetic liquids,” Phys. Rev. Lett. **79**, 749 (1997).

[203] S. Chandrasekhar F.R.S., *Liquid Crystals* (Cambridge University Press, 1993).

[204] K. Góral, K. Rzążewski, and T. Pfau, “Bose-Einstein condensation with magnetic dipole-dipole forces,” Phys. Rev. A **61**, 051601 (2000).

[205] J. Kim, B. Friedrich, D. P. Katz, D. Patterson, J. D. Weinstein, R. DeCarvalho, and J. M. Doyle, “Buffer-gas loading and magnetic trapping of atomic europium,” Phys. Rev. Lett. **78**, 3665 (1997).

[206] J. D. Weinstein, R. deCarvalho, J. Kim, D. Patterson, B. Friedrich, and J. M. Doyle, “Magnetic trapping of atomic chromium,” Phys. Rev. A **57**, R3173 (1998).

[207] S. Yi and L. You, “Trapped atomic condensates with anisotropic interactions,” Phys. Rev. A **61**, 041604 (2000).

[208] S. Yi and L. You, “Trapped condensates of atoms with dipole interactions,” Phys. Rev. A **63**, 053607 (2001).

[209] L. Santos, G. V. Shlyapnikov, P. Zoller, and M. Lewenstein, “Bose-Einstein condensation in trapped dipolar gases,” Phys. Rev. Lett. **85**, 1791 (2000).

[210] K. Góral and L. Santos, "Ground state and elementary excitations of single and binary Bose-Einstein condensates of trapped dipolar gases," Phys. Rev. A **66**, 023613 (2002).

[211] L. Santos, G. V. Shlyapnikov, and M. Lewenstein, "Roton-Maxon spectrum and stability of trapped dipolar Bose-Einstein condensates," Phys. Rev. Lett. **90**, 250403 (2003).

[212] A. Griesmaier, J. Werner, S. Hensler, J. Stuhler, and T. Pfau, "Bose-Einstein condensation of chromium," Phys. Rev. Lett. **94**, 160401 (2005).

[213] J. Stuhler, A. Griesmaier, T. Koch, M. Fattori, T. Pfau, S. Giovanazzi, P. Pedri, and L. Santos, "Observation of dipole-dipole interaction in a degenerate quantum gas," Phys. Rev. Lett. **95**, 150406 (2005).

[214] T. Lahaye, T. Koch, B. Frohlich, M. Fattori, J. Metz, A. Griesmaier, S. Giovanazzi, and T. Pfau, "Strong dipolar effects in a quantum ferrofluid," Nature **448**, 672 (2007).

[215] T. Koch, T. Lahaye, J. Metz, B. Frohlich, A. Griesmaier, and T. Pfau, "Stabilization of a purely dipolar quantum gas against collapse," Nat. Phys. **4**, 218 (2008).

[216] T. Lahaye, J. Metz, B. Fröhlich, T. Koch, M. Meister, A. Griesmaier, T. Pfau, H. Saito, Y. Kawaguchi, and M. Ueda, "d-wave collapse and explosion of a dipolar Bose-Einstein condensate," Phys. Rev. Lett. **101**, 080401 (2008).

[217] M. Lu, N. Q. Burdick, S. H. Youn, and B. L. Lev, "Strongly dipolar Bose-Einstein condensate of dysprosium," Phys. Rev. Lett. **107**, 190401 (2011).

[218] M. Lu, N. Q. Burdick, and B. L. Lev, "Quantum degenerate dipolar Fermi gas," Phys. Rev. Lett. **108**, 215301 (2012).

[219] K. Aikawa, A. Frisch, M. Mark, S. Baier, A. Rietzler, R. Grimm, and F. Ferlaino, "Bose-Einstein condensation of erbium," Phys. Rev. Lett. **108**, 210401 (2012).

[220] Q. Beaufils, R. Chicireanu, T. Zanon, B. Laburthe-Tolra, E. Maréchal, L. Vernac, J.-C. Keller, and O. Gorceix, "All-optical production of chromium Bose-Einstein condensates," Phys. Rev. A **77**, 061601 (2008).

[221] G. Bismut, B. Pasquiou, E. Maréchal, P. Pedri, L. Vernac, O. Gorceix, and B. Laburthe-Tolra, "Collective excitations of a dipolar Bose-Einstein condensate," Phys. Rev. Lett. **105**, 040404 (2010).

[222] B. Pasquiou, E. Maréchal, G. Bismut, P. Pedri, L. Vernac, O. Gorceix, and B. Laburthe-Tolra, "Spontaneous demagnetization of a dipolar spinor Bose gas in an ultralow magnetic field," Phys. Rev. Lett. **106**, 255303 (2011).

[223] B. Pasquiou, E. Maréchal, L. Vernac, O. Gorceix, and B. Laburthe-Tolra, "Thermodynamics of a Bose-Einstein condensate with free magnetization," Phys. Rev. Lett. **108**, 045307 (2012).

[224] G. Bismut, B. Laburthe-Tolra, E. Maréchal, P. Pedri, O. Gorceix, and L. Vernac, "Anisotropic excitation spectrum of a dipolar quantum Bose gas," Phys. Rev. Lett. **109**, 155302 (2012).

[225] N. R. Cooper, E. H. Rezayi, and S. H. Simon, "Vortex lattices in rotating atomic Bose gases with dipolar interactions," Phys. Rev. Lett. **95**, 200402 (2005).

[226] J. Zhang and H. Zhai, "Vortex lattices in planar Bose-Einstein condensates with dipolar interactions," Phys. Rev. Lett. **95**, 200403 (2005).

[227] S. Yi and H. Pu, "Vortex structures in dipolar condensates," Phys. Rev. A **73**, 061602 (2006).

[228] H. Pu, W. Zhang, and P. Meystre, "Ferromagnetism in a lattice of Bose-Einstein condensates," Phys. Rev. Lett. **87**, 140405 (2001).

[229] W. Zhang, H. Pu, C. Search, and P. Meystre, "Spin waves in a Bose-Einstein–condensed atomic spin chain," Phys. Rev. Lett. **88**, 060401 (2002).

[230] S. Yi, L. You, and H. Pu, "Quantum phases of dipolar spinor condensates," Phys. Rev. Lett. **93**, 040403 (2004).

[231] S. Yi and H. Pu, "Spontaneous spin textures in dipolar spinor condensates," Phys. Rev. Lett. **97**, 020401 (2006).

[232] L. Santos and T. Pfau, "Spin-3 chromium Bose-Einstein condensates," Phys. Rev. Lett. **96**, 190404 (2006).

[233] K. Gawryluk, M. Brewczyk, K. Bongs, and M. Gajda, "Resonant Einstein–de Haas effect in a rubidium condensate," Phys. Rev. Lett. **99**, 130401 (2007).

[234] M. Vengalattore, S. R. Leslie, J. Guzman, and D. M. Stamper-Kurn, "Spontaneously modulated spin textures in a dipolar spinor Bose-Einstein condensate," Phys. Rev. Lett. **100**, 170403 (2008).

[235] Y. Kawaguchi and M. Ueda, "Spinor Bose-Einstein condensates," Phys. Rep. **520**, 253 (2012).

[236] R. M. Wilson, S. Ronen, and J. L. Bohn, "Critical superfluid velocity in a trapped dipolar gas," Phys. Rev. Lett. **104**, 094501 (2010).

[237] C. Ticknor, R. M. Wilson, and J. L. Bohn, "Anisotropic superfluidity in a dipolar Bose gas," Phys. Rev. Lett. **106**, 065301 (2011).

[238] S. Ronen, D. C. E. Bortolotti, and J. L. Bohn, "Bogoliubov modes of a dipolar condensate in a cylindrical trap," Phys. Rev. A **74**, 013623 (2006).

[239] S. Ronen, D. C. E. Bortolotti, and J. L. Bohn, "Radial and angular rotons in trapped dipolar gases," Phys. Rev. Lett. **98**, 030406 (2007).

[240] R. M. Wilson, S. Ronen, J. L. Bohn, and H. Pu, "Manifestations of the roton mode in dipolar Bose-Einstein condensates," Phys. Rev. Lett. **100**, 245302 (2008).

[241] P. B. Blakie, D. Baillie, and R. N. Bisset, "Roton spectroscopy in a harmonically trapped dipolar Bose-Einstein condensate," Phys. Rev. A **86**, 021604 (2012).

[242] O. Dutta and P. Meystre, "Ground-state structure and stability of dipolar condensates in anisotropic traps," Phys. Rev. A **75**, 053604 (2007).

[243] T. Lahaye, T. Pfau, and L. Santos, "Mesoscopic ensembles of polar bosons in triple-well potentials," Phys. Rev. Lett. **104**, 170404 (2010).

[244] A. Bühler and H. P. Büchler, "Supersolid phase in atomic gases with magnetic dipole interaction," Phys. Rev. A **84**, 023607 (2011).

[245] R. M. Wilson and J. L. Bohn, "Emergent structure in a dipolar Bose gas in a one-dimensional lattice," Phys. Rev. A **83**, 023623 (2011).

[246] A. Maluckov, G. Gligorić, L. Hadžievski, B. A. Malomed, and T. Pfau, "Stable periodic density waves in dipolar Bose-Einstein condensates trapped in optical lattices," Phys. Rev. Lett. **108**, 140402 (2012).

[247] D. C. E. Bortolotti, S. Ronen, J. L. Bohn, and D. Blume, "Scattering length instability in dipolar Bose-Einstein condensates," Phys. Rev. Lett. **97**, 160402 (2006).

[248] R. Nath, P. Pedri, and L. Santos, "Phonon instability with respect to soliton formation in two-dimensional dipolar Bose-Einstein condensates," Phys. Rev. Lett. **102**, 050401 (2009).

[249] R. M. Wilson, S. Ronen, and J. L. Bohn, "Angular collapse of dipolar Bose-Einstein condensates," Phys. Rev. A **80**, 023614 (2009).

[250] S. Müller, J. Billy, E. A. L. Henn, H. Kadau, A. Griesmaier, M. Jona-Lasinio, L. Santos, and T. Pfau, "Stability of a dipolar Bose-Einstein condensate in a one-dimensional lattice," Phys. Rev. A **84**, 053601 (2011).

[251] J. Billy, E. A. L. Henn, S. Müller, T. Maier, H. Kadau, A. Griesmaier, M. Jona-Lasinio, L. Santos, and T. Pfau, "Deconfinement-induced collapse of a coherent array of dipolar Bose-Einstein condensates," Phys. Rev. A **86**, 051603 (2012).

[252] M. Fattori, G. Roati, B. Deissler, C. D'Errico, M. Zaccanti, M. Jona-Lasinio, L. Santos, M. Inguscio, and G. Modugno, "Magnetic dipolar interaction in a Bose-Einstein condensate atomic interferometer," Phys. Rev. Lett. **101**, 190405 (2008).

[253] M. Klawunn and L. Santos, "Hybrid multisite excitations in dipolar condensates in optical lattices," Phys. Rev. A **80**, 013611 (2009).

[254] P. Köberle and G. Wunner, "Phonon instability and self-organized structures in multilayer stacks of confined dipolar Bose-Einstein condensates in optical lattices," Phys. Rev. A **80**, 063601 (2009).

[255] H. Saito, Y. Kawaguchi, and M. Ueda, "Ferrofluidity in a two-component dipolar Bose-Einstein condensate," Phys. Rev. Lett. **102**, 230403 (2009).

[256] R. Nath and L. Santos, "Faraday patterns in two-dimensional dipolar Bose-Einstein condensates," Phys. Rev. A **81**, 033626 (2010).

[257] R. M. Wilson, C. Ticknor, J. L. Bohn, and E. Timmermans, "Roton immiscibility in a two-component dipolar Bose gas," Phys. Rev. A **86**, 033606 (2012).

[258] P. Pedri and L. Santos, "Two-dimensional bright solitons in dipolar Bose-Einstein condensates," Phys. Rev. Lett. **95**, 200404 (2005).

[259] I. Tikhonenkov, B. A. Malomed, and A. Vardi, "Anisotropic solitons in dipolar Bose-Einstein condensates," Phys. Rev. Lett. **100**, 090406 (2008).

[260] R. Nath, P. Pedri, and L. Santos, "Soliton-soliton scattering in dipolar Bose-Einstein condensates," Phys. Rev. A **76**, 013606 (2007).

[261] R. Nath, P. Pedri, and L. Santos, "Stability of dark solitons in three dimensional dipolar Bose-Einstein condensates," Phys. Rev. Lett. **101**, 210402 (2008).

[262] M. Baranov, "Theoretical progress in many-body physics with ultracold dipolar gases," Phys. Rep. **464**, 71 (2008).

[263] T. Lahaye, C. Menotti, L. Santos, M. Lewenstein, and T. Pfau, "The physics of dipolar bosonic quantum gases," Rep. Prog. Phys. **72**, 126401 (2009).

[264] M. A. Baranov, M. Dalmonte, G. Pupillo, and P. Zoller, "Condensed matter theory of dipolar quantum gases," Chem. Rev. **112**, 5012 (2012).

[265] D. J. Griffiths, "Hyperfine splitting in the ground state of hydrogen," Am. J. Phys. **50**, 698 (1982).

[266] S. Ronen, D. C. E. Bortolotti, D. Blume, and J. L. Bohn, "Dipolar Bose-Einstein condensates with dipole-dependent scattering length," Phys. Rev. A **74**, 033611 (2006).

[267] A. Derevianko, "Anisotropic pseudopotential for polarized dilute quantum gases," Phys. Rev. A **67**, 033607 (2003).

[268] G. E. Astrakharchik and Y. E. Lozovik, "Super-Tonks-Girardeau regime in trapped one-dimensional dipolar gases," Phys. Rev. A **77**, 013404 (2008).

[269] A. Micheli, G. Pupillo, H. P. Büchler, and P. Zoller, "Cold polar molecules in two-dimensional traps: Tailoring interactions with external fields for novel quantum phases," Phys. Rev. A **76**, 043604 (2007).

[270] R. Krems, B. Friedrich, and W. Stwalley, eds., *Cold molecules: Theory, Experiment, Applications* (CRC Press, 2009).

[271] S. Giovanazzi, A. Görlitz, and T. Pfau, "Tuning the dipolar interaction in quantum gases," Phys. Rev. Lett. **89**, 130401 (2002).

[272] G. E. Astrakharchik, J. Boronat, J. Casulleras, I. L. Kurbakov, and Y. E. Lozovik, "Weakly interacting two-dimensional system of dipoles: Limitations of the mean-field theory," Phys. Rev. A **75**, 063630 (2007).

[273] S. Giovanazzi, A. Görlitz, and T. Pfau, "Ballistic expansion of a dipolar condensate," J. Opt. B: Quantum Semiclass. Opt. **5**, 208 (2003).

[274] D. H. J. O'Dell, S. Giovanazzi, and C. Eberlein, "Exact hydrodynamics of a trapped dipolar Bose-Einstein condensate," Phys. Rev. Lett. **92**, 250401 (2004).

[275] C. Eberlein, S. Giovanazzi, and D. H. J. O'Dell, "Exact solution of the Thomas-Fermi equation for a trapped Bose-Einstein condensate with dipole-dipole interactions," Phys. Rev. A **71**, 033618 (2005).

[276] L. D. Landau, "The theory of superfluidity of helium II," J. Phys. USSR **5**, 71 (1941).

[277] L. D. Landau, "On the theory of superfluidity of helium II," J. Phys. USSR **11**, 91 (1947).

[278] L. Landau, "On the theory of superfluidity," Phys. Rev. **75**, 884 (1949).

[279] A. Griffin, *Excitations in a Bose-condensed Liquid* (Cambridge University Press, 2005).

[280] G. J. Kalman, P. Hartmann, K. I. Golden, A. Filinov, and Z. Donkó, "Correlational origin of the roton minimum," EPL **90**, 55002 (2010).

[281] R. P. Feynman, "Atomic theory of the two-fluid model of liquid helium," Phys. Rev. **94**, 262 (1954).

[282] R. P. Feynman and M. Cohen, "Energy spectrum of the excitations in liquid helium," Phys. Rev. **102**, 1189 (1956).

[283] M. Cohen and R. P. Feynman, "Theory of inelastic scattering of cold neutrons from liquid helium," Phys. Rev. **107**, 13 (1957).

[284] F. Zambelli, L. Pitaevskii, D. M. Stamper-Kurn, and S. Stringari, "Dynamic structure factor and momentum distribution of a trapped Bose gas," Phys. Rev. A **61**, 063608 (2000).

[285] P. Noziéres, "Is the roton in superfluid ^{4}He the ghost of a Bragg spot?" J. Low Temp. Phys. **137**, 45 (2004).

[286] H. Palevsky, K. Otnes, K. E. Larsson, R. Pauli, and R. Stedman, "Excitation of rotons in helium II by cold neutrons," Phys. Rev. **108**, 1346 (1957).

[287] H. Palevsky, K. Otnes, and K. E. Larsson, "Excitation of rotons in helium II by cold neutrons," Phys. Rev. **112**, 11 (1958).

[288] D. G. Henshaw and A. D. B. Woods, "Modes of atomic motions in liquid helium by inelastic scattering of neutrons," Phys. Rev. **121**, 1266 (1961).

[289] A. D. B. Woods, "Neutron inelastic scattering from liquid helium at small momentum transfers," Phys. Rev. Lett. **14**, 355 (1965).

[290] T. Regge, "Free boundary of He II and Feynman wave functions," J. Low Temp. Phys. **9**, 123 (1972).

[291] F. Dalfovo, "Structure of vortices in helium at zero temperature," Phys. Rev. B **46**, 5482 (1992).

[292] Y. Pomeau and S. Rica, "Model of superflow with rotons," Phys. Rev. Lett. **71**, 247 (1993).

[293] N. G. Berloff and P. H. Roberts, “Motions in a Bose condensate: VI. Vortices in a nonlocal model,” J. Phys. A: Math. Gen. **32**, 5611 (1999).

[294] S. Villerot, B. Castaing, and L. Chevillard, “Static spectroscopy of a dense superfluid,” J. Low Temp. Phys. **169**, 1 (2012).

[295] S. Stringari, “Dynamics of Bose-Einstein condensed gases in highly deformed traps,” Phys. Rev. A **58**, 2385 (1998).

[296] S. Giovanazzi and D. O’Dell, “Instabilities and the roton spectrum of a quasi-1D Bose-Einstein condensed gas with dipole-dipole interactions,” Eur. Phys. J. D **31**, 439 (2004).

[297] S. Sinha and L. Santos, “Cold dipolar gases in quasi-one-dimensional geometries,” Phys. Rev. Lett. **99**, 140406 (2007).

[298] Y. Pomeau and S. Rica, “Dynamics of a model of supersolid,” Phys. Rev. Lett. **72**, 2426 (1994).

[299] C. Josserand, Y. Pomeau, and S. Rica, “Coexistence of ordinary elasticity and superfluidity in a model of a defect-free supersolid,” Phys. Rev. Lett. **98**, 195301 (2007).

[300] S. Komineas and N. R. Cooper, “Vortex lattices in Bose-Einstein condensates with dipolar interactions beyond the weak-interaction limit,” Phys. Rev. A **75**, 023623 (2007).

[301] C. Ticknor, “Anisotropic coherence properties in a trapped quasi-two-dimensional dipolar gas,” Phys. Rev. A **86**, 053602 (2012).

[302] A. Macia, D. Hufnagl, F. Mazzanti, J. Boronat, and R. E. Zillich, “Excitations and stripe phase formation in a two-dimensional dipolar Bose gas with tilted polarization,” Phys. Rev. Lett. **109**, 235307 (2012).

[303] J. C. Cremon, G. M. Bruun, and S. M. Reimann, “Tunable Wigner states with dipolar atoms and molecules,” Phys. Rev. Lett. **105**, 255301 (2010).

[304] A. G. Litvak, V. A. Mironov, G. M. Fraiman, and A. D. Yunakovskii, “Thermal self-effect of wave beams in a plasma with a nonlocal nonlinearity,” Sov. J. Plasma Phys. **1**, 31 (1975).

[305] M. Peccianti, K. A. Brzdkiewicz, and G. Assanto, “Nonlocal spatial soliton interactions in nematic liquid crystals,” Opt. Lett. **27**, 1460 (2002).

[306] C. Conti, M. Peccianti, and G. Assanto, “Route to nonlocality and observation of accessible solitons,” Phys. Rev. Lett. **91**, 073901 (2003).

[307] M. Peccianti, C. Conti, A. Gaetano, D. L. Antonio, and C. Umeton, "Routing of anisotropic spatial solitons and modulational instability in liquid crystals," Nature **432**, 733 (2004).

[308] C. Conti, M. Peccianti, and G. Assanto, "Observation of optical spatial solitons in a highly nonlocal medium," Phys. Rev. Lett. **92**, 113902 (2004).

[309] M. F. Shih, M. Segev, and G. Salamo, "Three-dimensional spiraling of interacting spatial solitons," Phys. Rev. Lett. **78**, 2551 (1997).

[310] R. Richter and I. V. Barashenkov, "Two-dimensional solitons on the surface of magnetic fluids," Phys. Rev. Lett. **94**, 184503 (2005).

[311] F. Maucher, N. Henkel, M. Saffman, W. Królikowski, S. Skupin, and T. Pohl, "Rydberg-induced solitons: Three-dimensional self-trapping of matter waves," Phys. Rev. Lett. **106**, 170401 (2011).

[312] O. Bang, W. Krolikowski, J. Wyller, and J. J. Rasmussen, "Collapse arrest and soliton stabilization in nonlocal nonlinear media," Phys. Rev. E **66**, 046619 (2002).

[313] A. Pikovski, M. Klawunn, G. V. Shlyapnikov, and L. Santos, "Interlayer superfluidity in bilayer systems of fermionic polar molecules," Phys. Rev. Lett. **105**, 215302 (2010).

[314] A. C. Potter, E. Berg, D.-W. Wang, B. I. Halperin, and E. Demler, "Superfluidity and dimerization in a multilayered system of fermionic polar molecules," Phys. Rev. Lett. **105**, 220406 (2010).

[315] B. Wunsch, N. T. Zinner, I. B. Mekhov, S.-J. Huang, D.-W. Wang, and E. Demler, "Few-body bound states in dipolar gases and their detection," Phys. Rev. Lett. **107**, 073201 (2011).

[316] M. Dalmonte, P. Zoller, and G. Pupillo, "Trimer liquids and crystals of polar molecules in coupled wires," Phys. Rev. Lett. **107**, 163202 (2011).

[317] D.-W. Wang, M. D. Lukin, and E. Demler, "Quantum fluids of self-assembled chains of polar molecules," Phys. Rev. Lett. **97**, 180413 (2006).

[318] M. Klawunn, J. Duhme, and L. Santos, "Bose-Fermi mixtures of self-assembled filaments of fermionic polar molecules," Phys. Rev. A **81**, 013604 (2010).

[319] M. Stratmann, T. Pagel, and F. Mitschke, "Experimental observation of temporal soliton molecules," Phys. Rev. Lett. **95**, 143902 (2005).

[320] A. Hause, H. Hartwig, M. Böhm, and F. Mitschke, "Binding mechanism of temporal soliton molecules," Phys. Rev. A **78**, 063817 (2008).

[321] L.-C. Crasovan, Y. V. Kartashov, D. Mihalache, L. Torner, Y. S. Kivshar, and V. M. Pérez-García, "Soliton "molecules": Robust clusters of spatiotemporal optical solitons," Phys. Rev. E **67**, 046610 (2003).

[322] C. Yin, N. G. Berloff, V. M. Pérez-García, D. Novoa, A. V. Carpentier, and H. Michinel, "Coherent atomic soliton molecules for matter-wave switching," Phys. Rev. A **83**, 051605 (2011).

[323] U. A. Khawaja and H. T. C. Stoof, "Formation of matter-wave soliton molecules," New Journal of Physics **13**, 085003 (2011).

[324] P. I. C. Teixeira, J. M. Tavares, and M. M. Telo da Gama, "The effect of dipolar forces on the structure and thermodynamics of classical fluids," J. Phys. Cond. Matt. **12**, R411 (2000).

[325] H. P. Büchler, E. Demler, M. Lukin, A. Micheli, N. Prokof'ev, G. Pupillo, and P. Zoller, "Strongly correlated 2D quantum phases with cold polar molecules: Controlling the shape of the interaction potential," Phys. Rev. Lett. **98**, 060404 (2007).

[326] G. Pupillo, A. Griessner, A. Micheli, M. Ortner, D.-W. Wang, and P. Zoller, "Cold atoms and molecules in self-assembled dipolar lattices," Phys. Rev. Lett. **100**, 050402 (2008).

[327] I. S. Gradshteyn and I. M. Ryzhik, *Table of Integrals, Series, and Products*, 6th ed. (Academic Press, 2000).

[328] M. Faraday, "On a peculiar class of acoustical figures; and on certain forms assumed by groups of particles upon vibrating elastic surfaces," Phil. Trans. R. Soc. Lond. **121**, 299 (1831).

[329] M. C. Cross and P. C. Hohenberg, "Pattern formation outside of equilibrium," Rev. Mod. Phys. **65**, 851 (1993).

[330] D. Binks and W. van de Water, "Nonlinear pattern formation of Faraday waves," Phys. Rev. Lett. **78**, 4043 (1997).

[331] C. Szwaj, S. Bielawski, D. Derozier, and T. Erneux, "Faraday instability in a multimode laser," Phys. Rev. Lett. **80**, 3968 (1998).

[332] H. Abe, T. Ueda, M. Morikawa, Y. Saitoh, R. Nomura, and Y. Okuda, "Faraday instability of superfluid surface," Phys. Rev. E **76**, 046305 (2007).

[333] K. Staliunas, S. Longhi, and G. J. de Valcárcel, "Faraday patterns in Bose-Einstein condensates," Phys. Rev. Lett. **89**, 210406 (2002).

[334] K. Staliunas, S. Longhi, and G. J. de Valcárcel, “Faraday patterns in low-dimensional Bose-Einstein condensates,” Phys. Rev. A **70**, 011601 (2004).

[335] A. I. Nicolin, R. Carretero-González, and P. G. Kevrekidis, “Faraday waves in Bose-Einstein condensates,” Phys. Rev. A **76**, 063609 (2007).

[336] A. I. Nicolin, “Resonant wave formation in Bose-Einstein condensates,” Phys. Rev. E **84**, 056202 (2011).

[337] A. I. Nicolin, “Variational treatment of Faraday waves in inhomogeneous Bose-Einstein condensates,” Physica A **391**, 1062 (2012).

[338] A. Balaž and A. I. Nicolin, “Faraday waves in binary nonmiscible Bose-Einstein condensates,” Phys. Rev. A **85**, 023613 (2012).

[339] P. Engels, C. Atherton, and M. A. Hoefer, “Observation of Faraday waves in a Bose-Einstein condensate,” Phys. Rev. Lett. **98**, 095301 (2007).

[340] M. Modugno, C. Tozzo, and F. Dalfovo, “Detecting phonons and persistent currents in toroidal Bose-Einstein condensates by means of pattern formation,” Phys. Rev. A **74**, 061601 (2006).

[341] P. M. Morse and H. Feshbach, *Methods of Theoretical Physics, Part I* (McGraw-Hill, New York, 1953).

[342] F. Tisserand, *Traité de Mécanique Céleste, Tome III* (Paris, Gauthier-Villars et fils, 1894).

[343] A. I. Nicolin, Ph.D. thesis, The Niels Bohr Institute, Copenhagen, Denmark (2008).

[344] H.-Y. Lu, H. Lu, J.-N. Zhang, R.-Z. Qiu, H. Pu, and S. Yi, “Spatial density oscillations in trapped dipolar condensates,” Phys. Rev. A **82**, 023622 (2010).

[345] O. W. Dietrich, E. H. Graf, C. H. Huang, and L. Passell, “Neutron scattering by rotons in liquid helium,” Phys. Rev. A **5**, 1377 (1972).

[346] E. C. Svensson, A. D. B. Woods, and P. Martel, “Phonon dispersion in liquid helium under pressure,” Phys. Rev. Lett. **29**, 1148 (1972).

[347] P. R. Roach, J. B. Ketterson, B. M. Abraham, and M. Kuchnir, “Sound velocity in liquid ^{4}He under pressure,” J. Low Temp. Phys. **12**, 375 (1973).

[348] I. Iguchi, “Roton trapping by a vortex line,” Phys. Rev. A **6**, 1087 (1972).

[349] We assume the BEC away from the narrow regions of biconcave density profiles, see Ref. [239].

[350] T. D. Stanescu, B. Anderson, and V. Galitski, "Spin-orbit coupled Bose-Einstein condensates," Phys. Rev. A **78**, 023616 (2008).

[351] S. Sinha, R. Nath, and L. Santos, "Trapped two-dimensional condensates with synthetic spin-orbit coupling," Phys. Rev. Lett. **107**, 270401 (2011).

[352] The dynamics following roton instability has been previously discussed in Ref. [249]. However, in the considered work the roton confinement played no significant role, due to the low aspect ratio λ. Despite that, confinement effects may be inferred from an unpublished numerical simulation of collapse dynamics that can be found on the webpage of the authors of Ref. [249], `http://grizzly.colorado.edu/~bohn/movies/collapse.htm`. In our numerics, we have observed localized modulational instability for $\lambda \gtrsim 14$.

[353] N. G. Parker, C. Ticknor, A. M. Martin, and D. H. J. O'Dell, "Structure formation during the collapse of a dipolar atomic Bose-Einstein condensate," Phys. Rev. A **79**, 013617 (2009).

[354] Sufficiently large three-body losses and/or densities may also stabilize the system before the collapse occurs, provided that the time for the development of the modulational instability is comparable to $1/L_3\bar{n}^2$, where $\bar{n}$ is the average density. This becomes especially relevant if a_f is close to the instability threshold.

[355] The BEC presents also a small overall breathing due to the change of a, but this plays here a secondary role. We gauge this mode out by rescaling the radial coordinate r and the 2D density $n_0^{2\mathrm{D}}$ as $r \to r/f(t)$, $n_0^{2\mathrm{D}} \to n_0^{2\mathrm{D}} \times f(t)^2$, where $f(t) = R(1 + b\cos(2\pi t/\tau))$, with τ the breathing period, and b the breathing amplitude.

[356] The local spectrum should play also an important role in the stability spectroscopy of rotons recently proposed by J. P. Corson, R. M. Wilson, and J. L. Bohn, see arXiv:1301.1991.

[357] Effects of the roton confinement on Bragg spectroscopy may be already inferred from some results of Ref. [241].

[358] N. W. McLachlan, *Theory and applications of Mathieu functions* (Clarendon Press, 1947).

❧

Curriculum Vitae

1984	Born in Warsaw, Poland
2003	Matriculation, XIV Liceum Ogólnokształcące im. Stanisława Staszica, Warsaw, Poland
2003-2008	Physics studies, University of Warsaw, Poland
2008	Master Of Science in Theoretical Physics
2009-2013	PhD Fellowship, Leibniz University Hannover, Germany Centre for Quantum Engineering and Space-Time Research (QUEST)

Publications

1. Mattia Jona Lasinio, Kazimierz Łakomy, Luis Santos
   Roton confinement in trapped dipolar Bose-Einstein condensates
   submitted to Physical Review Letters, arXiv:1301.4907
2. Kazimierz Łakomy, Rejish Nath, Luis Santos
   Faraday patterns in coupled one-dimensional dipolar condensates
   Physical Review A **86**, 023620 (2012)
3. Kazimierz Łakomy, Rejish Nath, Luis Santos
   Soliton molecules in dipolar Bose-Einstein condensates
   Physical Review A **86**, 013610 (2012)
4. Kazimierz Łakomy, Rejish Nath, Luis Santos
   Spontaneous crystallization and filamentation of solitons in dipolar condensates
   Physical Review A **85**, 033618 (2012)
5. Kazimierz Łakomy, Zbigniew Idziaszek, Marek Trippenbach
   Thermal effects in light scattering from ultracold bosons in an optical lattice
   Physical Review A **80**, 043404 (2009)

◆

Acknowledgments

First and foremost I would like to express my sincere gratitude to my supervisor, Prof. Luis Santos, for his invaluable help and advice throughout the course of my PhD studies. The completion of this thesis would not have been possible without his scientific assistance, thoughtful guidance and the patience of a saint.

I owe a special debt of gratitude to Dr. Rejish Nath for his friendship, unfailing support, steadfast encouragement and hospitality in Dresden and India. I am also deeply grateful for numerous hours that we spent together discussing physics and collaborating. Most of the topics and concepts in this thesis came as a resolution of our debates. Ente hridhayam nirranja nanne!

I share the credit of my work also with Dr. Mattia Jona Lasinio whom I always have found ready to discuss and elucidate various, more or less puzzling problems that I would put in front of him. In particular, the last chapter of this thesis is the result of the project that we ran together. Further, he proved himself as a prime lunch and coffee chats companion and, when necessary, a sound opponent in disputes. Grazie mille!

Heartfelt thankfulness and appreciation are due to Dr. Adolfo del Campo. Thanks for the Russian poetry, being there to listen, a number of consolation drinks and unceasing encouragements to think independently and beyond the scope. Cheers gent!

I am indebted to Dr. Frank Deuretzbacher and Dr. Temo Vekua for many fruitful scientific discussions and prompt, and profound answers to my queries. I stand in awe of the prudent way you guys practice physics. I will also never forget the genuine sincerity that you have showed me.

A brief but very sincere acknowledgement is due to Dr. Philipp Hyllus and Dr. Hendrik Weimer. Thank you for the enjoyable time that we spent sharing the office.

Mihail Rabinovic has translated the Zusammenfassung in this thesis. Yet, what he did even better was to keep amusing me during gloomy days and to make me feel pleasurably more wise than I really am, when asking for

my opinions. Thank you Misha!

Special acknowledgement goes to Alex Cojuhovschi, for his assistance with IT related issues that come as an occupational hazard. More importantly, however, for exhilarating discussions and his open-minded attitude.

During these last four years I had a chance to attend many international conferences and meet there innumerable fascinating people. Some of them became my dear friends with whom I associate beautiful memories. I would like to take this chance to express my most warmhearted feelings to Maria Korppi (Basel oli todella hyvä!), Tim Langen (nächstes Mal in Wien wir gehen nach Chelsea zusammen!) and Ricard Menchón Enrich (alguns encara Xopets per provar a Barcelona!).

I took my first steps in the physics of ultracold quantum matter at the University of Warsaw, in the Institute for Theoretical Physics. There, for two years, I was benefiting from guidance and immense knowledge of Prof. Kazimierz Rzążewski, Prof. Marek Trippenbach and Prof. Zbigniew Idziaszek. I am utmost grateful for this time. It was the beginning of this intriguing scientific adventure that has continued with the work in this dissertation.

I could certainly not handle most of the office and red tape everyday problems if it was not for the friendly and helpful staff of the Institute for Theoretical Physics. With this respect, I would like to cordially acknowledge and thank to Ms. Emma Schwebs and Ms. Gitta Richter, and, especially, to Ms. Catharina Burmeister for being always there to help me out.

My work in Hannover has been possible through the PhD fellowship of the Center for Space-Time Research and Quantum Engineering (QUEST), an excellence cluster funded by the German Physical Society (Deutsche Physikalische Gesellschaft, DPG). I would like to thank both organizations for their generous support. As a member of QUEST I have been surrounded by wonderful colleagues who provided a rich and fertile environment to study and explore new ideas. This would have not been possible without the professional steering committee and its speaker Prof. Wolfgang Ertmer. Thank you for all the opportunities that you have provided me during this fellowship. Finally, I gratefully acknowledge the administrative staff of QUEST operated by Dr. Stefan Pfalz and Dr. Patrick Barthold. My most sincere gratitude goes to Ms. Birgit Ohlendorf who always cared for me in every tiniest detail of any possible matter. Thank you Birgit!

My friends from Poland have been a constant source of support throughout my graduate and postgraduate years. Thank you for just being there for me, rekindling the dreams.

Finally, I owe my deepest gratitude to my beloved mother. You have always taught me to reach for the stars. I just made another step towards them. *Dziękuję mamo.*

❧

Selbstständigkeitserklärung

Hiermit versichere ich, die vorliegende Doktorarbeit selbstständig und unter ausschliesslicher Verwendung der angegebenen Hilfsmittel angefertigt zu haben.

Hannover, den 29. Januar 2013

Kazimierz Łakomy